“SELF-HEALING” ORGANIC FLUOROPHORES FOR SINGLE-MOLECULE MICROSCOPY AND SPECTROSCOPY

A Dissertation

Presented to the Faculty of Weill Cornell Graduate School

of Medical Science

in Partial Fulfillment of the Requirements for the Degree of

Doctor of Philosophy

By

Qinsi Zheng

May 2016

“SELF-HEALING” ORGANIC FLUOROPHORES FOR SINGLE-MOLECULE MICROSCOPY AND SPECTROSCOPY

Qinsi Zheng

Cornell University 2016

Fluorescence provides a mechanism for achieving contrast in biological imaging that enables investigations of molecular structure, dynamics, and function at high spatial and temporal resolution. Small-molecule organic fluorophores have proven essential for such efforts and are widely used in advanced applications such as single-molecule and super-resolution microscopy. Yet, organic fluorophores, like all fluorescent species, exhibit instability in their emission characteristics, including blinking and photobleaching that limit their utility and performance. To overcome this limitation and to push the limit of biological imaging, we develop self-healing organic fluorophores, wherein the triplet state is intramolecularly quenched by a covalently attached stabilizer, exhibit markedly improved photostability for biological imaging *in vitro* and in living cells. Chapter 1 is a general introduction to fluorophores used for biological imaging and the photophysical framework for fluorophore stability. Chapter 2 overviews the methods used in this study. Chapter 3 is focused on the triplet-state-quenching mechanism of photostabilization in self-healing fluorophore. Chapter 4 discusses the generalization of this self-healing approach to organic fluorophores in different colors and structural categories. Chapter 5 presents that self-healing fluorophores improve single-molecule imaging in living cells. Chapter 6 presents a quantitative model for self-healing fluorophore photostability, leading to enhanced photostability that are not

attainable with previous photo-protection approaches. Chapter 7 addresses the future directions.

BIOGRAPHICAL SKETCH

Qinsi Zheng was born and raised in Foshan, China. While attending the Affiliated High School of South China Normal University, he enjoyed the very science-centric curriculum there and was inspired to pursue a career in science. He then moved to Beijing to attend Peking University with a major in chemistry, where he started his scientific exploration. He first worked with Dr. Zhongfan Liu to study carbon nanotubes, a material promising for microelectronics due to its nanometer size and excellent electronic properties. All semiconducting carbon nanotubes were synthesized as p type, but for microelectronics we also need n type, so Qinsi found a new method to make n-type carbon nanotubes by filling hydrazine inside the tubes. He was also fascinated by another kind of nanoscale machine - proteins - that can be synthesized with high quality and be assembled to perform complex functions. Together with his teammates at the International Genetically Engineered Machine competition, he taught bacterial cells to count by making a synthetic biochemical circuit. After these two valuable laboratory experiences, Qinsi found his interest in exploring at the interface between chemistry and biology, particularly in developing biophysical techniques to study complex biological systems that are inaccessible by traditional approaches. Hence, after enrollment in the Tri-Institutional PhD Program in Chemical Biology in New York, he joined Dr. Scott Blanchard's laboratory to develop photostable organic fluorophores for single-molecule biological imaging.

ACKNOWLEDGEMENTS

I would first like to acknowledge the extraordinary support of my mentor, Dr. Scott Blanchard. His fearless, ambitious, and dedicated pursuit of knowledge will be an inspiration throughout my career. My scientific exploration flourish in the nurturing environment he has created which aims to maximize the potential of students and postdocs. Scott is also intuitive in trouble-shooting our experiments, often within minutes after we had spent hours or even days on it. As a student came into a new country and culture, I also find his candidness invaluable.

I want to thank the faculty members on my thesis committee, Drs. Samie Jaffrey, Alexandros Pertsinidis, and Thomas Sakmar, for their time, guidance, and support. I am particularly grateful to them for being rigorous and critical, as well as for challenging me to do science that really makes a difference.

I also thank the current and former members in the Blanchard lab for their care and support along the way. They not only do great on their own projects, but also build an inter-dependent relationship and establish great infrastructures upon which we achieve excellence. In particular, I must acknowledge the exceptional support from our synthetic chemists Drs. Zhou Zhou and Hong Zhao. They have synthesized almost every compound that I have characterized in this dissertation. Without their excellence and efforts it would be impossible for me to perform this study. Like everyone else in the lab, I can focus a lot of my time and energy on the bench work because of the exceptional support of Roger Altman. His efforts, expertise and advice were critical for my training and growth as a scientist. I must also thank Dr. Daniel Terry and Dr. Manuel Juette. Together they keep our microscopy at the frontier of the field, and I own my skill of

optics and instrument control almost entirely to them. I am very grateful to Daniel for his outstanding software of data analysis, which I used almost every day.

I must also acknowledge the collaborators who contributed to this work. Most importantly, I would like to thank Dr. Steffen Jockusch and late Prof. Nicholas Turro at Columbia University, whose expertise on photochemistry and photophysics made this study possible. They demonstrated scholarship and professionalism as a scientist which I will strive for throughout my career. The cellular experiments were performed in the laboratory of Prof. Jonathan Javitch at Columbia University, with the help of Drs. Wesley Asher and Peter Geggier. The electrochemistry experiments were performed in the laboratory of Prof. Hector Abruna at Cornell University, with the help of Dr. Gabriel Rodriguez and Ryo Wakabayashi.

I am very grateful to the Tri-Institutional Ph.D. Program in Chemical Biology to provide such unique research opportunity as well as generous support. I am thankful to Prof. Derek Tan, Prof. Tim Ryan, Kathleen Pickering, and Margie Hinonangan-Mendoza for recruiting me into the program and support along the way.

Finally, I would like to thank my family: my parents; my wife Mengying Li; and our son Julian Zheng. Given their unconditional love and support, whatever I say would be too superficial.

TABLE OF CONTENTS

LIST OF FIGURES

LIST OF TABLES

LIST OF CHARTS

LIST OF SCHEMES

1. Introduction

Published previously in modified from:

Qinsi Zheng, Manuel F Juette, Steffen Jockusch, Michael R Wasserman, Zhou Zhou, Roger B Altman, Scott C Blanchard, Chemical Society Review, *Ultra-stable organic fluorophores for single-molecule research*, 2014, 43, pp1044-1056

1.1 Summary

This chapter aims to provide background information related to the work discussed in subsequent chapters. Fluorescence provides a mechanism for achieving contrast in biological imaging that enables investigations of molecular structure, dynamics, and function at high spatial and temporal resolution. Small-molecule organic fluorophores have proven essential for such efforts and are widely used in advanced applications such as single-molecule and super-resolution microscopy. Yet, organic fluorophores, like all fluorescent species, exhibit instabilities in their emission characteristics, including blinking and photobleaching that limit their utility and performance. Here, we review the photophysics and photochemistry of organic fluorophores as they pertain to mitigating such instabilities, with a specific focus on the development of stabilized fluorophores through derivatization. Self-healing organic fluorophores, wherein the triplet state is intramolecularly quenched by a covalently attached stabilizers, exhibit markedly improved photostabilities. We discuss the potential for further enhancements towards the goal of developing ‘‘ultra-stable’’ fluorophores spanning the visible spectrum and how such fluorophores are likely to impact the future of single-molecule research.

1.2 Fluorophore for fluorescence imaging

Fluorescence imaging, which affords high specificity and imaging contrast,[4] has proven to be an indispensable tool for advancing our understanding of biological systems.[5] Although biomolecules often contain intrinsic fluorophores, such as aromatic amino acids, that can be used to interrogate biological functions, extrinsic fluorophores,[6] such as small-molecule organic fluorophores,[7, 8] fluorescent proteins,[9, 10] and inorganic semiconductor particles (quantum dots),[11] have high absorbance cross sections and fluorescence quantum yields that dramatically increase image contrast and have therefore become essential for imaging. Extrinsic fluorophores spanning the visible spectrum are now available that can be specifically attached to almost any biomolecule of interest. These probes can thus serve as versatile messengers of dynamic and functional information in a diverse array of systems that would otherwise be hidden.[5] Small-molecule organic fluorophores are the smallest of the known extrinsic fluorophores–only a hundredth to a thousandth the size of fluorescent proteins and quantum dots[12, 13] **(Figure 1.1)**. Correspondingly, when properly positioned, organic fluorophores are the least perturbing to the system under interrogation.

The use of organic fluorophores over the last century has greatly advanced our knowledge and understanding of biological systems.[5] These essential tools have been used for staining distinct cellular compartments,[6] for pH and analyte sensing *in vitro* and in living cells,[14] and for detecting intermolecular interactions *via* changes in fluorophore excitation, emission, and tumbling properties.[5] They have also been used as essential reagents for immunofluorescence, proteomics, as well as a host of medical

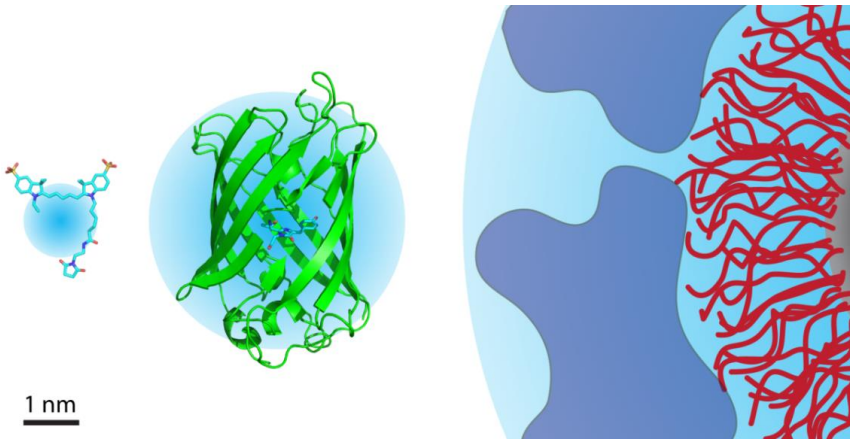

Figure 1.1. Size comparison of extrinsic fluorophores. From left to right: the organic fluorophore Cy5 (maleimide conjugate), green fluorescent protein, and a quantum dot coated with a passivating polymer layer (red) and a bioconjugating molecule layer (blue). Cyan spheres represent hydrodynamic radii.[1-3]

diagnostic tools.[5, 6] In each application, the appropriate organic fluorophore maximizes signal and minimizes noise. In this regard, the choice of fluorophore proves paramount to successful outcomes.

While organic fluorophores lack the *per se* genetic encodability of fluorescent proteins and can be less photostable than quantum dots, a number of recently developed methods enable the problem of encodability to be overcome[15-17] as well as dramatic improvements in photostability (reviewed here) that markedly expand their utility and performance in almost every imaging application. In this chapter, we focus our discussion on the use and performance of organic fluorophores in investigations using single-molecule fluorescence as excellent reviews of fluorescent proteins and quantum dots can be found elsewhere.[1, 9, 11, 12, 18-21]

Since the first single-molecule fluorescence measurements on biological samples at ambient temperatures were made in the 1990s,[22, 23] the quest to image biological systems one molecule at a time has grown exponentially.[24] The driving force behind

this trend is the emerging understanding that time-dependent fluctuations in the structure and dynamics of molecular systems are essential aspects of function that are lost, or at least obscured, in bulk investigations.[22-24] Single-molecule methods also enable the quantification of heterogeneous molecular populations and the tracking of asynchronous events in real time,[22-24] information that is inaccessible at the ensemble scale. *In vitro* analyses of motor protein function,[25, 26] RNA folding and catalysis,[27] transcription,[28] role of dynamics in molecular structure, dynamics, and function. Single-molecule investigations in living cells,[29-38] although still nascent as a field, have further revolutionized our understanding of the transient and stochastic nature of cellular processes and the fundamentally dynamic nature of biological systems.

Yet despite the remarkable progress that has already been achieved, the continued advance of single-molecule research requires new technologies to address the high demands placed on the chemical and physical properties of the fluorophores employed.[8] The instability of fluorophores –including their propensity to switch between bright and dark states (blinking) and permanently terminate fluorescence (photobleaching) –compromises the regularity and duration of photon emission.[7, 8] Depending on the nature of the fluorophore species, the illumination intensity, as well as the environmental conditions, blinking events can range from rare to frequent and last from microseconds to minutes. Blinking can arise for a variety of reasons. In the case of organic fluorophores, transient dark states may occur due to reversible isomerization of the conjugated π orbital system, resulting in temporary formation of a weakly fluorescent or non-fluorescent isomers and thus cycles of bright and dark

states.[8] Blinking may also arise from triplet or radical states of the fluorophores, which are non-fluorescent and have long lifetimes, as discussed in Section 1.3.[8] Photobleaching is defined as the permanent loss of fluorescence from light-emitting fluorescent species.

Such phenomena, which stem from fluorophore- and environment-specific photophysical and photochemical reactions,[7, 8] limit the spatial and temporal resolution and diminish the information content of the experiment. Therefore, efforts to characterize and to understand each fluorophore's distinct properties play a critical role in the evolution of fluorophores for distinct applications. Advancements in these areas offer the promise of further broadening the scope and depth of information that can be gained through single-molecule imaging as well as the types of biological that can be interrogated. Here, we discuss our translation,[39] DNA recombination,[40, 41] splicing,[42] telomere maintenance,[43, 44] reverse transcription,[45] chromatin remodeling,[46] and membrane transport[47-49] have already lead to unprecedented insights that have advanced our knowledge of the best estimate of the road ahead and the likely obstacles that will need to be overcome to make further progress.

Although blinking can be exploited for reconstructing super-resolution images of cellular structures,[50-52] for most single-molecule imaging applications, stochastic blinking, which spans from microsecond to minute timescales, reduces the number of photons emitted per unit time to the detriment of signal quality, resolution and imaging time.[53] Blinking can also be misinterpreted as biologically relevant events,[54, 55] and significantly hamper efforts to track individual fluorophores in complex environments.[56-58] Bright, slow-photobleaching and non-phototoxic[59-61]

fluorophores with stable fluorescence intensity are correspondingly in great demand. Below, we discuss key challenges associated with the generation of organic fluorophores spanning the visible spectrum with such performance characteristics and how such properties may be associated with reduced phototoxicity in complex biological settings[59-61]. Such species are referred to here as "ultra-stable" organic fluorophores and progress towards their development is reviewed in the context of recent advances in the field.

1.3 Origins of fluorophore instability

Our discussion of mitigating fluorophore instability necessarily begins with a brief review of the photophysics and photochemistry underpinning organic fluorophore performance. (**Figure 1.2**).[62] A fluorophore molecule in the ground state (**S_0** in **Figure 1.2**) that is illuminated with light of appropriate wavelength may absorb a photon to transition into an excited state, where the efficiency of this process is determined by the illumination intensity and the fluorophore's extinction coefficient. Following rapid (ca. picoseconds), solvent-mediated relaxation, the fluorophore resides in the lowest vibrational level of the first singlet excited state (**S_1** in **Figure 1.2**). The excitation process can also be described in the framework of molecular orbital theory,[62] where an electron within the highest occupied molecular orbital (**HO** in **Figure 1.2**) transitions to the lowest unoccupied (**LU** in **Figure 1.2**) molecular orbital.

A fluorophore in S_1 can return to the S_0 state through either a radiative (fluorescence [**F**] in **Figure 1.2**) or a non-radiative (internal conversion [**IC**] in **Figure 1.2**) relaxation pathway, at timescales on the order of 10^{-10} – 10^{-9} seconds (for fluorophores typically used in single-molecule imaging).[7, 63, 64] Due to rapid vibrational

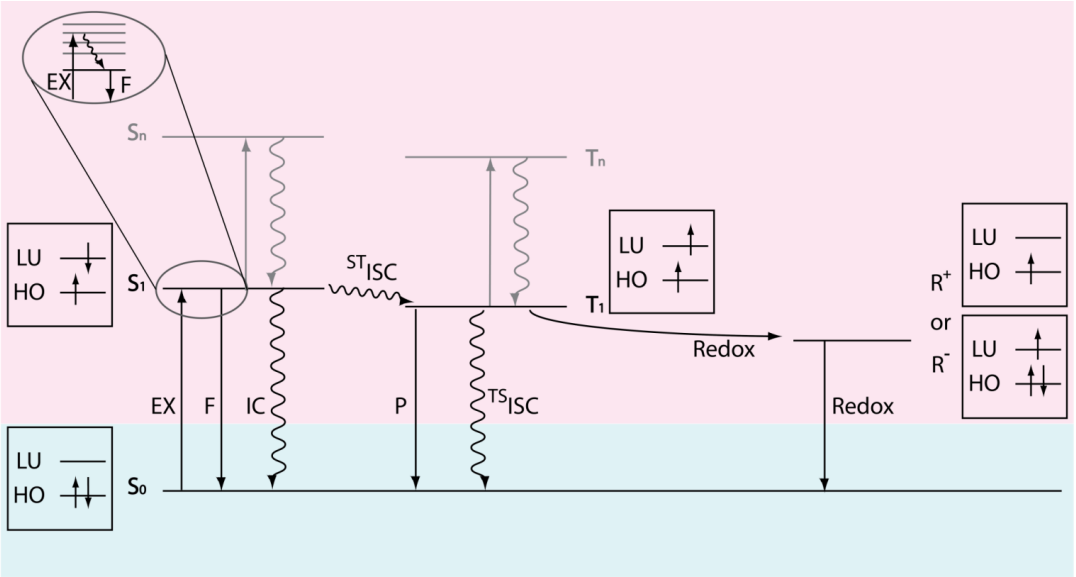

Figure 1.2. The state energy diagram and the electron spin configuration for fluorophore excitation and deactivation pathways. S0: the ground state of the fluorophore molecule; S1: the first singlet excited state; T1: the first triplet excited state; R+: cationic radical state; R-: anionic radical state; Sn and Tn (n > 1): h igher-energy singlet and triplet excited state, respectively; EX: excitation by photon absorption; F: fluorescence; IC: internal conversion; ISC: intersystem crossing; P: phosphorescence; Redox: reduction or oxidation. The boxes show the electron and spin configurations for the corresponding states. HO: highest occupied molecular orbital for the fluorophore molecule; LU: lowest unoccupied molecular orbital.

relaxation following excitation, the energy of the emitted photon from S_1 is lower than the excitation photon, resulting in an increase in wavelength ranging from 5-50 nm (Stokes shift).[62]

While an ideal fluorophore rapidly cycles between S_1 and S_0, resulting in regular photon emission, deviations from this simple two-state model feature prominently in the experimentally observed behaviours of organic fluorophores. For instance, a fluorophore in S_1 can also undergo intersystem crossing (**ISC** in **Figure 1.2**) to a non-fluorescent triplet excited state (**T_1** in **Figure 1.2**). Although ISC to T_1 is typically a rare event for organic fluorophores used in single-molecule imaging (< 0.01),[65-68] its high energy and long lifetime (typically 10^{-6} – 10^{-4} seconds)[66, 69-72] make it a key determinant of fluorophore performance. Excursions to the triplet state attenuate the observed photon emission rate (blinking) and open chemical pathways to irreversible damage (photobleaching). For example, fluorophores in T_1 are particularly active in electron transfer reactions[62] that result in the formation of non-fluorescent radical species (**R^+** and **R^-** in **Figure 1.2**) and subsequent degradation of the fluorophore. Here, oxidation or reduction of the fluorophore can be mediated by a solvent impurity (e.g. metal ions), molecular oxygen (O_2), components of the biological molecule to which it is attached or another fluorophore. Molecular oxygen, present at a concentration of approximately 0.3 mM in aqueous solutions at ambient pressure,[73] is a ubiquitous and reactive participant in reactions with organic fluorophores. Electron transfer from a triplet fluorophore to molecular oxygen produces a superoxide radical (O_2^-) and a non-fluorescent, cationic state (R^+) of the fluorophore. Energy transfer from a triplet fluorophore to molecular oxygen produces excited singlet oxygen ($^1O_2$), an oxidizing

agent stronger than ground state molecular oxygen. Superoxide radicals and singlet oxygen, along with other downstream reactive oxygen species (ROS), including $HO\cdot$, $HO_2\cdot$, and H_2O_2, can cause photobleaching by reacting with the fluorophore[74-76] and phototoxicity by reacting with nearby biomolecules.[61, 77, 78]

The aforementioned discussion provides a simplified framework for understanding the experimentally observed instability of organic fluorophores (**Figure 1.3**). While the ideal fluorophore cycles exclusively between the S_0 and S_1 states, leading to a non-blinking and long-lasting fluorescent signal, such behavior is never achieved in practice because the rate of intersystem crossing to the triplet state is non-negligible. A simple calculation illustrates this point. Approximately 100 detected photons per time point are needed to achieve a sufficient signal-to-noise ratio (SNR) for a single-molecule measurement.[8] Assuming that the quantum yield of triplet state formation (Φ_{ISC}) is 0.001, the quantum yield of fluorescence (Φ_{fl}) is 0.5, and the efficiency of photon detection is 10%,[8] a fluorophore will make about two transitions to T_1 during each integration period.

In air-saturated solutions, reactions between molecular oxygen and T_1 are rapid (on the order of 10^6 s^{-1} [79]), leading to substantial ROS generation and rapid photobleaching (**Regime 1** in **Figure 1.3**). In the absence of molecular oxygen, radical states of the fluorophore may be rapidly formed through electron transfer with its surroundings (**Regime 2** in **Figure 1.3**). As R^+ and R^- radical states of the fluorophore are non-emissive and can be long lived, pronounced blinking and photobleaching occur. As will be discussed in detail below, triplet state quenchers (**TSQ** in **Figure**

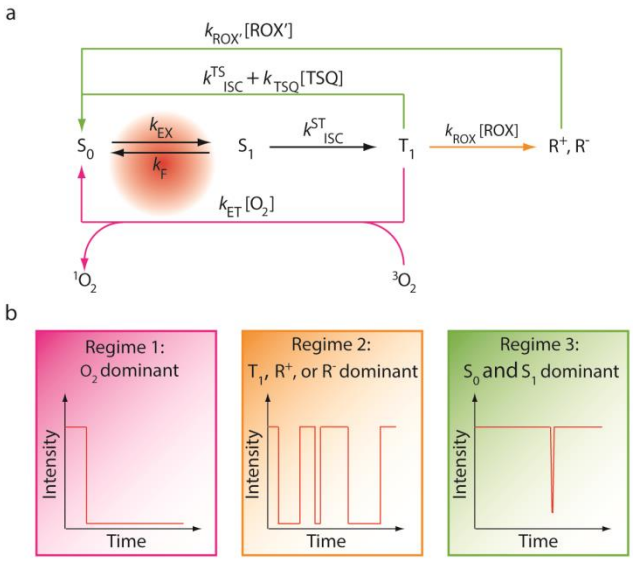

Figure 1.3. The nature of fluorophore instability. (a) A framework for understanding the nature of fluorophore instability. (b) Kinetic regimes that lead to different behaviors of a fluorophore. TSQ: triplet state quencher; ROX and ROX': reducing or oxidizing agents. t_{EXP}: the exposure time for each frame of the measurement. Regime 1 occurs when $k_{ET}[O_2] >> k^{TS}_{ISC}+k_{TSQ}[TSQ]$, $k_{ROX}[ROX]$, and the fluorophore photobleaches quickly. Regime 2 occurs when $k_{ROX}[ROX] >> k_{ET}[O_2]$, $k^{TS}_{ISC} + k_{TSQ}[TSQ]$; $k_{ROX'}[ROX'] \leq 1/ t_{EXP}$, and the fluorophore blinks frequently. Regime 3 occurs when $k^{TS}_{ISC}+ k_{TSQ}[TSQ] >> k_{ET}[O_2]$, $k_{ROX}[ROX]$;
or $k_{ROX}[ROX] >> k_{ET}[O_2]$, $k^{TS}_{ISC} + k_{TSQ}[TSQ]$; $k_{ROX'}[ROX'] >> 1/ t_{EXP}$, and the fluorophore lasts long and rarely blinks.

1.3) and reducing and oxidizing agents (**ROX** in **Figure 1.3**) can quench T1 and radical states[70, 72, 80] to recover the ground state. When such quenching occurs rapidly, triplet and radical states are shortened resulting in a non-blinking and long-lasting fluorescent signal (**Regime 3** in **Figure 1.3**).

Reactions independent of the triplet state may also contribute to fluorophore instability. The following two examples are relevant to many applications. First, excited states higher than S_1 and T_1 can be produced by the absorption of one or multiple photons (eg. $S_0 \rightarrow S_n$, $S_0 \rightarrow S_1 \rightarrow S_n$, and $S_0 \rightarrow T_1 \rightarrow T_n$) (**Figure 1.2**). However, since S_n and T_n generally relax to S_1 or T_1 (ca. femtoseconds to picoseconds) faster than they undergo other transitions (Kasha's rule),[62] higher excited states are usually not explicitly discussed in the context of fluorophore photophysics. Nevertheless, an excess of photobleaching are often observed in single-molecule Förster Resonance Energy Transfer (smFRET) and in multi-color excitation studies, which typically demand intense illumination, suggesting an involvement of S_n or T_n states.[79, 81-83] Second, the polymethine chain in cyanine fluorophores in the S_1 excited state can undergo cis-trans isomerization to produce poorly fluorescent cis isoforms, leading to attenuations in brightness, including microsecond timescale fluctuations and blinking.[7, 84-86]

1.4 Fluorophore stabilization through oxygen depletion

Given that the rate constant for quenching of fluorophore triplet states by molecular oxygen is on the order of $10^9\ M^{-1}s^{-1}$,[62] the effective rate of triplet state quenching in

air-saturated solutions approaches 10^6 s^{-1}. This rate is substantially faster than the intrinsic decay of triplet states for most organic fluorophore species (ca.5-50 x 10^6 s^{-1}). In the absence of high concentrations (e.g. > 1 mM) of oxidants or reductants,

the rate of triplet state quenching by molecular oxygen is also faster than the formation of radical states. Thus, in the presence of molecular oxygen, where the triplet state lifetime on the order of 1 μs, fluorophore blinking stemming from the formation of radical states is typically negligible. While this may be a preferred regime for live cell single-molecule imaging and some *in vitro* systems, the generation of ROS can lead to rapid fluorophore photobleaching (**Regime 1** in **Figure 1.3**; **Figure 1.4a**) and unwanted phototoxicity[59-61].

Molecular oxygen's recognized role in the photobleaching of organic fluorophores has motivated extensive investigations into practical means of removing it from solution. Dissolved oxygen can be efficiently removed by degassing techniques and saturating the solution with oxygen-free gases.[87] However, such methods are prone to variability and reverse rapidly. For this reason, enzymatic oxygen scavenging systems have become the method of choice for many fluorescence applications.[88-91] This is particularly true in the case of single-molecule imaging, where the demand for fluorophore performance is greatest. The GOD:CAT system, comprised of glucose, glucose oxidase and catalase, and the PCA/PCD system, comprised of protocatechuic acid (PCA) and protocatechuate-3,4-dioxygenase (PCD), are the most widely employed. Alternative methods include the usage of pyranose oxidase, D-glucose, and catalase,[90] or methylene blue and thiol,[91] but such systems are less common and have yet to be fully characterized.

In an air sealed container, the PCA/PCD system can reduce the molecular oxygen concentration to approximately 3 µM when operating properly.[89] In doing so, the

a

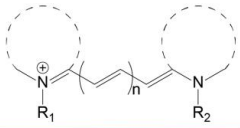

b

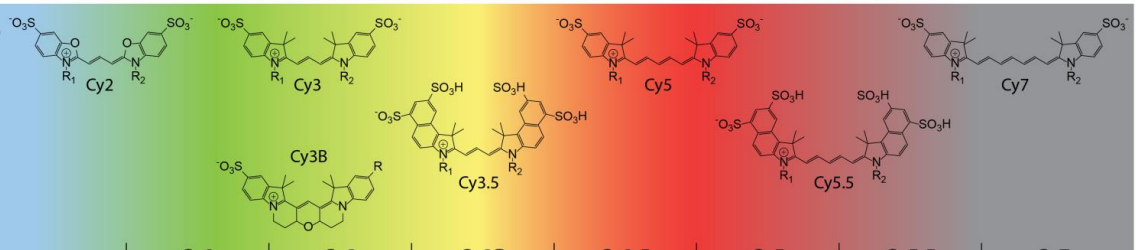

	Cy2	Cy3	Cy3B	Cy3.5	Cy5	Cy5.5	Cy7
λ_{abs} (nm)	489 nm [i,a]	550 nm [i,a]	559 nm [i,a]	581 [i,a]	649 nm [i,a]	675 nm [i,a]	747 nm [i,a]
λ_{fl} (nm)	506 nm [i,a]	570 nm [i,a]	570 nm [i,a]	596 [i,a]	670 nm [i,a]	694 nm [i,a]	776 nm [i,a]
ε_{max} ($10^5 M^{-1}cm^{-1}$)	1.3 [ii,b,*]	1.5 [iii,a] 1.5 [v,a/b]	1.3 [iii,a]	1.2 [xiv,a] 1.25 [xiv,c]	2.2 [iv,b,*] 2.5 [v,a/b]	1.9 [xiv,a] 1.95 [xiv,c]	2.5 [vi,b,*] 2.0 [v,a/b]
τ_{fl} (ns)	0.2 [vii,a]	0.2 [vii,a] < 0.3 [iii,a] 0.18 [xiii,a]	2.8 [iii,a] 2.7 [xiii,a]	[–]	0.9 [vii,a] 0.98 [iv,b,*]	[–]	0.4 [vii,a]
Φ_{fl}	0.05 [viii,b,*] 0.04 [xi,e,*] 0.053 [xii,c,*]	0.04 [iii,a] 0.09 [xiii,a] 0.04 [v,a] 0.09[v,b]	0.67 [iii,a] 0.85 [xiii,a]	0.14 [xiv,a] 0.28 [xiv,c]	0.21 [iv,b,*] 0.27 [v,a] 0.4 [v,b]	0.23 [xiv,a] 0.24 [xiv,c]	0.28 [vi,b,*]
τ_{tr} (µs)	[–]	3.9 [ix,c]	[–]	[–]	63 [x,d] 60 [iv,b,*]	[–]	[–]
Φ_{isc}	< 0.001 [xi,e,*]	< 0.001 [iv,e,*] 0.03 [ix,c]	[–]	[–]	< 0.003 [iv,b,*]	[–]	[–]

Figure 1.4. Photophysical properties of Cyanine fluorophores. (a) Generic structure of cyanine fluorophores. (b) Structures of commercially available cyanine fluorophores along with important spectroscopic properties. Despite the ubiquitous use of cyanine fluorophores, important properties like triplet state lifetimes and ISC quantum yield are often not readily available. λ_{abs}, λ_{em} – wavelengths of absorption, emission maximum; ε_{max} – extinction coefficient; τ_{fl}, τ_{tr} – lifetimes of fluorescence and triplet state; Φ_{fl}, Φ_{isc} – quantum yields of fluorescence and intersystem crossing. The R groups represent the various linkers available for bioconjugation of the fluorophores.

Source: [i] Dempsey et al. 2011;[92] [ii] Kassab 2002;[61] [iii] Cooper et al. 2004;[93] [iv] Chibisov et al. 1996;[66] [v] Mujumdar et al. 1993;[94] [vi] Rurack and Spieles 2011;[95] [vii] unpublished data; [viii] Ponterini and Caselli 1992;[96] [ix] Jia et al. 2007;[71] [x] Zheng et al. 2012;[72] [xi] Chibisov 1977;[97] [xii] Roth and Craig 1974;[98] [xiii] Sanborn et al. 2007;[99] [xiv] Mujumdar et al. 1996.[100] Solvent: [a] Water; [b] Ethanol; [c] Methanol; [d] Acetonitrile; [e] Butanol. [*] non-sulfonated form; [–] no data available.

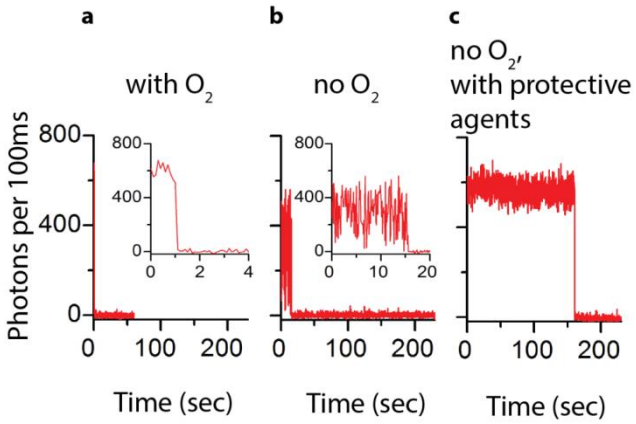

Figure 1.5. Representative single-molecule fluorescence traces for Cy5. Cy5 was imaged in (a) air saturated buffer, (b) deoxygenated buffer, and (c) deoxygenated buffer plus 1mM COT, NBA, and Trolox.

collision frequency between the fluorophore and molecular oxygen is lowered by roughly two orders of magnitude (from ~1 μs^{-1} to ~0.01 μs^{-1}). Although the removal of molecular oxygen from the solution can reduce fluorophore photobleaching rates by an order of magnitude or more (**Figure 1.5a** and **b**), doing so accentuates the redox characteristics of the fluorophore's triplet state. In solution conditions and biological settings, this typically results in severe blinking (**Figure 1.5b**) due to the formation of radical states lasting anywhere from several milliseconds to hours (**Regime 2** in **Figure 1.3**).[101] As we discuss below, improved fluorophore performance can be realized through the addition of exogenous chemical additives as well as fluorophore engineering.

1.5 Fluorophore stabilization by solution additives

A small but growing number of specific chemical additives –collectively referred to here and elsewhere[79] as stabilizers –have been identified that afford significant improvements in fluorophore performance. Stabilizer may operate through a wide range of mechanisms. However, they are generally characterized by their capacity to reduce fluorophore photobleaching rates, to increase the mean photon emission rate, to reduce variances in fluorescence intensity, and to reduce blinking frequency.[53, 80, 102]

The reducing agent, β-mercaptoethanol, was one of the first stabilizer to be employed for fluorophore stabilization.[103] Consistent with the idea that radical species contribute to poor fluorophore performance, the antioxidants cysteamine, N-propyl gallate, ascorbic acid, *p*-phenylenediamine and 1,4-diazabicyclo[2.2.2]octane (DABCO), have since been found to reduce the apparent blinking and photobleaching rates in bulk and single-molecule imaging.[53, 70, 86, 102, 104-106] Some of these compounds

constitute the active ingredients in commercially available anti-fading agents employed for fixed cell imaging applications.[107]

Chemicals such as 1,3,5,7 cyclooctatetraene (COT)[39, 79, 102, 108] 4-nitrobenzylalchohol (NBA),[39, 102, 108] and Trolox[53, 79, 102, 104] are on the shortlist of preferred compounds for fluorophore stabilization. The combined use of COT, NBA and Trolox under oxygen scavenging conditions can drastically increase the mean fluorescence intensity as well as the duration of photon emission (**Figure 1.5c**).[102] Although these reagents were understood to operate through a collision-based mechanism and to exhibit the greatest benefits when used in combination, the precise mechanisms of these stabilizers were not known at the time that they were initially employed.[53, 79, 102, 104] The utility of solution-based stabilizers as a strategy for fluorophore stabilization is highlighted by the fact that stabilizers have been used for the vast majority of single-molecule fluorescence applications over the past decade.

A significant advance in the use of stabilizers for fluorophore photostabilization has been the development of reducing and oxidizing systems (ROXS).[80] These systems elegantly address the tendency of organic fluorophores to enter dark states *via* the formation of radical fluorophore species that are directly on path to photobleaching (**Figure 1.2**). The proper balance of reducing agents, such as ascorbic acid and n-propyl gallate, and oxidizing agents, such as methylviologen, can reduce the lifetime of the triplet state by forcing the formation of fluorophore radicals that can then be quickly returned to the ground state by providing a readily available source of redox agents (**Regime 3** in **Figure 1.3**). ROXS can also reduce the lifetime of spontaneously formed

radical states through similar means. Trolox and two commercially available anti-fading agents (Vectashield and Ibidi-MM) have also been shown to function through ROXS mechanisms.[107, 109] Importantly, ROXS has proven effective for controlling the duration of bright and dark states for a variety of commercially available fluorophores by adjusting the concentration of reducing and oxidizing agents used. Sub-millimolar ROXS concentrations generally leads to reversible blinking, which can be exploited for super-resolution applications based on stochastic blinking,[110] while at millimolar concentrations and above, redox agents collide with the fluorophore on the microsecond timescale, resulting in much shorter triplet and radical state lifetimes.[80] Under such conditions, ROXS can significantly increase fluorophore stability by effectively short-circuiting photobleaching pathways. However, ROXS performance is strongly dependent on fluorophore type and experimental demands. It also functions by enforcing the entry into dark states and thus only appears to eliminate blinking when imaging at integration times substantially slower than the blinking frequency.

Research in the dye laser field dating back to the 1960s demonstrated that certain agents can increase fluorophore brightness and photostability by operating through a triplet-triplet energy transfer mechanism.[111] For this mechanism to be efficient, the triplet energy of the fluorophore (donor) must be higher than the triplet energy of the triplet state quencher (acceptor). In the presence of molecular oxygen, the triplet energy of the quencher should also be lower than the triplet-singlet energy gap of molecular oxygen (~94 kJ/mol) to prevent singlet oxygen generation. COT, which has a low-energy triplet state (~92 kJ/mol),[112, 113] fits this description and has recently been shown to greatly improve fluorophore stability in single-molecule imaging in aqueous

environments.[47, 102, 114]

Despite the remarkable advancements afforded by solution-based stabilizers, such approaches face severe constraints. First, the benefit to fluorophore performance by exogenous stabilizers depends on the collision frequency.[102] Thus, millimolar concentrations are typically required for stabilizing effects. This concentration regime is at, or near, the solubility limit for many of these compounds. Correspondingly, stabilizers may lead to a non-specific inhibition of biological activities and their effects must be carefully examined for each system under investigation. Second, the hydrophobic nature and redox properties of stabilizers pose serious limitations for investigations of biological systems at the membrane or in living cells. Indeed, it has now been shown that COT, NBA and Trolox interact with biological membranes to quantitatively alter the function of integral membrane proteins.[115] Third, the effects of stabilizers may depend on the fluorophore and the labeling context.[80, 102] Such considerations pose significant challenges for ROXS-based stabilization strategies in particular, as the redox properties of organic fluorophores are dependent on fluorophore type, solution conditions, and biological context. These issues suggest that a universal, fluorophore-independent solution for optimizing photostability using this approach may not exist.

1.6 Self-healing fluorophores

To address the aqueous insolubilities and potential toxicities exhibited by stabilizers, we have recently turned to a strategy of chemically engineering organic fluorophores to improve their performance.[72, 116, 117] Efforts along these lines have been successfully employed previously to develop fluorophores for the dye laser field,[118]

to improve the aqueous solubility,[119] and to develop fluorescence-based biosensors.[14] As indicated above, we have focused our recent endeavors on the cyanine fluorophores (**Figure 1.4**), although we believe the mechanistic insights from these investigations are likely applicable to other fluorophore classes.

Building on the observation that the stabilizers COT, NBA and Trolox operate through a concentration-dependent mechanism,[102] we set out to covalently conjugate them to the fluorogenic center to achieve the highest effective concentration possible. In our initial efforts,[117] we focused on the commercially available cyanine fluorophore, Cy5, one of the most widely employed organic fluorophores in fluorescence and FRET imaging. Cy5 serves an important role in cellular imaging and FRET due to its red-shifted emission properties but is prone to frequent blinking and rapid photobleaching in the absence of stabilizers. In this work, we chose a generalizable synthetic strategy in which a bis-N-hydroxysuccinimide activated Cy5 fluorophore was coupled to amine-activated COT, NBA and Trolox molecules to create fluorophores linked to these stabilizers through a flexible 13-atom linker (termed Cy5-COT(13), Cy5-NBA(11), and Cy5-Trolox(11), respectively; **Scheme 1**).

Remarkably, these fluorophores showed little blinking and reduced photobleaching rates compared to the parent Cy5 fluorophore in distinct biological contexts (linked to a DNA molecule *in vitro*, and to the Dopamine D2 receptor on the surface of living cells). Consistent with the hypothesis that covalent attachment of the stabilizer would increase the effective local concentration, each of the conjugates performed better than Cy5 with the respective stabilizer in solution at near-saturating (1 mM) concentration. Improvements in photostability were also found in oxygenated buffers, where stabilizers

in solution had little or no effect.[117] These findings showed that a single, proximally linked stabilizer could mediate photostabilization of the Cy5 fluorophore. Coined "self-healing fluorophores",[120] Tinnefeld and Cordes speculated that the observed photostabilization could be mediated by ping-pong redox chemistry *via* the conjugated stabilizer, thereby mitigating the formation of triplet and radical states directly.[120]

Despite the enhanced photostability for the self-healing Cy5 derivatives, key open questions remained in order to use self-healing fluorophores to push the limit of biological imaging: (1) to investigate the mechanism of enhanced photostability for self-healing fluorophores; (2) to generalize the self-healing approach to organic fluorophores in different color and structural categories; (3) to prove that they can advance single-molecule measurement of biological processes *in vitro* and in living cells; (4) to understand the design principles of self-healing fluorophores that can guide further development. This dissertation presents my studies addressing these four open questions. Chapter 2 overviews the methods used in this study. Chapter 3 is focused on the triplet-state-quenching mechanism of photostabilization in self-healing fluorophore. Chapter 4 discusses the generalization of this self-healing approach to organic fluorophores in different colors and structural categories. Chapter 5 presents that self-healing fluorophores improve single-molecule imaging in living cells. Chapter 6 presents a quantitative model for self-healing fluorophore photostability, leading to enhanced photostability that are not attainable with previous photo-protection approaches. Chapter 7 addresses the future directions.

2. Material and methods

A part of this chapter was previously published in modified form:

Roger B Altman, Daniel S Terry, Zhou Zhou, Qinsi Zheng, Peter Geggier, Rachel A Kolster, Yongfang Zhao, Jonathan A Javitch, J David Warren and Scott C Blanchard, *Cyanine fluorophore derivatives with enhanced photostability.* Nature Methods (2012) 9, 68–71

Roger B Altman, Qinsi Zheng, Zhou Zhou, Daniel S Terry, J David Warren and Scott C Blanchard, *Enhanced photostability of cyanine fluorophores across the visible spectrum.* Nature Methods (2012) 9, 428–429

Qinsi Zheng, Steffen Jockusch, Zhou Zhou, Roger B. Altman, J. David Warren, Nicholas J. Turro, and Scott C. Blanchard, Journal of Physical Chemistry Letters, *On the Mechanisms of Cyanine Fluorophore Photostabilization*. 2012, 3 (16), pp 2200–2203

Qinsi Zheng, Steffen Jockusch, Zhou Zhou, Roger B. Altman, and Scott C. Blanchard, Journal of Physical Chemistry Letters, *The Contribution of Reactive Oxygen Species to the Photobleaching of Organic Fluorophores*. 2014, 90 (2), pp 448-454

2.1 Generation of fluorophore–labeled DNA duplexes

A 21-nucleotide DNA, 5′-(5AmMC6)CATGACCATGACCATGACCAG (3BioTEG)-3′, was chemically synthesized containing a 5′ amino modifier with a six-carbon linker (5AmMC6) for fluorophore linkage and an additional 3′ biotin moiety attached via a 22-atom tetra-ethyleneglycol (TEG) spacer (3BioTEG) (Integrated DNA

Technologies). A complementary strand was synthesized with a C_6-amino thymine at various positions (indicated by asterisks) (5′-CTGGTCATGGTCAT*GGT*CAT*G-3′).

Each DNA strand was individually labeled with either commercially available N-hydroxysuccinimide (NHS) ester activated fluorophore Cy5 (GE Healthcare) or newly generated TSQ-linked compounds (Supplementary Note) through the following procedure: lyophilized DNAs were resuspended in double-distilled (dd)H_2O and adjusted to 50 μM in 50 mM potassium borate buffer (pH 8.1) with 200 mM KCl. Labeling was achieved by adding a fivefold molar excess of NHS-reactive fluorophore or TSQ resuspended in dimethyl sulfoxide (DMSO) in a 10-μl reaction. After incubation at 37 °C for 30 min, all reactions were quenched with 0.2 μl of 1 M Tris-acetate pH 7.5 at 25 °C for 2 min. Complementary strands were hybridized by mixing the two in equimolar ratios, briefly heating to 90 °C followed by passive cooling to room temperature (23 °C). Unbound fluorophore was removed using 300 μl of diethylaminoethyl (DEAE) cellulose resin equilibrated with 10 mM Tris-acetate (pH 7) with 200 mM ammonium chloride. Hybrids were diluted in column buffer for binding, then after extensive washing to liberate free fluorophore, the DNA was eluted with 10 mM Tris-acetate (pH 7) with 1 M ammonium chloride. Labeled fractions were pooled (~200 μl total), diluted in 1 ml of buffer A (1.7 M ammonium sulfate, 10 mM ammonium acetate pH 5.85) and applied over an (FPLC) phenyl 5PW column (Tosoh Bioscience) using a 60-min gradient from buffer A to B (10% methanol and 10 mM ammonium acetate; pH 5.85). The major peak of interest was collected and used for single-molecule experiments.

2.2 Single-molecule imaging of fluorophore-labeled DNA duplexes in vitro

All experiments were performed using a laboratory built, prism-based total internal reflection fluorescence (TIRF) apparatus as previously described[102] at specified illumination intensities in T50 buffer (10 mM Tris acetate (pH 7.5) and 50 mM KCl), containing 5 mM β-mercaptoethanol, 1 mM 3,4-dihydroxybenzoic acid (PCA) and 50 nM protocatechuate 3,4-deoxygenase (PCD) (Sigma-Aldrich). Biotinylated DNA molecules were immobilized via a biotin-streptavidin interaction in microfluidic channels constructed on quartz slides[102, 121]. Fluorescence from surface-immobilized molecules, illuminated via the evanescent wave generated by total internal reflection of a 640 nm (Coherent) laser source, was collected using a 1.27 numerical aperture (NA), 60× water-immersion objective (Nikon) and imaged onto a Cascade Evolve 512 electron-multiplying charge-coupled device (EMCCD) camera (Photometrics). Data were acquired using Metamorph software (Universal Imaging Corporation) collecting at a frame rate of 10–100 s^{-1}. Bulk studies were performed by immobilizing a saturating amount of molecules under deoxygenated and oxygenated conditions. Fluorescence decay curves were created by averaging intensity over the field of view for each frame and fitting to single-exponential distributions.

2.3 Kinetic analysis of fluorescence time traces

The photophysical properties of fluorophores were investigated using automated software built in-house using Matlab (MathWorks) as previously described[102]. Traces were extracted from wide-field TIRF movies by finding peaks of fluorescence intensity at least 8 s.d. above background noise and summing the intensity of 4 total pixels encompassing each peak. Neighboring peaks closer than 2.1 pixels were removed.

To reduce analytical error, traces were only used for analysis if they passed the following criteria: signal-background noise ratio >10, single-step photobleaching and background noise levels within 4 s.d. from the mean.

To extract kinetic parameters of blinking and photobleaching, the fluorescence traces were normalized to the mean fluorescence intensity of each dataset and idealized using the segmental *K*-means (SKM) algorithm[122] and a three-state model with one fluorescent (on) state, a transient dark state (blinking) and a permanent dark state (photobleaching). τ_{on} was calculated by fitting the cumulative distribution (survival plot) to an exponential function. Total τ_{on} was calculated by taking the mean of the distributions of the total time spent in the on state in each trace. Fluorescence intensity was calculated from analog-to-digital units using a conversion provided by the manufacturer. Photon counts were calculated by multiplying total τ_{on} with fluorescence intensity.

2.4 Cell culture and media

Flp-in Chinese hamster ovary (CHO) cells (Invitrogen) were stably transfected with pcDNA6/TR (Invitrogen), and single clones were selected with 15 μg ml^{-1} blasticidin and 100 μg ml^{-1} zeocin. The clone with the lowest basal expression and highest induction ratio in response to overnight treatment with 1 μg ml^{-1} tetracycline was stably transfected with a pcDNA5/FRT/To-IRES construct encoding the Metabotropic glutamate receptor 2 (mGlu2) with a SNAP tag (NEB) fused to its N terminus, and single clones were selected in 200 μg ml^{-1} hygromycin in the continued presence of 15 μg ml^{-1} blasticidin. To reduce receptor expression for ease of single-molecule tracking, the Kozak sequence was mutated to thymine at the −3 and +4 position sites, and

the *CMV* enhancer sequence was partly deleted by digestion with NruI and SnaBI (from position 209 to 591) and religation. Cells were maintained in Ham's F-12 medium (Cellgro) containing 10% FBS and 1% glutamine at 37 °C in 5% CO_2, in the presence of blasticidin (15 μg ml^{-1}) and hygromycin (200 μg ml^{-1}). Cells were used without tetracycline induction to limit receptor expression.

2.5 Cell labeling and preparation for TIRF imaging

When cells reached ~70% confluence, they were washed with PBS, resuspended in enzyme-free cell dissociation buffer (Millipore) and incubated in suspension with 10 nM Benzylguanine(BG)-derivatives of fluorophores (in 0.1% (vol/vol) DMSO and PBS) for 1 h at 37 °C. BG-derivatives of fluorophores were prepared by standard procedures in which O6-(4-(aminomethyl)benzyl)guanine (BG) was linked to NHS-derivatives of fluorophores, followed by high-performance liquid chromatography (HPLC) purification. This concentration was chosen based on fluorescence-activated cells sorting (FACS) analysis to label only ~5% of the surface receptors to facilitate particle tracking. Cells were then washed twice with 0.1% DMSO and Dulbecco's phosphate-buffered saline (DPBS) (Cellgro) and once with 0.1% BSA and DPBS. Cells were seeded on fibronectin-coated (0.1 μg $μl^{-1}$) (Sigma-Aldrich), 25 mm, #1.5 glass coverslips (Warner Instruments) and incubated in phenol-red–free DMEM/F12 medium (Gibco) containing 10% FBS and 1% glutamine for at least 1 h. Before use, new coverslips were cleaned with an optical lens cleaner (Sparkle; A.J. Funk and Co.), followed by incubation for 1.5 h in a 1:0.25:5 solution of hydrogen peroxide and ammonium hydroxide in deionized water at 75 °C. Coverslips were subsequently rinsed in deionized water, then rinsed in 100% ethanol, rapidly dried with filtered air and

passed several times over a flame. Before imaging, the coverslip with cells attached was washed seven times in PBS, the coverslip was assembled into an imaging chamber (RC-40LP, Warner Instruments) and the chamber was filled with Hank's balanced salt solution (HBSS) (Gibco) (1.26 mM calcium chloride, 0.493 mM magnesium chloride, 0.407 mM magnesium sulfate, 5.33 mM potassium chloride, 0.441 mM potassium phosphate monobasic, 4.17 mM sodium bicarbonate, 137.93 mM sodium chloride, 0.338 mM sodium phosphate dibasic and 5.56 mM D-glucose). Immediately before imaging, PCA and PCD were diluted in HBSS to reach a final concentration of 1 mM and 50 nM, respectively, in the imaging chamber.

2.6 Single-molecule imaging of mGlu2 receptor in living cells

Image sequences of single D2 receptors were measured using an objective-based TIRF microscope (IX81 with CellTIRF illuminator, Olympus) equipped with a 100× oil-immersion objective (100xUAPON NA 1.49, Olympus). Focus drift during data acquisition was minimized by using a laser autofocus system (ZDC2, Olympus) in continuous focusing mode. To establish evanescent wave illumination of receptor labeled BG-Cy5 derivatives, the excitation light beam of a red laser (640 nm, 100 mW, Olympus) was focused into the back focal plane of the objective at an angle of incidence of 76.21°, resulting in an approximate penetration depth of 90 nm. The average laser intensity during each measurement at the specimen plane was ~0.5 kW cm^{-2}. Fluorescence emission was separated from excitation light using a full-multiband filter set (LF405/488/561/635, Semrock) in combination with a single-bandpass filter (FF01-685/40, Semrock) and recorded with an EMCCD camera (Evolve 512, Photometrics) at a time resolution of 40 ms.

2.7 Laser Flash Photolysis measurement for the triplet state of the fluorophores

Laser flash photolysis experiments employed the pulses from a Spectra-Physics GCR 150-30 from a Nd:YAG laser (355 nm, ~ 5 mJ/pulse, 5 ns) and a computer-controlled system, which has been described previously[123]. For the data presented in chapter 3, acetonitrile solutions containing the Cy5 derivatives and BP were prepared and deoxygenated by argon purging. The concentrations of the Cy5 derivatives and BP were selected for optimum signal kinetics to achieve efficient triplet energy transfer from BP triplets to Cy5, but minimize self-quenching of Cy5 triplets by Cy5 ground state molecules. To accommodate the different concentrations, quartz cells of different optical path length and different experimental geometry were selected (10 x 10 mm and 6 x 4 mm in right angel pump/probe geometry; 2 x 10 mm in front face pump/probe geometry). For the data presented in chapter 6, 10 μM oxothioxanthone(OTX)-derivatives of Cy5 and Cy5-COT fluorophores was used to efficiently pump the fluorophore to triplet excited state through intramolecular triplet energy transfer. 10 x 10 mm quartz cells and right angel pump/probe geometry were used.

2.8 Ensemble fluorophore bleaching experiments

Fluorophores (5 μM or 26 μM for Cy5; 5 μM for Cy5-COT, Cy5-NBA and Cy5-Trolox; 10 μM for ATTO 655 and ATTO 647N) were dissolved in solvent (H_2O, D_2O, $CHCl_3$, $CDCl_3$, acetontrile or 100 mM Tris-acetate aqueous solution at pH 7.5). Samples (2 mL) were examined in a 1 cm cuvette, illuminated with a 300 W Tungsten halogen lamp, using an RG570 longpass filter to block short-wavelength light. Absorbance spectra of each fluorophore were measured using a UV–vis spectrometer (Agilent 8453).

The decrease in the absorption was used to estimate the relative rate of fluorophore photobleaching over the first 2 min using a linear fit.

2.9 Measurement of Singlet oxygen generation

Singlet Oxygen Sensor Green (SOSG; Invitrogen) experiments were performed in aqueous buffer as previously described[124] in a 1 cm cuvette containing 2 mL of 100 mM Tris-acetate (pH 7.5), SOSG (2 μM) fluorophore (5 or 10 μM). Samples were illuminated for fixed periods of time with a 300 W Tungsten halogen lamp in conjugation with a RG570 longpass filter. After each photolysis period, the fluorescence of SOSG was recorded over a range of 510–630 nm using 504 nm for excitation.

Due to the incompatibility of SOSG with organic solvent, 9,10-diphenylanthracene (DPA) was used to detect singlet oxygen in acetonitrile. DPA exhibits strong absorbance at 373 and 393 nm, and forms 9,10-endoperoxide, a compound that has no absorbance above 350 nm (**Figure 3.13.A**). The absorption of DPA was measured with a UV–vis spectrometer (Agilent 8453).

2.10 Fluorescence quantum yield measurements

Fluorescence spectra of solutions containing 0.7 μM Cy5, Cy5-COT, Cy5-NBA or Cy5-Trolox were recorded with a spectrofluorometer (Fluorolog 3; HORIBA Jobin Yvon), using an excitation wavelength of either 649 (aqueous Tris buffer, pH 7.5) or 654 nm (acetonitrile). The fluorescence quantum yield was calculated using Cy5 in aqueous solution (ϕ = 0.20[94]) as a standard.

2.11 Fluorescence lifetime measurements

Fluorescence lifetimes were measured by time correlated single photon counting (TC-SPC) with an OB920 spectrometer (Edinburgh Analytical Instruments) in conjunction with a pulsed diode laser emitting at 659 nm. Fluorescence decay traces were monitored at 670 nm.

2.12 Phosphorescence measurements

Solutions of the fluorescence dyes in ethanol/iodomethane (2:1, v/v) in 3 mm quartz tubes (inner diameter) were frozen at 77 K in a optical liquid N_2 quartz dewar. Iodomethane was added to increase intersystem crossing into the triplet state. The frozen samples inside the quartz dewar were excited with a pulsed Spectra Physics GCR-150-30 Nd:YAG laser (532 nm, ca. 1 mJ/pulse, 7 ns pulse length) or excited with chopped (20 Hz) cw lasers at 473 nm and 633 nm. The time-resolved phosphorescence spectra at 1 ms after pulsed excitation and a gate width of 2 ms were recorded on an Acton Spectrograph (SpectraPro-2150) in conjunction with an intensified CCD detector (PI-MAX from Princeton Instruments) with fiber optics attachment.

2.13 Reduction and oxidation potential measurements

Cyclic voltammetry was performed in DMSO using glassy carbon electrodes against an Ag/AgCl reference electrode and a platinum wire as a counter electrode at a scan rate of 100 mV/s, with 0.1 M tetrabutylammonium perchlorate as the electrolyte. Prior to measurement, the solution was purged with nitrogen gas for 15 min. All electrochemical measurements were made with a Hokuto Denko

HSV-100 potentiostat. To test whether solvent significantly affects the reduction/oxidation (redox) potential of fluorophores, a subset of fluorophores (Cy5, ATTO655, Alexa633, and fluorescein) was measured with water or water/DMSO mixture as solvent. No significant change of redox potential was detected.

3. The mechanism of self-healing fluorophore photostabilitzation

Published previously in modified from:

Qinsi Zheng, Steffen Jockusch, Zhou Zhou, Roger B. Altman, J. David Warren, Nicholas J. Turro, and Scott C. Blanchard, Journal of Physical Chemistry Letters, *On the Mechanisms of Cyanine Fluorophore Photostabilization*. 2012, 3 (16), pp 2200–2203

Qinsi Zheng, Steffen Jockusch, Zhou Zhou, Roger B. Altman, and Scott C. Blanchard, Journal of Physical Chemistry Letters, *The Contribution of Reactive Oxygen Species to the Photobleaching of Organic Fluorophores*. 2014, 90 (2), pp 448-454

3.1 Summary

Cyanine fluorophores exhibit greatly improved photostability when covalently linked to stabilizers, such as cyclooctatetraene (COT), nitrobenzyl alcohol (NBA) or Trolox. However, the mechanism by which photostabilization is mediated has yet to be determined. Here we present spectroscopic evidence that COT, when covalently linked to Cy5, substantially reduces the lifetime of the Cy5 triplet state, and that the degree of triplet state quenching correlates with enhancements in photostability observed in single-molecule fluorescence measurements. By contrast, NBA and Trolox did not quench the Cy5 triplet state under our conditions suggesting that their mechanism of photostabilization is different from COT and may quench the triplet state through electron transfer. We further showed that these self-healing fluorophores

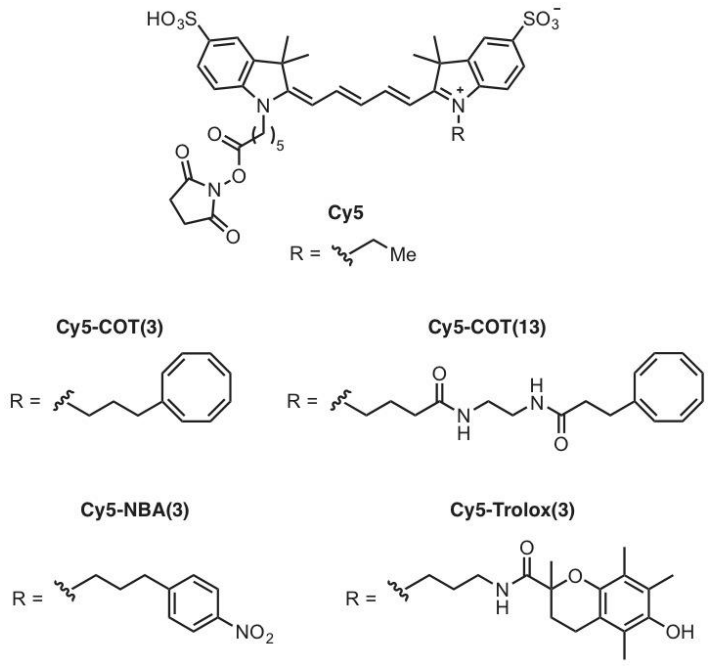

Chart 3.1. Structures of Cy5 derivatives used in this study.

generate less reactive oxygen species than parent Cy5 fluorophore and other organic fluorophores, suggesting exhibit reduced phototoxicity. These findings provide insights into the mechanisms of fluorophore photostabilization that may lead to improved fluorophore designs for biological imaging applications.

3.2 Introduction

Over the past decade, fluorescence microscopy has seen revolutionary advancements in both sensitivity and resolution, highlighted by the recent development of single-molecule fluorescence.[24, 125] However, the inherent instabilities and potential toxicities of the fluorophores employed are a current limitation. Organic fluorophores are highly prone to intermittent fluorescence (blinking) and photo-induced degradation (photobleaching), which reduce the amplitude and duration of the experimental signal.[8, 24] Consequently, there is an increasing demand for the development of new strategies that enable fluorophore photostabilization. Recently, we demonstrated that photostabilization of cyanine fluorophores can be achieved by covalently linking the fluorophore to a "stabilizer" such as cyclooctatetraene (COT), nitrobenzyl alcohol (NBA) and Trolox (Chart 3.1).[116, 117] We observed an up to 70-fold increase in the duration of fluorescence prior to entering a non-fluorescent state.

The major pathway for photobleaching of most organic fluorophores is photo-oxidation by reactive oxygen species, such as singlet oxygen and peroxides, which are thought to arise from reactions between molecular oxygen and fluorophore triplet states.[7] However, removal of molecular oxygen (a triplet quencher) often induces severe blinking, primarily due to fluorophore triplet state-induced processes.[8, 24] It had been suggested that the stabilizers (e.g. COT, NBA and Trolox) quench the triplet

states to restore the fluorophore to the singlet ground state (S_0).[70, 109, 120] Several mechanisms for this triplet quenching have been suggested. For example, the quenching of rhodamine fluorophore triplet states by COT present in the solution has been suggested to proceed through an energy transfer mechanism.[70] Studies with Trolox and ATTO fluorophores suggested that Trolox restores the fluorophore ground state from the triplet state through a reduction-oxidation (red-ox) mechanism,[109] and that a single Trolox molecule may operate through a "ping-pong" red-ox mechanism to enhance photostability.[120] The mechanism of NBA-mediated photostabilization is not clear, but may also operate through red-ox cycles.[120] However, unambiguous experimental proof of the involved mechanisms are still lacking. Here, we examined whether enhanced photostability of the Cy5 fluorophore, when covalently linked to stabilizers (COT, NBA or Trolox) (Chart 3.1) can be specifically attributed to a triplet state quenching mechanism using laser flash photolysis (time-resolved transient absorption spectroscopy).

$$\mathrm{BP} \xrightarrow[(355\,\mathrm{nm})]{h\nu} {}^1\mathrm{BP}^* \longrightarrow {}^3\mathrm{BP}^* \xrightarrow[-\,\mathrm{BP}]{+\,\mathrm{Cy5}} {}^3\mathrm{Cy5}^* \qquad (1)$$

3.3 Cy5-COT exhibited shortened triplet state lifetime

Because the formation of triplet states of Cy5 is inefficient (triplet quantum yield < 0.003) upon direct excitation,[66] a triplet sensitizer was employed to more efficiently populate the Cy5 triplet state (^{3}Cy5*) through an energy transfer mechanism (eq 1). Benzophenone (BP) was selected as a sensitizer, because of its high triplet quantum yield and higher triplet energy (289 kJ/mol)[73] compared to Cy5 (154

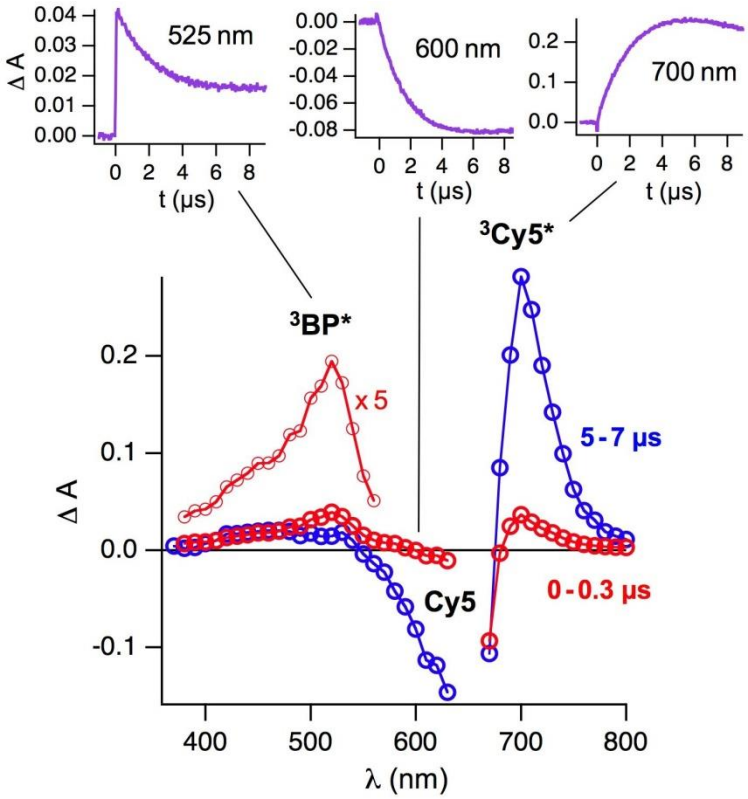

Figure 3.1. Transient absorption spectra of Cy5. Transient absorption spectra recorded at different delay times after the laser pulse (355 nm, 5 ns pulse width) of deoxygenated acetonitrile solutions of BP (5 mM) and Cy5 (22 μM). The insets show kinetic traces at different observation wavelength.

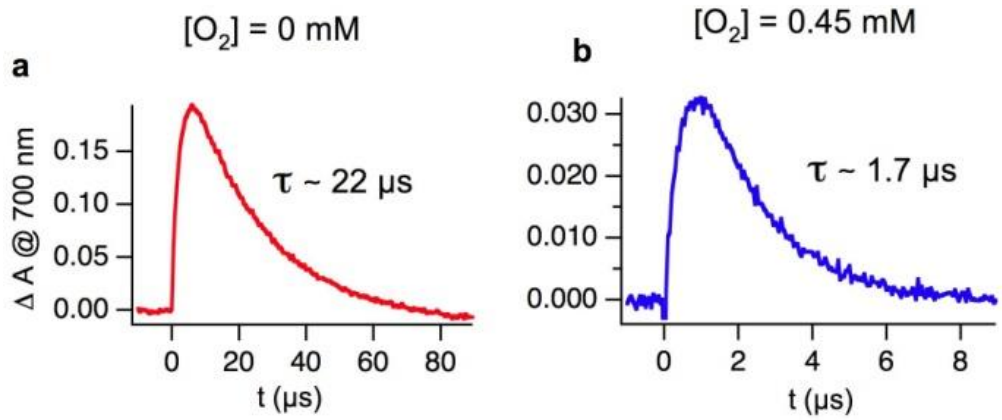

Figure 3.2. The effect of oxygen on the transient absorption traces for Cy5. Transient absorption traces recorded at 700 nm after pulsed laser excitation (355 nm, 5 ns pulse width) of acetonitrile solutions of BP (5 mM) and Cy5 (22 μM). The solutions were purged with argon (a) or a gas mixture of 95% N_2 and 5% O_2. Optical path length = 6 mm.

kJ/mol)[126].In addition, BP can be selectively excited at 355 nm, where Cy5 shows negligible absorption.

Deoxygenated acetonitrile solutions containing BP and Cy5 were irradiated with light pulses from a Nd-YAG laser at 355 nm (5 ns pulse width) to generate transient absorption kinetic traces across the visible spectrum. From these traces, transient absorption spectra at different times after the laser pulse were constructed (**Figure 3.1**). Directly after the laser pulse (**Figure 3.1**, red line) the spectrum is dominated by the triplet absorption of BP, which is known to show a peak at 525 nm.[73] After several microseconds (**Figure 3.1**, blue line) the BP triplet decayed under bleaching of Cy5

ground state absorption (~650 nm) and a new transient absorption at 700 nm appeared. As shown in the insets of **Figure 3.1**, the three processes, decay of ^{3}BP* (observed at 525 nm), bleaching of Cy5 (monitored at 600 nm) and growth of the new transient at 700 nm, occur with very similar kinetics. Assignment of this new transient at 700 nm as the triplet state absorption of Cy5 was subsequently confirmed by performing quenching studies in the presence of a small amount of oxygen (0.45 mM; generated by bubbling the acetonitrile solution with a gas mixture of 5% O_2 and 95% N_2).[73] Consistent with its potent, triplet state quenching properties, in the presence of O_2 the lifetime of the 700 nm transient was reduced to 1.7 µs compared to ~22 µs in the absence of O_2 (**Figure 3.2**). The quenching of the 700 nm transient was paralleled by recovery of Cy5 in the ground state (monitored at 600 nm). In line with this assignment, other cyanine dyes also show triplet state absorption at 700 nm.[66, 127] Conversely, the *cis*-conformation of ground state Cy5 is also known to absorb in this spectral region.[66, 126, 127] However, the observed quantitative quenching of the

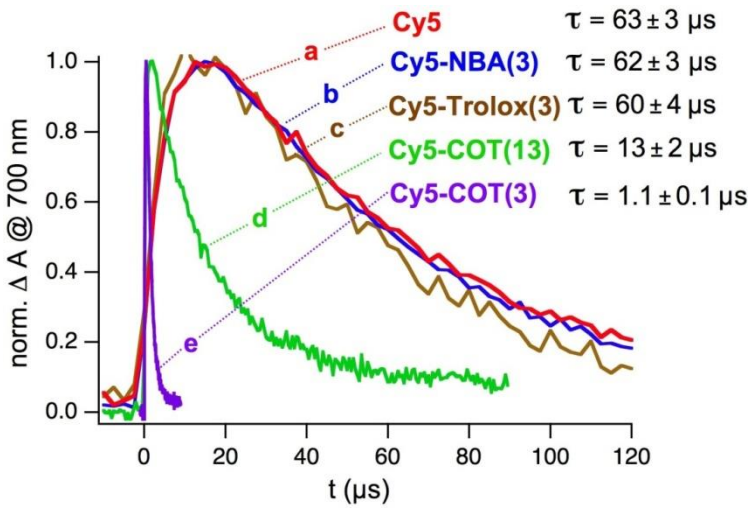

Figure 3.3. Transient absorption spectra of Cy5 and its derivatives. Cy5 triplet absorption traces recorded at 700 nm after pulsed laser excitation. The laser is at 355 nm with 5 ns pulse width. Experiments were performed with deoxygenated acetonitrile solutions of BP (a-d: 3 mM; e: 10 mM) and Cy5 derivatives (a-d: 10 ± 1 µM; e: 82 µM). The triplet lifetimes (τ) derived from a kinetic fitting model considering the growth kinetics due to energy transfer from 3BP* to Cy5. Details and the fitted traces are shown in the Supporting Information, Figures 4 and 8.

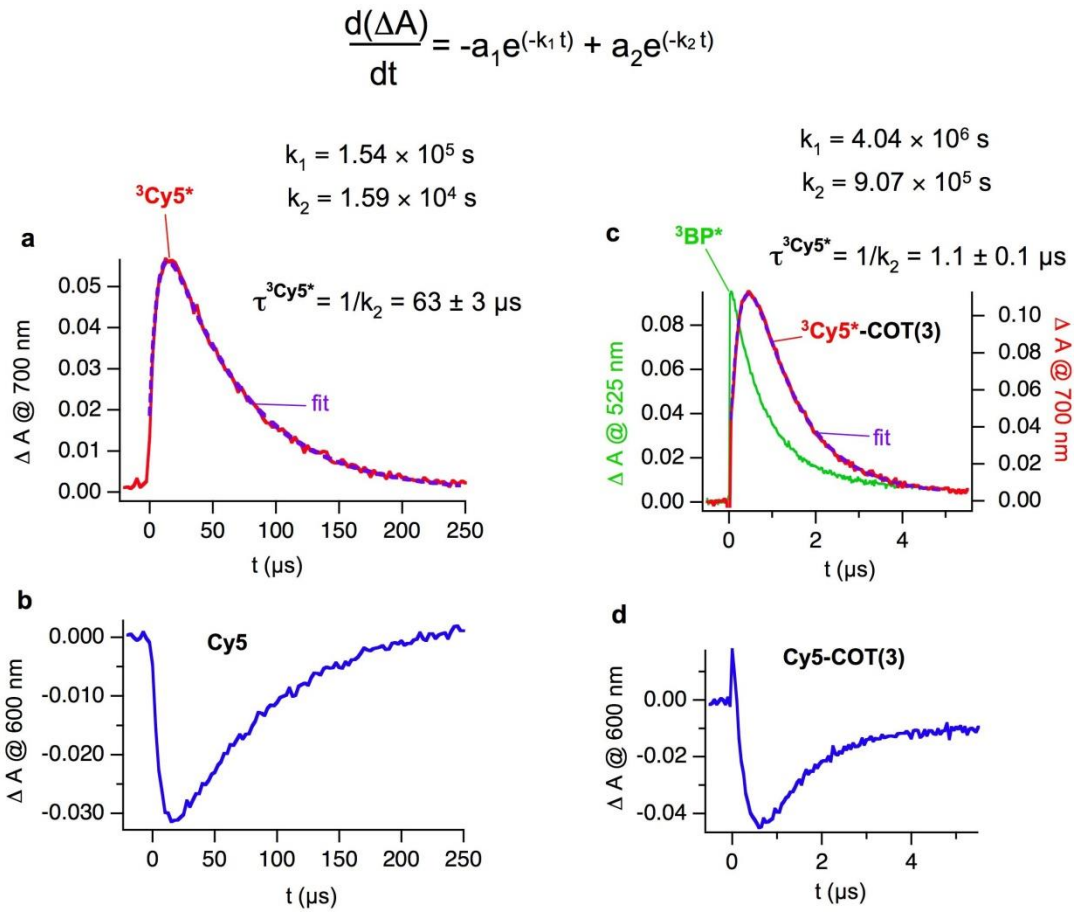

Figure 3.4. Transient absorption spectra of Cy5 and Cy5-COT(3) at different wavelength. Transient absorption traces after pulsed laser excitation (355 nm, 5 ns pulse width) of deoxygenated acetonitrile solutions of BP (a, b: 3 mM; c, d: 10 mM) and Cy5 (a, b: 10 µM) or Cy5-COT(3) (c, d: 82 µM). Optical path length 10 mm (a, b) or 2 mm (c, d). The transients were fitted (purple line) to a biexponential function, which accounts for the growth kinetics (k_1) and decay (k_2) of Cy5 triplets.

transient by O_2 demonstrates that the contribution of the ground state *cis*-conformer (which is not quenched by O_2) to the transient absorption at 700 nm is negligible. Therefore, we conclude that the transient at 700 nm observed under our experimental conditions using the BP sensitization strategy (eq 1) is correctly assigned to ^{3}Cy5* and this transient can be used to investigate Cy5 triplet state quenching by the covalently linked stabilizers. However, some minor contribution of the *cis*-conformer to the transient absorption at 700 nm cannot be excluded, especially at longer time scales.

A series of Cy5 derivatives with covalently linked stabilizers (Chart 3.1) were synthesized following procedures analogous to those previously described.[116, 117] In addition to different stabilizers (COT, NBA and Trolox), the length of the spacer between Cy5 and the stabilizer was also varied. Laser flash photolysis experiments in argon-saturated acetonitrile solutions using BP as the sensitizer were performed on each of the Cy5 derivatives. Transient absorption bands similar to unsubstituted Cy5 (**Figure 3.1**) were observed. However, significant differences were seen in the kinetic features of their triplet absorption at 700 nm (**Figure 3.3**). The initial growth in transient absorption is caused by the energy transfer process from ^{3}BP* to the Cy5 chromophore analog eq 1, which then is followed by the decay of the Cy5 triplet state. The concentrations of the Cy5 derivatives were optimized in order to ensure accurate triplet lifetime determination. High concentration, while advantageous by increasing the rate of triplet energy transfer (eq 1), had the negative effect of decreasing the Cy5 triplet lifetime due to self-quenching by ground state Cy5. Exceedingly low concentrations decreased the signal intensity at 700 nm and also substantially reduced the rate at which ^{3}Cy5* was populated. In addition, a low enough laser power was used to eliminate the

quenching of ^{3}Cy5* by triplet-triplet annihilation. The growth kinetic was deconvoluted from the decay in order to accurately determine the triplet lifetimes of the Cy5 derivatives (**Figure 3.4**). The triplet lifetimes obtained are listed in **Figure 3.3**. Cy5-NBA(3) (b) and Cy5-Trolox(3) (c) show triplet lifetimes, which are indistinguishable from the lifetime of unsubstituted Cy5 (a) (60-63 μs). However, the COT-linked derivatives (d,e) showed significantly reduced triplet lifetimes. Cy5-COT(3), the derivative with the shortest linker between the cyanine chromophore and COT has the shortest triplet lifetime (1.1 μs), and is two orders of magnitude shorter than the triplet lifetime of the unsubstituted Cy5.

COT is known to have a low-energy ("relaxed") triplet state with an energy of ~92 kJ/mol[112, 113] whereas the triplet energy of Cy5 is significantly higher (154 kJ/mol)[126]. Therefore, energy transfer from ^{3}Cy5* to COT is energetically favorable. The energy transfer mechanism between triplet donors and COT has been investigated in detail.[113] The energy transfer process generates COT triplet states and returns the cyanine chromophore to the ground state. The recovery of the cyanine fluorophore to the ground state was directly observable by laser flash photolysis (**Figure 3.4d**).

3.4 Triplet state lifetime anti-correlate with fluorophore photostability

To examine whether this COT-mediated triplet state quenching and rapid ground state recovery correlates with the observed photostability of the cyanine fluorophore, single-molecule fluorescence measurements were performed, as previously

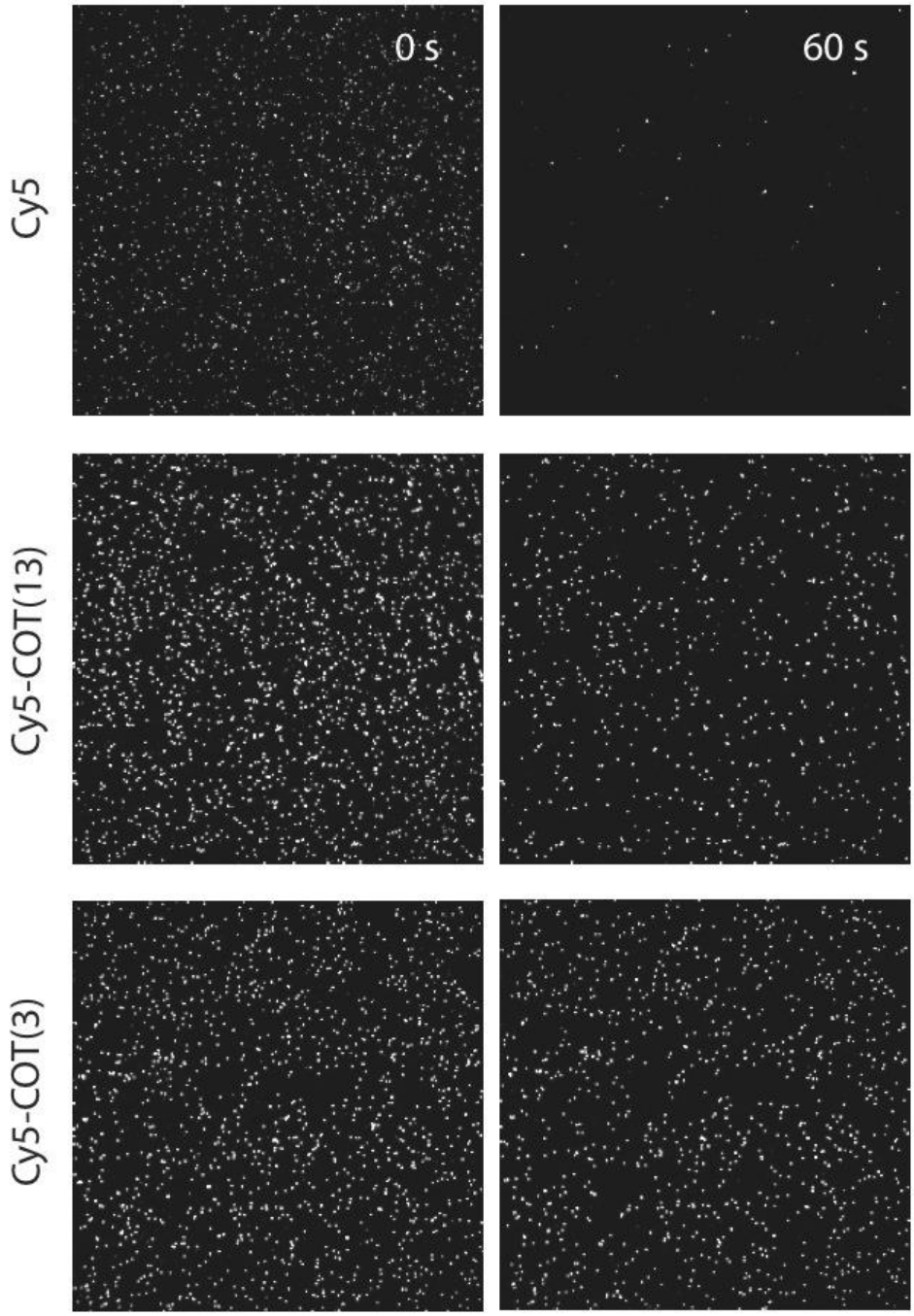

Figure 3.5. Single-molecule image of Cy5 and its derivatives. Single-molecule images of duplex DNA oligonucleotide labeled with Cy5, Cy5-COT(13) and Cy5-COT(3) under deoxygenated solution conditions using a total internal reflection microscope with 641 nm illumination.

described,[116] where the Cy5 derivatives were conjugated to double stranded DNA, a model system to study fluorophore stability on biomolecules. **Figure 3.5** shows representative images of these systems using a total internal reflection fluorescence microscope with illumination at 641 nm. By tracking the fluorescence of individual molecules over time, the intensity and duration of fluorescence, as well as the kinetics of blinking and photobleaching could be quantified. Visual inspection of individual fluorescence traces revealed that the time period of fluorescence before blinking or photobleaching was longest for Cy5-COT(3) and shortest for the unsubstituted Cy5 (**Figure 3.6**). By quantifying the number of photons detected for each ensemble of single molecules (>500 for each data set; Table 3.1), we found that the average duration of fluorescence increased from Cy5 to Cy5-COT(13) to Cy5-COT(3) in a manner that was inversely correlated with the triplet lifetime. This finding shows that the triplet state is a key intermediate for fluorophore blinking and photobleaching and that COT photostabilizes the cyanine fluorophore by reducing the duration that the fluorophore spends in the triplet state. A shortened triplet lifetime reduces the probability of fluorophore transformation reactions from the triplet state and reduces the probability of reactive oxygen species production, such as singlet oxygen, which is generated by interaction of triplet excited states with molecular oxygen. It must be noted that the interaction of COT triplet states, which are generated by energy transfer quenching from ^{3}Cy5* to COT, does not lead to singlet oxygen as the triplet energy of COT (~92 kJ/mol)[112] is slightly lower than the energy of singlet oxygen (94 kJ/mol).

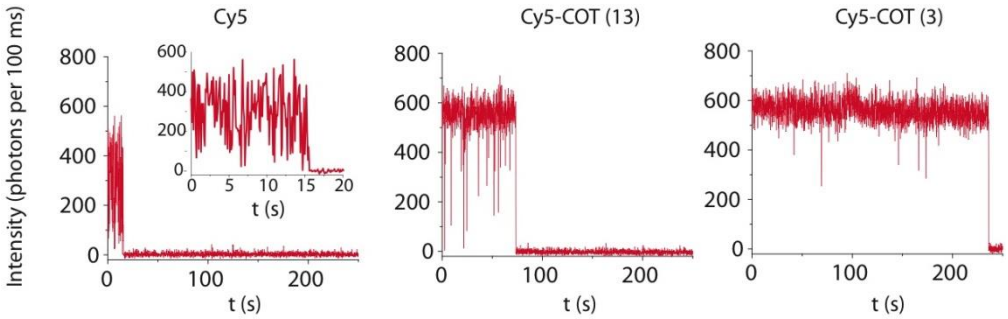

Figure 3.6. Representative single-molecule fluorescence traces for Cy5, Cy5-COT(13) and Cy5-COT(3). Fluorophores were covalently linked to DNA oligonucleotides and imaged using a total internal reflection microscope under continuous laser excitation (641 nm).

Table 3.1. Average number of photons detected before photobleaching or blinking in single-molecule measurements and triplet lifetime ($\tau_{triplet}$) of Cy5 derivatives.

	Average number of photons (10^4 photons)	$\tau_{triplet}$ (μs)
Cy5	2.1 ± 0.1	63 ± 3
Cy5-COT(13)	40 ± 4	13 ± 2
Cy5-COT(3)	99 ± 6	1.1 ± 0.1
Cy5-NBA(3)	10 ± 1	62 ± 3
Cy5-Trolox(3)	22 ± 2	60 ± 4

By contrast, shortening of the triplet lifetime was not observed for Cy5-NBA(3) and Cy5-Trolox(3) under our experimental conditions, but both Cy5 derivatives showed increased photostability compared to unsubstituted Cy5 (**Figure 3.3** and **Table 3.1**). This finding suggests that NBA and Trolox operate to stabilize the cyanine fluorophore through different mechanisms, which do not target the Cy5 triplet state directly. Possible stabilization mechanisms of NBA and Trolox could involve passivation of reactive oxygen species and radicals, which can damage the fluorophore. However, a red-ox mechanism where ^{3}Cy5* is deactivated by Trolox and NBA through a electron exchange mechanism ("ping-pong")[120] appears unlikely under our conditions, because no measurable reduction of the triplet lifetime was observed for Cy5-NBA(3) and Cy5-Trolox(3). To test if the short linker between Cy5 and NBA or Trolox might sterically hinder the electron transfer, a larger more flexible 11-atom linker chain was also tested. However, no reduction of the Cy5 triplet lifetime was observed (**Figure 3.7**).

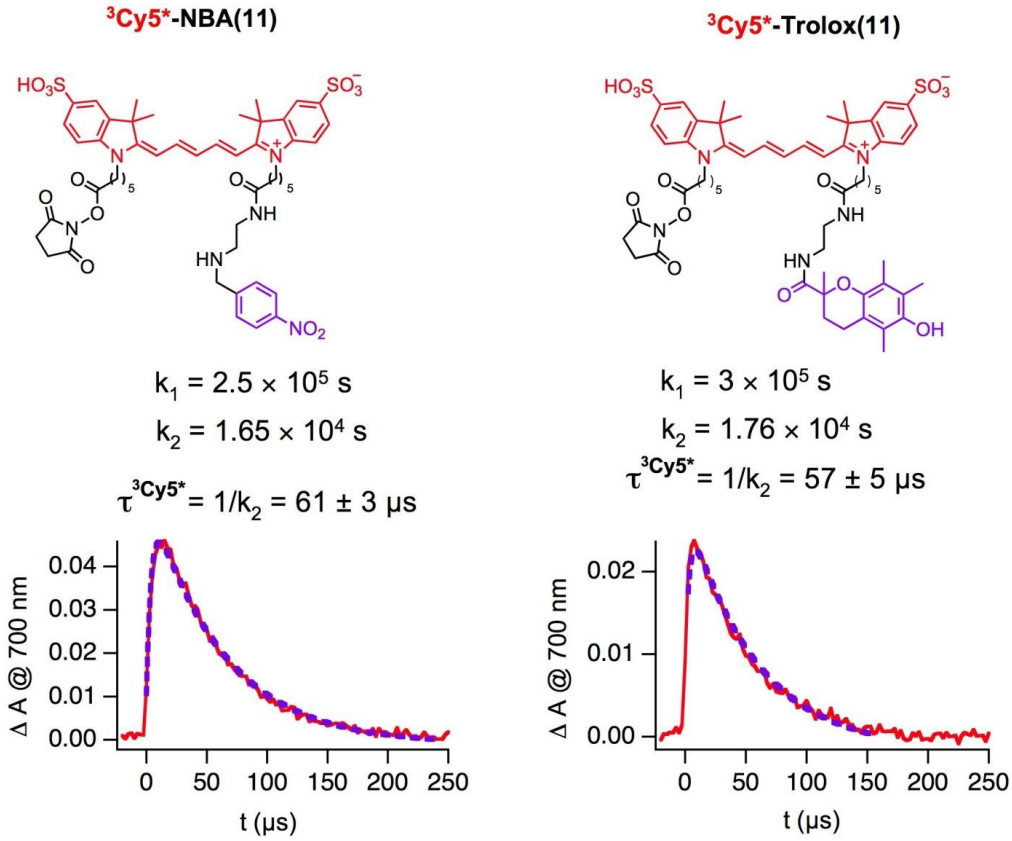

Figure 3.7. Transient absorption spectra of Cy5-NBA(11) and Cy5-Trolox(11). Cy5 triplet absorption traces recorded at 700 nm after pulsed laser excitation (355 nm, 5 ns pulse width) of deoxygenated acetonitrile solutions of BP (3 mM) and Cy5 derivatives (10 ± 1 µM). The transients were fitted (purple line) to a biexponential function, which accounts for the growth kinetics (k_1) and decay (k_2) of Cy5 triplets.

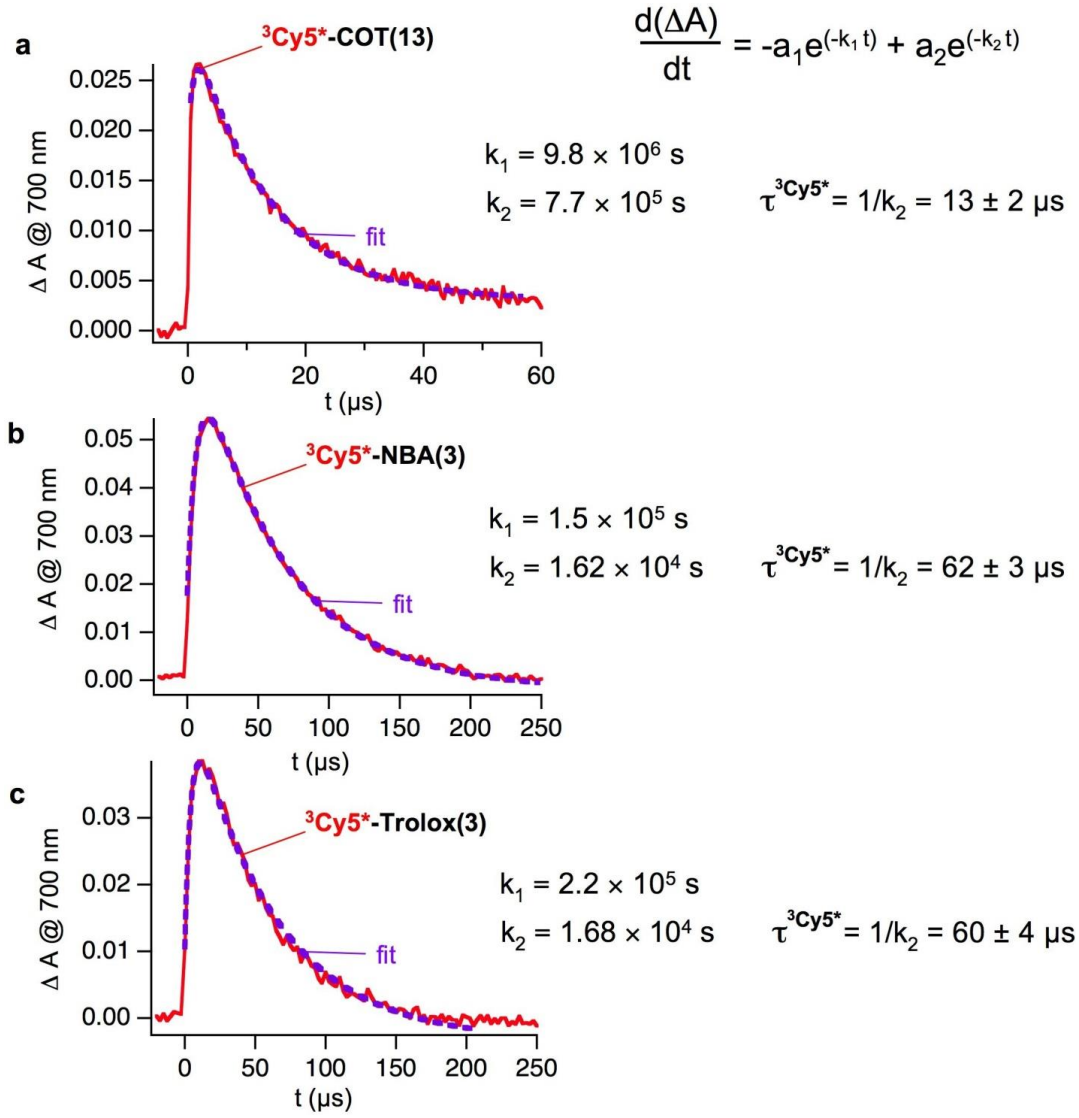

Figure 3.8. Transient absorption traces for Cy5-COT(13), Cy5-NBA(3), and Cy5-Trolox(3). Transient absorption traces at 700 nm after pulsed laser excitation (355 nm, 5 ns pulse width) of deoxygenated acetonitrile solutions of BP (3 mM) and Cy5-COT(13) (a), Cy5-NBA(3) and Cy5-Trolox(3) (10 ± 1 µM). Optical path length 10 mm. The transients were fitted (purple line) to a biexponential function, which accounts for the growth kinetics (k_1) and decay (k_2) of Cy5 triplets.

3.5 Self-healing fluorophores generate less reactive oxygen species

Molecular oxygen plays a critical role in fluorophore photobleaching and phototoxicity [7, 8, 59, 62] as it can participate in two probable reactions with an excited fluorophore. First, energy transfer can occur from a fluorophore in the triplet excited state to molecular oxygen leading to the formation of energetically excited singlet oxygen. Second, electron transfer can occur from the triplet fluorophore to molecular oxygen leading to the formation of a superoxide radical (**Scheme 1**) [62, 76]. Singlet oxygen and superoxide radical, along with other oxidizing species formed subsequently (**Scheme 1**), are collectively termed reactive oxygen species (ROS) which can degrade fluorophores [7, 74-76, 128] and damage biomolecules in various contexts [59, 77, 78, 129, 130].

To examine whether the PA-conjugated fluorophores produce less singlet oxygen, we attempted to spectroscopically measure singlet oxygen *via* its phosphorescence emission band at 1270 nm [131] upon fluorophore illumination. However, under the conditions of the experiment (5 μM fluorophore at room temperature), the yield of singlet oxygen was too low to be reliably detected using this approach (data not shown). We therefore used Singlet Oxygen Sensor Green (SOSG) as an indirect probe of singlet oxygen generation. SOSG itself is weakly-fluorescent due to intramolecular electron transfer quenching and becomes highly fluorescent following cycloaddition of singlet oxygen (**Figure 3.9a**) [124].

Initially, singlet oxygen and photobleaching resulting Cy5 illumination (>570nm) were tracked by monitoring fluorophore absorption and SOSG emission spectra as a

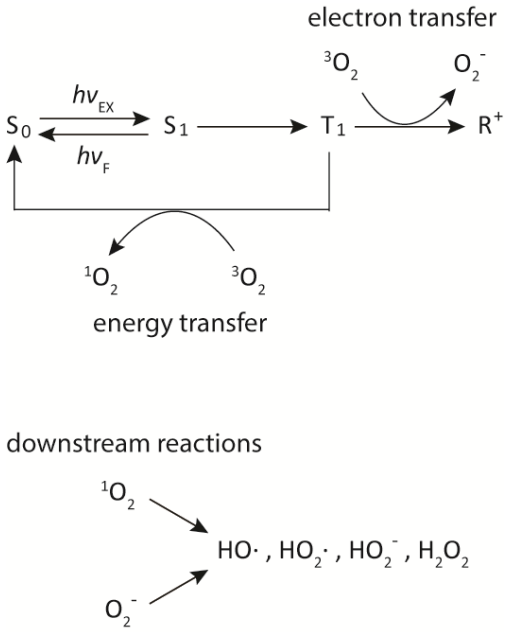

Scheme 3.1. Some probable steps to ROS via the reactions between molecular oxygen (3O2) and the fluorophore. S_0: fluorophore in ground state; S_1: fluorophore in the singlet excited state; T_1: fluorophore in the triplet state; R^+: fluorophore in the radical cationic state.

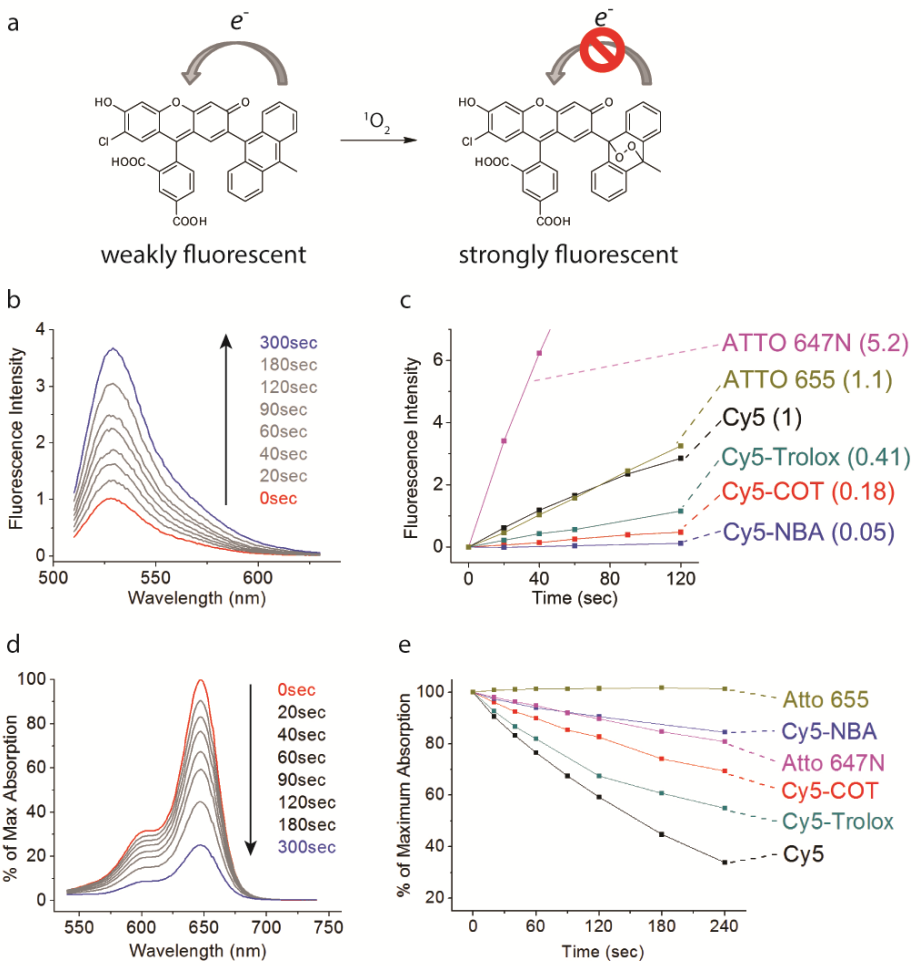

Figure 3.9. Generation of singlet oxygen for Cy5 and its derivatives. (a) The mechanism of singlet oxygen ($^1O_2$) induced fluorescence of SOSG. (b) The emission spectra of SOSG upon illumination of Cy5. (c) $^1O_2$ generation, reported by the increase of SOSG fluorescence, for distinct fluorophores at different illumination time. The relative rates of $^1O_2$ generation compared to the Cy5 fluorophore are shown in parentheses. (d) The absorption spectrum of Cy5 observed at different illumination time. (e) The decrease of Cy5, Cy5-COT, Cy5-NBA, Cy5-Trolox, ATTO 647N, and ATTO 655 absorption at 647nm as a function of illumination time. Experiments were performed in 100 mM Tris-acetate buffered aqueous solution, pH=7.5.

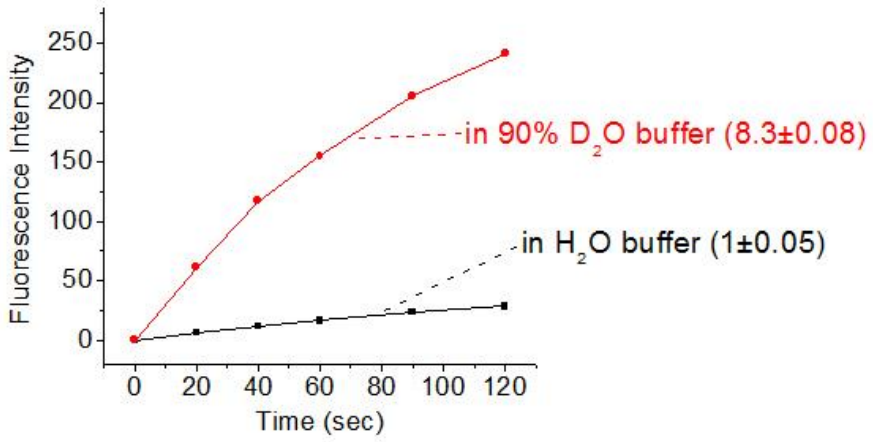

Figure 3.10. Comparison of singlet oxygen generation in water and deuterated water. Relative rate of singlet oxygen generation, in H_2O solution and in 90% D_2O solution, reported by the increase of SOSG fluorescence integrated from 518 to 538 nm. Experiments were performed with 0.7 µM Cy5 in 100 mM Tris-acetate buffered solution (pH=7.5).

function of illumination time (647 nm and 528 nm, respectively) (**Figure 3.9b,d**). As expected, the observed increase of SOSG fluorescence emission paralleled the decrease of Cy5 absorption. The increase in SOSG fluorescence was confirmed to arise from its specific reaction with singlet oxygen by performing the same measurement in 90% deuterated water, where the lifetime of singlet oxygen is significantly extended (see discussion above). The rate of SOSG fluorescence increase was enhanced by approximately 8 fold in solution in 90% D_2O (**Figure 3.10**).

In parallel, the rates of singlet oxygen generation were also measured for Cy5-COT, Cy5-NBA, Cy5-Trolox, ATTO 655 and ATTO 647N. As observed for the experiment of Cy5, SOSG fluorescence increased upon illumination of each fluorophore (**Figure 3.9c,e**). All three PA-conjugated fluorophores exhibited lower rates of singlet oxygen generation, which paralleled their increased photostability compared to Cy5. Specifically, Cy5-Trolox, Cy5-COT and Cy5-NBA exhibited 2.5-fold, 5-fold and 20-fold reductions in the rate of singlet oxygen generation, respectively (**Figure 3.9c; Table 3.2**). By contrast, ATTO 655 exhibited rates of singlet oxygen generation that were similar to those observed for Cy5, while ATTO 647N generated singlet oxygen at a rate that was approximately 5-fold greater than Cy5 (**Figure 3.9c**). These data imply that Cy5-PA fluorophores may be significantly less phototoxic than Cy5, ATTO 647N, and ATTO 655 in biological contexts.

To further explore the generation of ROS, we examined the rates of hydroxyl radical (HO·) formation using the probe Aminophenyl fluorescein (APF) [132]. Upon reaction with hydroxyl radicals, APF converts to fluorescein, a highly fluorescent species [132] (**Figure 3.11a**). Aqueous solutions containing APF and individual

Table 3.2. A summary of the data. 100mM Tris acetate buffer (pH=7.5) was used in all experiments in aqueous buffer. All of the rates were normalized to the corresponding numbers for Cy5.
[a] [94]

Solvent		Cy5	Cy5-COT	Cy5-NBA	Cy5-Trolox
aqueous	Relative rate of single-molecule photobleaching	1±0.2	0.29±0.02	0.27±0.02	0.42±0.04
	Relative rate of ensemble photobleaching	1±0.2	0.45±0.03	0.24±0.04	0.78±0.06
	Relative rate of $^1O_2$ generation	1±0.05	0.18±0.01	0.05±0.01	0.41±0.01
	Relative rate of hydroxyl radical generation	1±0.03	0.43±0.01	0.235±0.004	0.367±0.009
	Fluorescence lifetime (ns)	0.92±0.02	0.95±0.02	0.59±0.02	0.76±0.03
	Fluorescence quantum yield	0.20[a]	0.20	0.07	0.11
acetonitrile	Relative rate of ensemble photobleaching	1±0.08	0.50±0.01	1.0±0.1	0.9±0.1
	Relative rate of $^1O_2$ generation	1±0.08	0.57±0.06	0.92±0.06	0.86±0.06
	Fluorescence lifetime (ns)	1.11±0.03	1.18±0.05	0.93±0.04	1.02±0.03
	Fluorescence quantum yield	0.22	0.22	0.18	0.19
	Triplet state lifetime (μs)	63±3	1.1±0.1	62±3	60±4

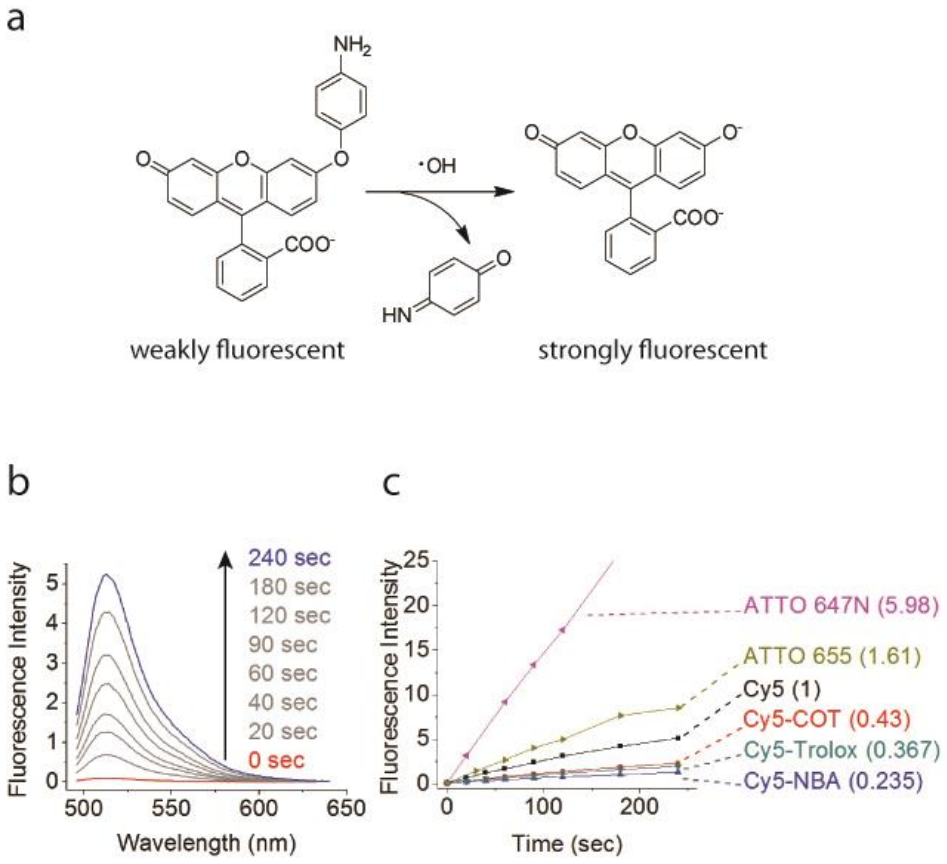

Figure 3.11. Generation of hydroxyl radical for Cy5 and its derivatives. (a) The mechanism of hydroxyl radical detection with APF. (b) The emission spectra of APF at different time points of the photo-illumination of Cy5. (c) The generation of hydroxyl radical, reported by the increase of APF fluorescence, upon illumination of Cy5, Cy5-COT, Cy5-NBA, Cy5-Trolox, ATTO 655, and ATTO 647N. In the parenthesis are the relative rates of hydroxyl radical generation.

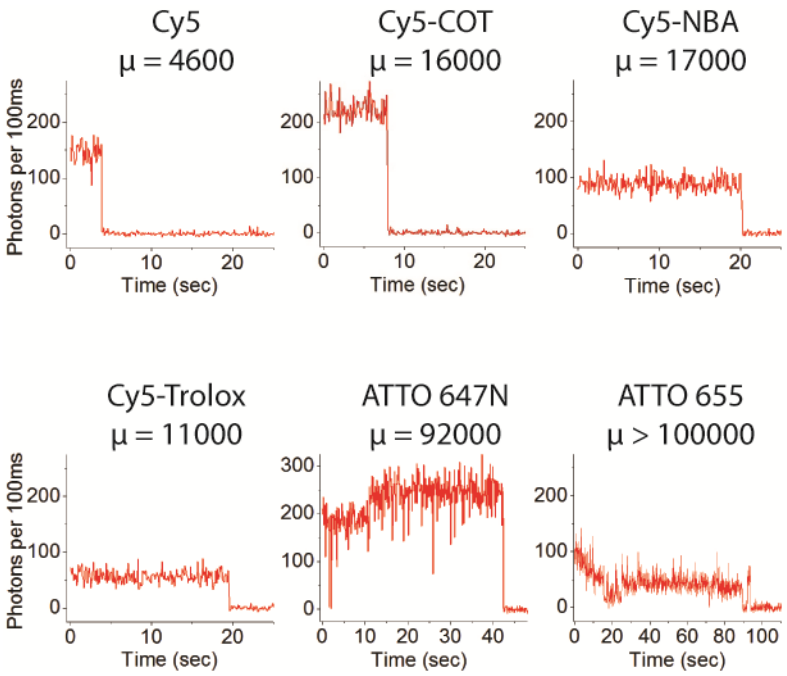

Figure 3.12. Representative single-molecule fluorescence traces for Cy5, Cy5-COT, Cy5-NBA, Cy5-Trolox, ATTO 647N, and ATTO 655. Fluorophores were covalently linked to DNA oligonucleotides and imaged in air-saturated aqueous solution using a total internal reflection microscope under continuous laser excitation (641 nm). μ is the average number of detected photons before fluorophore photobleaching.

fluorophores showed marked increases in fluorescein fluorescence (λ_{max}= 518 nm) as a function of illumination time (**Figure 3.11b**). Consistent with their reduced rates of singlet oxygen generation, the PA-conjugated fluorophores (Cy5-COT, Cy5-NBA and Cy5-Trolox) exhibited significantly reduced rates of hydroxyl radical generation (**Figure 3.11c**). These data provide supporting evidence that the Cy5-PA fluorophores may be less phototoxic than the Cy5, ATTO 647N, and ATTO 655.

To directly examine the performance of fluorophores in single-molecule fluorescence measurement in ambient oxygen conditions, each fluorophore was conjugated to a double-stranded DNA oligonucleotide and imaged under a total internal reflection fluorescence microscope [116]. Visual inspection of fluorescence traces from individual molecules revealed that most of ATTO 647N and ATTO 655 molecules showed substantial transient dark states and intensity fluctuations, while Cy5, Cy5-COT, Cy5-NBA, and Cy5-Trolox rarely blinked or fluctuated (**Figure 3.12**). By tracking the fluorescence of many single molecules (>1000) over time (**Figure 3.12**), the fluorescence intensity and the photobleaching rates were quantified. To compare each fluorophore's photobleaching rate, μ (the average numbers of photons detected from individual fluorophore prior to photobleaching) was calculated. As anticipated from prior investigations [116], the Cy5-COT, Cy5-NBA, and Cy5-Trolox fluorophores exhibited significantly reduced rates of photobleaching (**Table 3.2**), emitting up to 4-fold more photons than Cy5 prior to photobleaching (**Figure 3.12**). As previously reported [116], the COT-conjugated fluorophore displayed a roughly 30% increase in brightness relative to Cy5 (**Figure 3.12**). By contrast, both Cy5-NBA and Cy5-Trolox conjugates investigated here were substantially dimmer than Cy5 (~30% and 50%,

respectively; **Figure 3.12**), likely due to the electron transfer between the PA and Cy5 singlet excited state. The slow-photobleaching, non-blinking, and non-fluctuating properties of the Cy5 derivatives investigated here render them suitable for single-molecule quantitative measurements, such as fluorescence resonance energy transfer, anisotropy, and stoichiometry. By contrast, the fluctuating emission behaviors of ATTO 647N and ATTO 655 make them more suitable for single-molecule tracking.

In previous studies [72], we showed that Cy5-COT, but not Cy5-NBA and Cy5-Trolox, exhibits shortened triplet state lifetime compared to Cy5 (**Table 3.2**). However, our previous measurements were exclusively performed in acetonitrile. Here we have shown that each of the Cy5-PA fluorophores exhibit reductions in photobleaching rates and in ROS generation, implying that in aqueous solution Cy5-COT, Cy5-NBA, and Cy5-Trolox possess substantially shorter triplet state lifetime than Cy5. These data suggest that the effects of NBA and Trolox are strongly solvent-dependent: in aqueous solution they effectively quench the triplet state of Cy5, likely through an electron-transfer mechanism [120, 133], whereas in acetonitrile they do not quench the triplet state due to the solvent-dependent nature of the electron transfer where radical states form [62]. The rate of electron transfer is known to be affected by solvent polarity [134]. By contrast, COT can quench the Cy5 triplet state in both solvents because of the solvent-independent nature of triplet-triplet energy transfer [62, 72]. This mechanism is supported by a further comparison of fluorophore properties in aqueous solution and in acetonitrile: the fluorescent lifetime, the fluorescent quantum yield, the photobleaching rate and the singlet oxygen generation

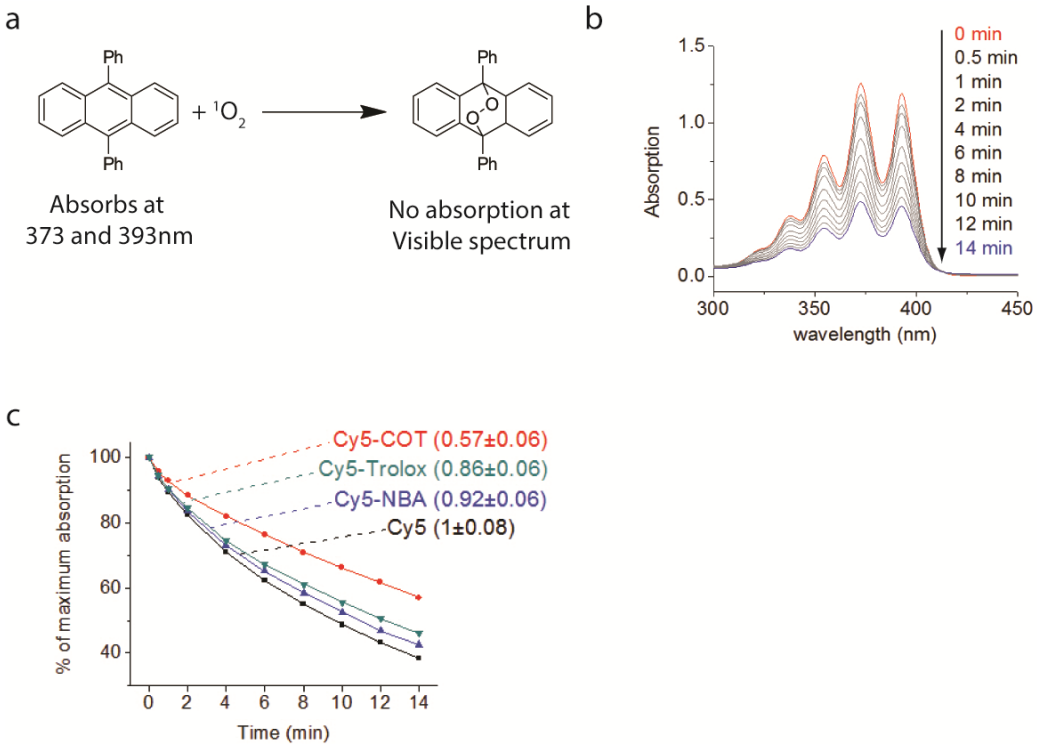

Figure 3.13. Reactivity to singlet oxygen for Cy5 and its derivatives. (a) The reaction of $^1O_2$ with 9,10-diphenylanthracene. (b) The spectrum of 9,10-diphenylanthracen absorption during photobleaching of Cy5 (5 µM) in acetonitrile. (c) In the parentheses are the relative rates of singlet oxygen generation reported by the decrease of absorption at 393nm.

rate for Cy5-NBA and Cy5-Trolox were strongly solvent-dependent, while these properties for Cy5 and Cy5-COT were only weakly solvent-dependent (**Table 3.2; Figure 3.13**).

3.6 Conclusion

In summary, we have observed that Cy5 derivatives containing covalently linked COT have significantly reduced Cy5 triplet lifetimes due to intramolecular energy transfer quenching, which regenerates the Cy5 fluorophore ground state. The triplet lifetimes correlate well with the photostability in single-molecule fluorescence experiments, where Cy5-COT(3), with the shortest triplet lifetime, showed the highest photostability. It also suggests that COT is a robust and potentially general agent that can be used to improve photostability of organic fluorophores especially when covalently linked in close proximity to the fluorogenic center. We further showed that self-healing fluorophores generate less ROS than conventional fluorophores do, suggesting they are less phototoxic.

4. Intramolecular triplet energy transfer is a general approach to improve fluorophore photostability

part of this chapter was previously published in modified form:

Roger B Altman, Qinsi Zheng, Zhou Zhou, Daniel S Terry, J David Warren and Scott C Blanchard, *Enhanced photostability of cyanine fluorophores across the visible spectrum.* Nature Methods (2012) 9, 428–429

4.1 Summary

Bright, long-lasting and non-phototoxic organic fluorophores are essential to the continued advancement of biological imaging. Traditional approaches towards achieving photostability, such as the removal of molecular oxygen and the use of small-molecule additives in solution, suffer from potentially toxic side effects, particularly in the context of living cells. The direct conjugation of small-molecule triplet state quenchers, such as cyclooctatetraene (COT), to organic fluorophores has the potential to bypass these issues by restoring reactive fluorophore triplet states to the ground state through intra-molecular triplet energy transfer. Such methods have enabled marked improvement in the photostability of Cy5. However, the generality of this strategy to chemically and structurally diverse fluorophore species has yet to be examined. Here, we show that the proximal linkage of COT increases the photon yield of a diverse range of organic fluorophores widely used in biological imaging applications, demonstrating that the intra-molecular triplet energy transfer mechanism is a potentially general approach for improving organic fluorophore performance and photostability.

4.2 Introduction

Single-molecule and super-resolution fluorescence imaging techniques have yielded unprecedented breakthroughs in a diverse range of biological systems and shed new light on cellular structure and organization[24, 135]. Such methods rely critically on the availability and performance of bright fluorescent probes spanning the visible and near infrared spectrum (400 – 800 nm) that exhibit high brightness and photostabilities. However, the inherent photo-chemical and photo-physical instabilities and related photo-toxicities of fluorescent species remain limiting features of most imaging applications[59, 60, 129, 136].

Fluorophore photo-instabilities, which manifest as intermittent dark states and irreversible photobleaching, compromise imaging duration, signal-to-noise ratios (SNR) and the spatial and temporal resolution that can be achieved[7, 8, 137]. Phototoxicity, which arises from the generation of reactive oxygen species through excitation of a fluorophore, can perturb the system under investigation[59, 60, 129]. Experimental control of these factors is particularly challenging in complex biological settings where the fluorophore's physical environment may be confined or changing over time. As a consequence of these limitations, many biological systems and questions remain beyond the reach of imaging methods that require the maximization of finite photon budgets or a minimization of time, such as single-molecule or super-resolution imaging[8, 18, 136]. Hence, a general approach to increase fluorophore photostability would enable these powerful imaging modalities to open new biological frontiers and have the potential impact of broadly advancing the boundaries of numerous fluorescence applications.

The most commonly employed strategies to improve organic fluorophore photostability require the removal of molecular oxygen.[88, 89] and the addition of small-molecule stabilizers, such as cyclooctatetraene (COT)[39], nitrobenzylalcohol (NBA)[102], Trolox (TX)[53, 138], and a combination of reducing and oxidizing chemicals (ROXS)[80]. While such methods have a proven capacity to increase fluorophore performance in a range of biological settings, they are restricted by their fluorophore-specific impacts, the solubility limits of extant stabilizers (ca. 1 mM), and their potential to exhibit biological toxicities[115], particularly in live-cells[31].

It has been recently shown that cyanine-class organic fluorophores can be intra-molecularly photostabilized by the covalent attachment of a single COT, NBA, or TX molecule in proximity of the fluorogenic center[72, 116, 117]. Mechanistic studies have since revealed that Trolox and NBA, like other small-molecules employed for ROXS[80], operate by redox chemistries on fluorophores trapped in relatively long-lived, non-fluorescent excited states[72, 120, 133, 139]. Such mechanisms, which necessarily entail the generation of charged intermediates, are strongly dependent on the fluorophores employed and the environment setting. Stabilizers operating *via* electron transfer also have the potential to quench singlet excited states[62], thus reducing fluorophore brightness by reducing their effective fluorescence quantum yield. By contrast, COT operates through a triplet-triplet energy transfer mechanism that recovers the fluorophore from triplet states without charge separation[72]. As most organic fluorophores that absorb in the visible spectrum have triplet state energies higher than that of COT, we hypothesized that the proximal attachment of COT may provide a potentially general approach to improve fluorophore photostability. Here, we show that

the proximal attachment of a single COT molecule improved the performance of a broad range of chemically distinct organic fluorophores, suggesting that intra-molecular triplet energy transfer is a potentially general strategy for improving organic fluorophore photostability.

4.3 Generality for Cyanine fluorophores across the visible spectrum

Our recent demonstration[116] that proximally linked 'protective' agents can yield substantial improvements in the performance of the cyanine fluorophore Cy5 motivated us to develop more photostable fluorophores spanning the visible spectrum. Such fluorophores would enable a broad range of applications and experimental demands. Here, using strategies identical to those previously described[116], we show that marked enhancements in performance can also be achieved for other widely used members of the cyanine class, Cy2, Cy3, Cy3.5, Cy5.5 and Cy7 (**Figure 4.1a**) when coupled to individual cyclooctatetraene (COT), nitrobenzyl alcohol (NBA) and Trolox molecules.

We quantified each fluorophore's performance (**Figure 4.1b**) using single-molecule fluorescence imaging techniques. This method gives access to a number of salient properties of individual fluorophores under continuous laser excitation including the apparent brightness of fluorescent states and the rates at which transient and permanent non-fluorescent states are entered ('blinking' and 'photobleaching',

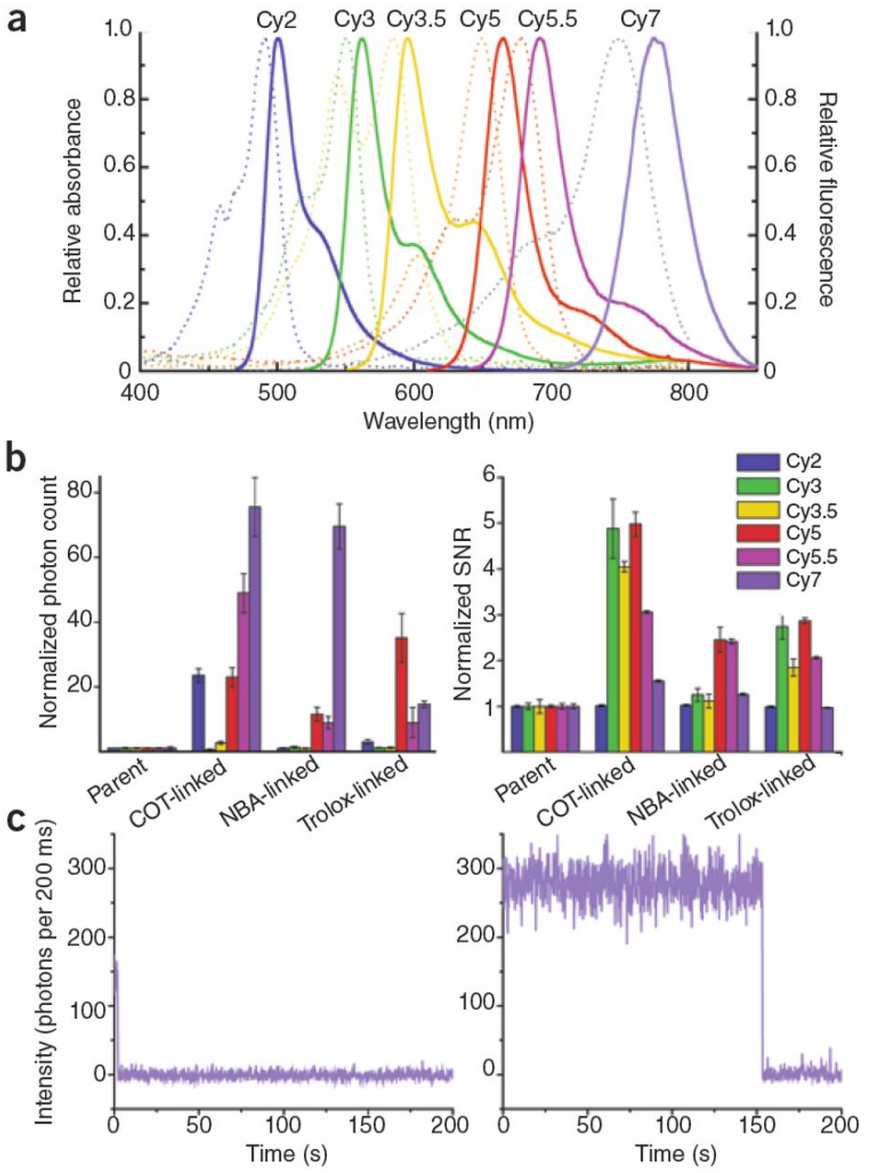

Figure 4.1. Enhanced photostability for Cy5 derivatives across the visible spectrum. (**a**) Absorbance (dotted lines) and fluorescence (solid lines) spectra of the cyanine-class fluorophores. (**b**) Average number of photons detected before the fluorophore entered dark states (left) and the average SNR of fluorescence, a measure of the variance in signal intensity over time (right), observed for the COT-, NBA- and Trolox-linked fluorophore derivatives of Cy2, Cy3, Cy3.5, Cy5, Cy5.5 and Cy7. All values were normalized to that of the corresponding parent compounds. Error bars, s.d. (n = 3 experiments). (**c**) Representative Cy7 (left) and Cy7-COT (right) single-molecule fluorescence traces showing the average enhancement in performance (~70-fold) observed for Cy7-COT relative to Cy7.

respectively). These measures can then be used to assess the average number of photons emitted by a fluorophore before entering a dark state (the duration of fluorescence (t_{on}) × mean fluorescence intensity) and the effective signal-to-noise ratio (SNR) of fluorescence, a parameter that reports on the variance in a flourophore's photon emission rate (**Figure 4.1b**). These data reveal that the performance of each cyanine-class fluorophore tested is enhanced when linked to single stabilizers. Notably, these positive effects varied substantially for each fluorophore type. For instance, each of the COT-linked fluorophores showed dramatic enhancements in overall performance. For Cy2-COT, we observed an ~25-fold increase in the number of photons emitted before a dark-state transition. For Cy3-COT and Cy3.5-COT, this parameter changed very little, but the SNR of fluorescence for both molecules increased approximately four- to fivefold. Cy5.5-COT and Cy7-COT showed 50- and 70-fold increases, respectively, in the number of photons emitted before entering a dark state. Consequently, the average Cy5.5-COT and Cy7-COT molecule could be continuously imaged for ~3 min at an SNR >7:1 (**Figure 4.1c**). Consistent with our previous work[116], we observed only modest improvements for most NBA-linked fluorophores. However, we observed an almost 70-fold enhancement of photon count for Cy7-NBA. Trolox, which shows the most favorable impact on the performance of the Cy5 fluorophore[116], also had relatively modest beneficial effects for the other cyanine-class fluorophores.

These data provide compelling evidence that the strategy of proximally linking stabilizers to the fluorogenic center to enhance its performance can be generalized. However, the high variability in a yield of benefits observed for the cyanine class suggests the need for a deeper understanding of how stabilizers provide

photostabilization. Plausible mechanisms for mediating enhancements in fluorophore performance include cycles of reduction and oxidation, triplet-triplet energy transfer and exciplex-type relaxation[62]. As suggested by Tinnefeld and Cordes[120], the enhancements in performance of Trolox-linked fluorophores may arise through favorable reduction-oxidation cycles with the fluorogenic center. However, the results we obtained suggest that the benefits of such a mechanism may be restricted to the Cy5 and Cy5.5 fluorophores, which perhaps reflects an appropriate matching of their redox potentials. By contrast, we observed more substantial and general enhancements for each of the COT-linked cyanine fluorophores. Given the estimated triplet energy and redox potential of COT (unpublished data) and COT's propensity for triplet-triplet energy transfer[70], these findings suggest that a triplet-triplet energy transfer mechanism may be the most generally effective means for cyanine fluorophore photostabilization. Forward progress toward quantifying the relative weights and impacts of each pathway for distinct fluorophores will enable additional improvements in the activities of these known stabilizers. Insights of this kind may also aid the discovery of new compounds and the implementation of new strategies to meet the specific demands of distinct fluorophore types. Ultimately, continued efforts on these fronts may yield strategies that can be generalized for tailoring fluorophore performance for a broad array of distinct experimental demands.

4.4 Generality for fluorophores in different structural categories

Spontaneous energy transfer can occur when the excited-state energy of a stabilizer is lower than that of a fluorophore[62]. COT’s reported triplet state energy of approximately 92 kJ/mol[112, 113, 140] is substantially lower than the triplet state

energies of most commonly used organic fluorophores employed for biological imaging applications (*ca.* 100-200 kJ/mol[62]). Importantly, the energy of COT's first singlet excited state (S_1, >400 kJ/mol) is markedly higher than the S_1 energy of organic fluorophores (ca. 150-300 kJ/mol)[113]. Thus, COT imparts little to no impact on fluorophore brightness. These characteristics render COT a promising, general triplet state quencher candidate for improving the performance of organic fluorophores commonly used in biological imaging applications. Based on this rationale, and direct evidence that COT mediates intramolecular photostabilization for certain cyanine dyes spanning the visible spectrum[117], we examined whether COT can mediate intramolecular photostabilization of the following chemically and structurally diverse organic fluorophores: Cyanines (Cy3B, Cy5, DY654); Carbopyronines (ATTO647N); Oxazines (ATTO655); Rhodamines (TMR, ATTO565, Alexa633, Alexa568); and Fluoresceins (fluorescein) (**Figure 4.2**).

In order to enforce the proximity of COT to each of these fluorophore species, while bypassing fluorophore-specific synthesis challenges and potentially negative impacts on fluorophore solubility, N-hydroxysuccinimide (NHS)-activated COT and fluorophore molecule were linked to the 3'- and 5'-ends, respectively, of complementary strands of a short, double-stranded DNA oligonucleotides 21-base pairs in length (**Scheme 4.1**). Thus positioned, collisional interactions are expected to occur with a high frequency[116]. The performance of each fluorophore was examined in this context at the single-

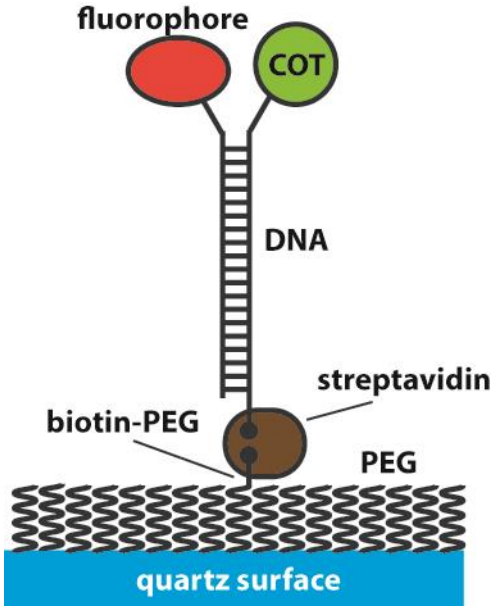

Scheme 4.1. Assembly of fluorophores on quartz surfaces in close proximity to COT using DNA base pairing and biotin-streptavidin binding.

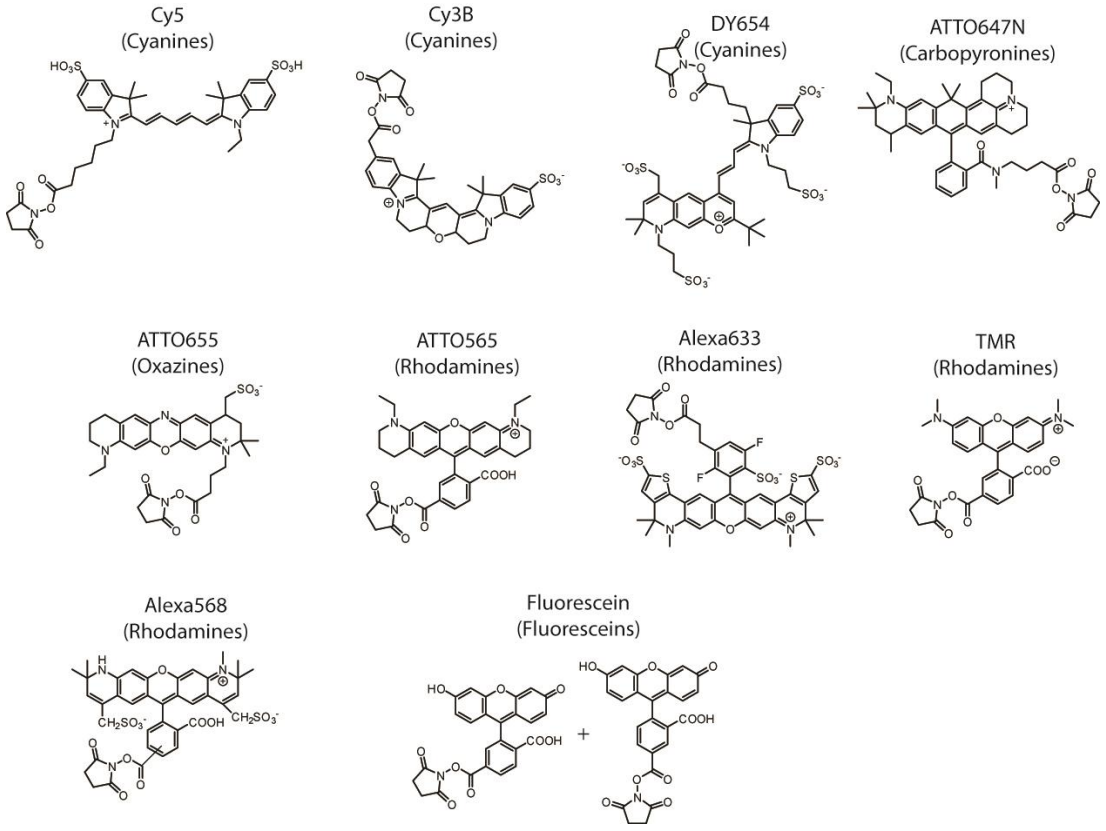

Figure 4.2. Chemical structures of the fluorophores used in this study.

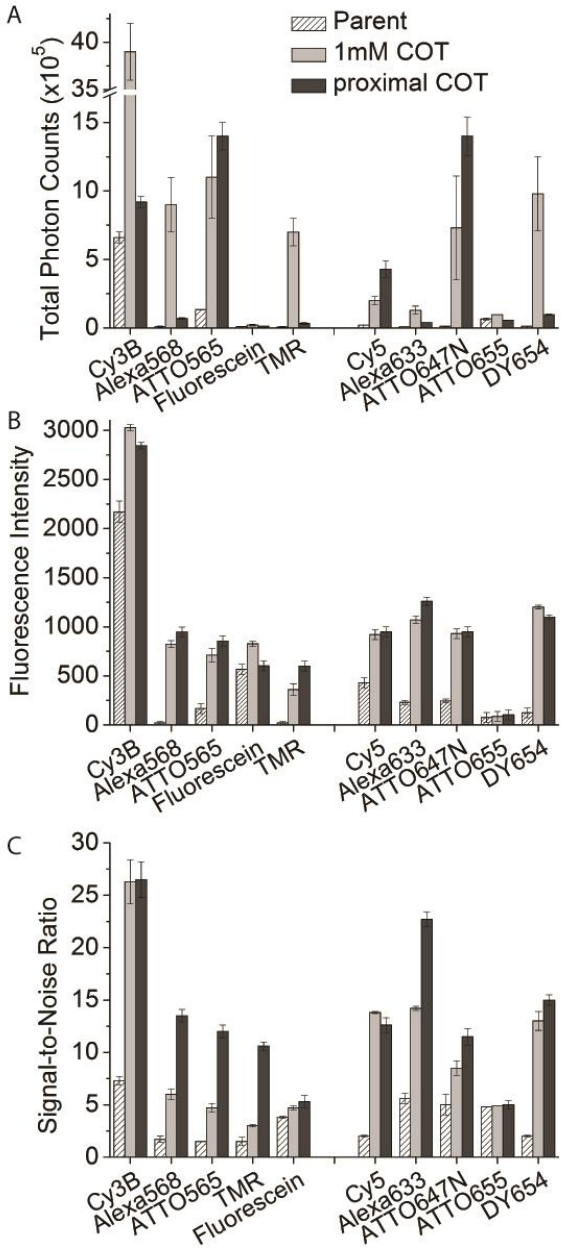

Figure 4.3. Enhanced photostablity for fluorophores at different structural categories. (A) Total photon counts, (B) number of photons detected from individual fluorophores per unit time (Brightness), and (C) signal-to-noise ratio of different fluorophores in deoxygenated buffer (hatch bars), in deoxygenated buffer with 1mM COT (grey bars), or in deoxygenated buffer with a single proximal COT (black bars). Error bars indicate standard deviation of three measurements.

molecule scale by tethering the opposite end of the DNA duplex to a passivated-quartz, microfluidic device *via* a biotin-streptavidin interaction such that fluorophore excitation and emission performance could be examined under solution conditions using a prism-based, wide-field total-internal-reflection fluorescence (TIRF) microscope[116].

Absolute and comparative fluorophore performance evaluations were based on the number of photons detected from individual fluorophores per unit time (brightness), the variance in the fluorescence signal detected (SNR = (average of fluorescence intensity)/(standard deviation of fluorescence intensity)) as well as the total number of photon detected (photon counts) prior to photo-induced degradation and signal loss (**Figure 4.3**). Each fluorophore was also examined in the same context without proximally attached COT and with 1 mM COT in solution. All experiments were performed in a buffered saline solution (50 mM Tris-Acetate, 50 mM KCl) supplemented with an enzymatic oxygen scavenging system (see Chapter 2 for methods) to remove oxygen from the buffer.

To quantify the effectiveness of the proximal COT molecule in this context, we benchmarked its impact for specific cyanine fluorophores, where beneficial impacts have been previously documented[72, 116, 117]. As anticipated from these investigations, the photostability of both Cy5 and Cy3B were significantly improved. The Cy5 fluorophore exhibited a 50-fold increase in total photon count, a 2-fold increase in brightness, and a 2.5-fold increase in SNR. As expected, these effects were more pronounced than when 1 mM COT was present in solution (**Figure 4.3**)[102, 117]. The impact of proximally linked

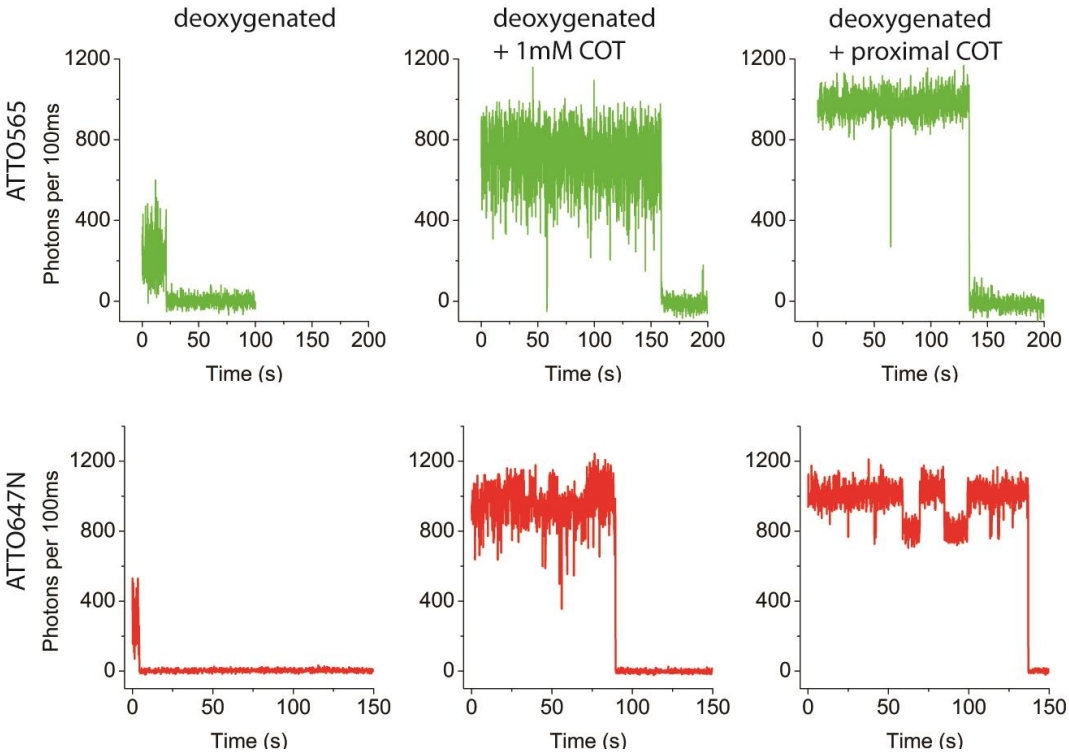

Figure 4.4. Representative single-molecule fluorescence traces for ATTO565 and ATTO647N. Each fluorophores were imaged in deoxygenated buffer, in deoxygenated buffer with 1mM COT, or in deoxygenated buffer with proximal COT.

COT was significant, albeit less pronounced, for Cy3B (~4 fold increase in SNR and 20% increase in brightness and photon counts), whereas Cy3B was strongly photostabilized (~6-fold increase in photon counts) with 1 mM COT in solution (**Figure 4.3**). Analogous impacts were observed for DY654, also a cyanine-class fluorophore. The reason why Cy3B and DY654 are less responsive to proximally linked COT is not presently clear. We speculate, however, that this observation may relate to differences in the probability of effective collisions between COT and the Cy3B/DY654 fluorophore when proximally conjugated.

We next tested the impact of proximally linked COT for representative fluorophores of distinct structural families. Here, we observed that the photostability of each of the fluorophores examined, with the exception of ATTO655 and fluorescein, was enhanced by a proximally linked COT molecule (**Figure 4.3**). For ATTO647N, a fluorophore widely used for single-molecule and super-resolution measurements[141-144], proximal COT provided a 120-fold increase in photon count, a 4-fold increase in brightness, and a 2.5-fold increase in SNR (**Figure 4.3** and **4.4**). A substantial, albeit relatively modest impact, was also observed with COT in solution (Figure 4.3 and 4.4). Analogous impacts were observed for ATTO565 (**Figure 4.3** and **4.4**). The proximally linked COT molecule also improved the photostability of Alexa568, Alexa633, and TMR. Here, the impacts were, however, more modest in nature, exhibiting ~4-8 fold increases in photon counts and in SNRs. These specific fluorophores exhibited more pronounced increases in photostability when 1 mM COT was present in solution (**Figure 4.3**).

We therefore conclude that the photostability of most organic fluorophores can be markedly improved by a single, proximally linked COT molecule and that the precise extent of the observed enhancement varies dramatically for each fluorophore species. These fluorophore-specific distinctions may be attributed to differences in triplet energy transfer rate and/or differences in the competing photochemical processes, such as redox reactions from the triplet excited states. Under the conditions of the present experiments, redox partners include an enzymatic oxygen scavenging system as well as the oligonucleotides to which the fluorophore is attached. To investigate why COT exhibited distinct impacts on fluorophore photostabilities when proximally linked in a manner such that relatively uniform collision frequencies are enforced, the redox potentials of each fluorophore were measured using cyclic voltammetry[145]. Here, we hypothesized that a fluorophore's responsiveness to COT reflects differences in the rates of competing chemical pathways that generate radical fluorophore species which COT is unable to rescue. According to the Marcus theory, the rate of electron transfer in the normal region increases with the thermodynamic driving force of the reaction[146]. Here, the responsiveness of a fluorophore to COT is expected to be lowered when the rate of gaining or losing electrons shortens the triplet state lifetime[137, 147] such that redox reactions are faster than the rate of triplet energy transfer with COT.

The reduction potentials of the triplet state for each fluorophore were estimated using the Rehm-Weller equation: $E_{red}^{T} = eE_{red}^{0} + E_T + C$, where E_{red}^{0} is the first one-electron reduction potential of the ground state obtained by cyclic voltammetry (**Figure 4.5, Table 4.1**), E_T is the triplet state energy of the fluorophore obtained by phosphorescence (**Figure 4.6, Table 4.1**), and e is the unit charge[62]. In aqueous solutions, the columbic

attraction energy *C* can be neglected due to the high polarity of water[62]. Consistent with the notion that fast electron transfer between the triplet fluorophore and its environment competes with triplet energy transfer to COT, both fluorescein and ATTO655, the two fluorophores for which COT had a negligible impact, exhibited the highest E_{red}^{T} (**Table 1**). By contrast, the fluorophores improved by COT tended to exhibit lower E_{red}^{T}, consistent with the notion that a fluorophore's responsiveness to COT-mediated intra-molecular triplet state quenching is determined by the rates of competing redox reactions from the triplet state. The absence of direct correlations between E_{red}^{T} and COT responsiveness is not presently known but may relate to other factors affecting the rates of charge transfer, such as the frequency of productive collisions between the fluorophore and COT, as well as the reorganization energies in these structurally distinct fluorophores[146].

4.5 Conclusion

The present observations demonstrate that photostabilization through intra-molecular triplet energy transfer is a potentially general approach for improving the experimental performance of organic fluorophores of various structures in biological settings. We observe, however, that the effectiveness of this approach is strongly dependent on the nature of the fluorophore. Our data suggest that competing electron transfer processes, which are highly fluorophore specific,

Table 4.1. Triplet state energy, reduction potential from the ground state, and reduction potential from the triplet state for the fluorophores. DY654 and Alexa568 do not show measurable reduction peak in cyclic voltammetry measurement.
* phosphorescence of ATTO655 was not detectable. The E_T of ATTO655 is estimated to be 0.2 eV lower than the energy of the first singlet excited state (1.81 eV)

Fluorophore	TMR	ATTO647N	Cy5	Cy3B	Alexa633	ATTO565	Fluore-scein	ATTO655
E_T (eV)	1.72	1.46	1.48	1.66	1.55	1.72	1.98	1.6*
E_{red}^0 (V vs Ag/Ag+)	-1.58	-1.23	-1.24	-1.40	-1.175	-1.25	-1.40	-0.635
E_{red}^T (eV)	0.14	0.23	0.24	0.26	0.38	0.47	0.58	1.0

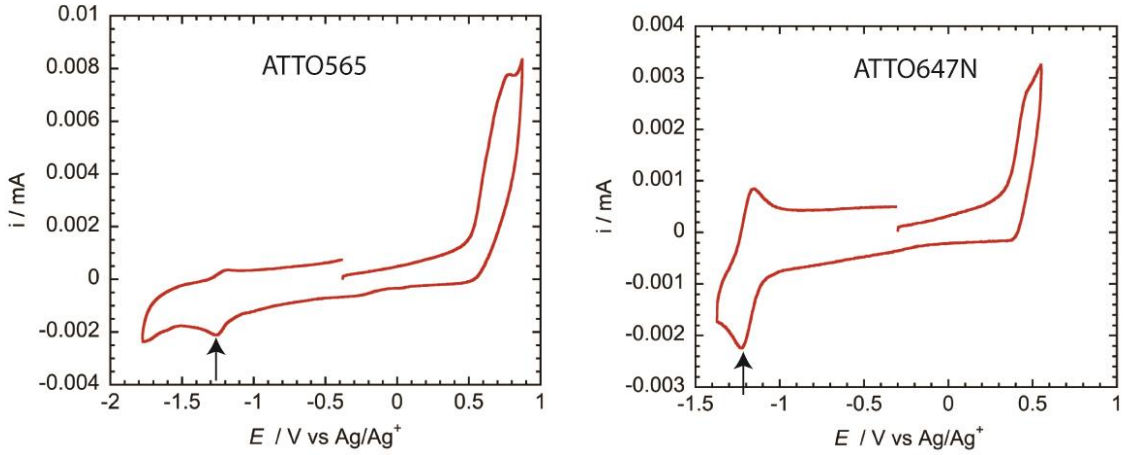

Figure 4.5. Representative cyclic voltammograms for ATTO565 (left) and ATTO647N (right). The reduction peak potentials are indicated by the arrows.

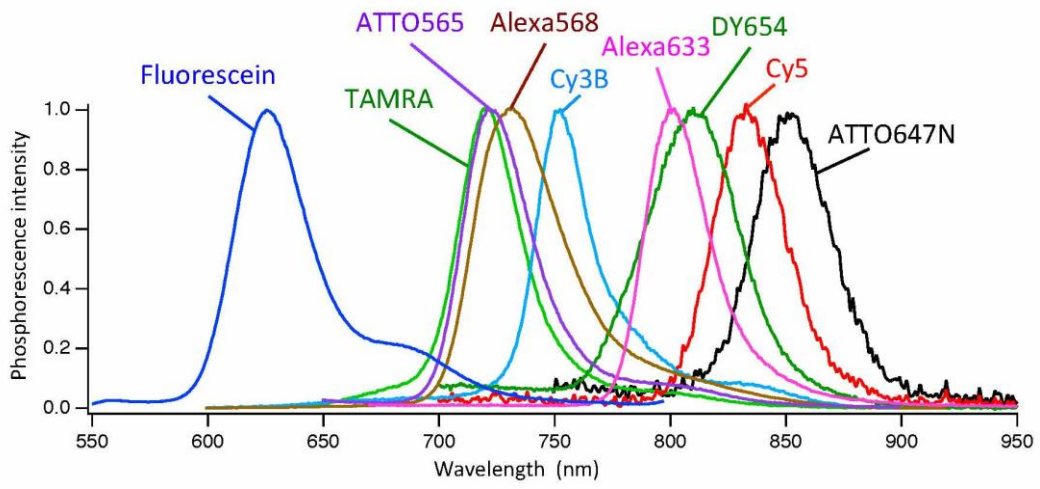

Figure 4.6. Phosphorescence spectra of the fluorophores. Fluorophores were in ethanol/iodomethane glass (2:1, v/v) at 77 K with excitation at 473 nm (fluorescein), 532 nm (TAMRA, ATTO565, Alexa568, Cy3B) or 633 (Alexa633, DY654, Cy5, ATTO647N). The wavelengths of each phosphorescence maxima were converted to the triplet state energy (E_T) of the fluorophores.

may be the explanation for the observed differences in effectiveness. To obtain increased photostability, the relative rates of intra-molecular triplet energy transfer need to be substantially faster than the rates of electron transfer from/to the triplet state of the fluorophore. The rate of intra-molecular triplet energy transfer when sufficiently rapid has the potential to shield the fluorophore from redox damage even in the presence of highly reactive species such as molecular oxygen, which is present at nearly millimolar concentrations in aqueous solutions. These observations rationalize future efforts aimed at developing general synthetic strategies for linking COT, or other compounds capable of intra-molecular triplet energy transfer, directly to a range of organic fluorophores where their performance can be examined in diverse imaging contexts. For example, a fluorophore may be first coupled to an "adapter molecule" where a COT is covalently linked, before being labelled to the biomolecule of interest. Here it will be particularly impactful to examine whether such methods can be extended to organic fluorophore species commonly employed for live-cell imaging, such as TMR and the near-IR emitting silicon-rhodamine (SiR)[136, 148, 149], where fluorophore performance in complex cellular milieus are particularly demanding and prone to exhibit undesirable phototoxicities.

5. Self-healing fluorophores improve cellular imaging at single-molecule scale

5.1 Summary

Despite the demonstrated enhanced photostability of *in vitro* conditions with purified components, it remains an open question that whether self-healing fluorophores exhibit enhanced photostability in a more complex environments. Here we showed similar improvement of photostability in fixed cells and in living cells, which is better than parent fluorophores with stabilizers in solution. These data demonstrate that self-healing fluorophores can extend the temporal scale of cellular imaging, in bulk as well as at single-molecule scale.

5.2 Introduction

The data in previous chapter have shown that self-healing fluorophores exhibit increased photostability through shortening the fluorophore triplet state, and that the linkage to cyclooctatetraene (COT) is a general approach to improve fluorophore photostability for organic fluorophore across the spectrum and in different structural categories. Despite the demonstrated enhanced photostability of *in vitro* conditions with purified components, it remains an open question that whether self-healing fluorophores exhibit enhanced photostability in a more complex environments.

Fluorescence imaging enables specific, non-invasive, and quantitative measurements of biological process in living cells and *in vivo*. Various methods of advanced fluorescence microscopy, including single-molecule[24] and super-resolution[150]

microscopy, have the potential to reveal cellular processes at unprecedented spatiotemporal resolution, but their application has been limited by a number of factors, including the limited photostability of fluorophores[8, 136]. Here we aim to address this limitation by applying self-healing fluorophores with improved photostability for cellular fluorescence imaging at single-molecule scale.

In collaboration with Prof. Jonathan Javitch at Columbia University, we select the dimerization of G-protein Coupling Receptors (GPCR) as a model system to characterize the fluorophore performance in living cells. Receptor dimerization is typically the first step of the induction of intracellular signaling after ligand binding, and is fairly common for the GPCR super family[151]. Despite this importance, the dimerization of GPCR has not been directly measured at its native environment at single-molecule resolution. Here we use single-molecule Förster Resonance Energy Transfer (smFRET)[152] to characterize the dimerization of GPCR.

5.3 Result and Discussion

To specifically label the fluorophore to the targeted protein, we use SNAP tag, a self-labelling protein tags [153] (See chapter 2 for the details of experimental methods). SNAP was first fused with the targeted protein. After protein expression, the benzylguanine (BG)- derivatives of the fluorophores were incubated with the cells. SNAP catalyzes the ligation of fluorophore to the Cysteine at its active site, with BG as a leaving group. After washing off the free dyes, cells were put on the coverslip and imaged under the microscopy. Here we used the objective-based total-internal-reflection fluorescence (TIRF) microscopy to measure the labeled membrane proteins.

To benchmark the fluorophore performance, we fused SNAP tag to the N-terminus (extracellular end) of mGlu2, a GPCR that forms constitutive dimer.

smFRET measurement requires two fluorophores, one donor and one acceptor, with high brightness and high photostability. In addition, fast labelling and low-nonspecific binding are required for live-cell imaging. We first select commercial-available fluorophores that fulfil these requirements. Several fluorophores (e.g. ATTO647N) exhibit high brightness and photostability but have high background due to non-specific binding, and therefore are not suitable for live-cell imaging [154]. Based on the data collected by Dr. Wesley Asher and Dr. Peter Geggier at the laboratory of Prof. Jonanthan Javitch as well as others [154], we chose DY549 and Alexa647 as the donor and acceptor, respectively, that are most suitable for this measurement.

Next, we applied the self-healing fluorophores for the same measurement and compare with the DY549-Alexa647 dye pairs. To test the non-specific binding to living cells, we expressed the mGlu2 proteins without fused to SNAP tag (mock cells) and use the same labelling protocol. with the First generation self-healing fluorophores containing two sulfonate groups[137] exhibit high non-specific binding to the cellular membrane (**Figure 5.1.B**), which is probably due to the hydrophobicity of the fluorophore. Indeed, elution time in reverse-phase HPLC C18 column with an aqueous mobile phase shows that these fluorophores (Cy3-2S-COT(N3) and Cy5-2S-COT(N3)) is more hydrophobic than the DY549 and Alexa647. Other fluorophores with high non-specific binding to living cells, such as ATTO647N and Cy3B, also exhibit large elution time (i.e. high hydrophobicity). Therefore, elution time in the C18

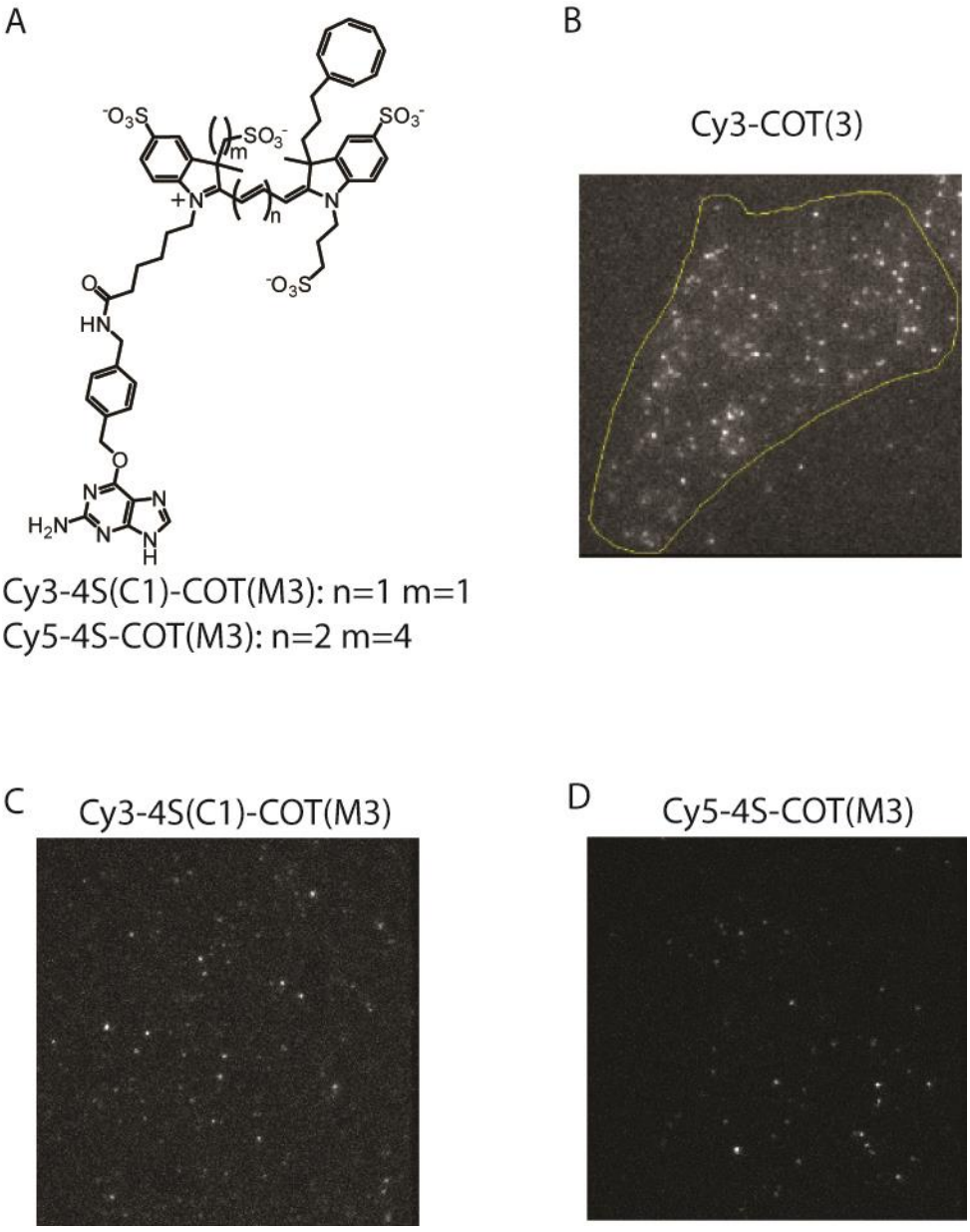

Figure 5.1. Non-specific binding of self-healing fluorophores. (A) The structures of Cy3-4S(C1)-COT(M3) and Cy5-4S-COT(M3) fluorophores. The non-specific binding of (B) Cy3-4S(C1)-COT(M3) , and Cy5-4S-COT(M3) to Mock cells. Each image contains one cell.

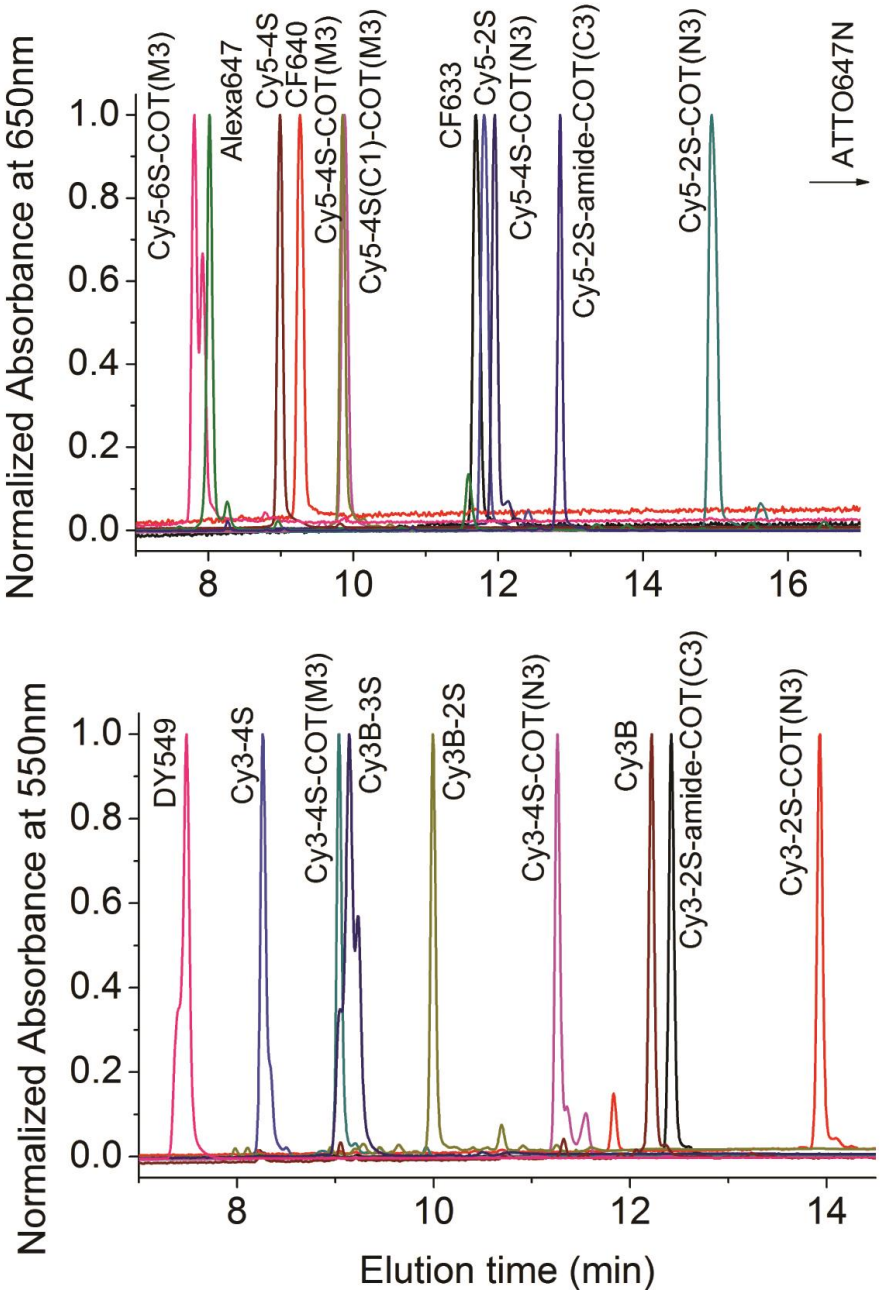

Figure 5.2. Comparison of aqueous solubility for self-healing fluorophores and common organic fluorophores. Fluorophores are benchmarked for aqueous solubility by comparing their relative elution times using reverse-phase HPLC with an aqueous mobile phase.

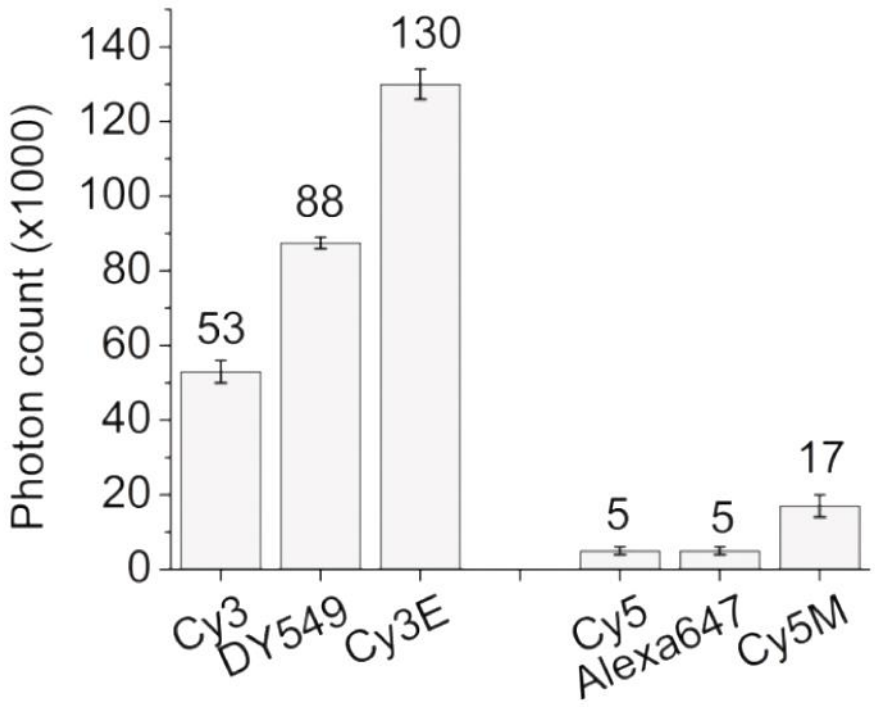

Figure 5.3. Photon counts of fluorophores labeled on SNAP tag. All measurements were performed in buffer with ambient oxygen. Cy3, DY549, and Cy3-4S(C1)-COT(M3) (Cy3E) were illuminated with a 532 nm laser at 150W/cm^2. Cy5, Alexa647, and Cy5-4S-COT(M3) (Cy5M) were illuminated with a 639 nm laser at 100W/cm^2.

Table 5.1. Photobleaching time (sec) of single-molecule FRET (smFRET) measurement at fixed cells. Two dyes pairs were labeled to mGlu2-SNAP fusion protein and the cells were fixed before smFRET measurements at different conditions. The concentration of stabilizers was 1mM COT:cyclooctatetraene; NBA: 4-nitrobenzyl alcohol; MV: methyl viologen; AA: ascorbic acid.

	DY549 and Alexa647	Cy3-4S(C1)-COT(M3) and Cy5-4S-COT(M3)
50% O_2	10	35
0% O_2	7	100
0% O_2+COT	8	
0% O_2+COT, NBA, Trolox	37	
0% O_2+MV, AA	55	

column provides a simple assay for fluorophore hydrophobicity and non-specific binding to living cells.

To reduce the hydrophobicity of the self-healing fluorophores, we first introduce two more sulfonate groups to the fluorophores (Cy5-4S-COT(N3) and Cy3-4S-COT(N3)). They exhibit reduced hydrophobicity, but still higher than the Alexa647 and DY549. We then distribute the sulfonate groups evenly around the fluorophore, which leads to the synthesis of fluorophore Cy3-4S(C1)-COT(M3) and Cy5-4S-COT(M3) (**Figure 5.1.A**). These two fluorophores have further smaller retention time than the previous self-healing fluorophores (albeit still higher than DY549 and Alexa647) (**Figure 5.2**), and low non-specific binding to the mock cells (**Figure 5.1.C** and **D**), with which we can specifically labeled the extracellular targets. We next labeled these fluorophore to purified SNAP protein and characterized their photostability *in vitro* with ambient oxygen. Like other self-healing fluorophores, they exhibited higher photostability than the parent fluorophores (Cy3 and Cy5, respectively) as well as DY549 (by 50%) and Alexa647 (by 240%), the two commercial available fluorophores selected for smFRET imaging (**Figure 5.3**).

To benchmark the fluorophore photostability in cellular context, we performed smFRET measurement for the two dye pairs (DY549 and Alexa647, as well as Cy3-4S(C1)-COT(M3) and Cy5-4S-COT(M3)) at various conditions and recorded the measurement time before one the fluorophore photobleaches (photobleaching time) (**Table 5.1**). The conditions include imaging buffer with 50% or 0% of saturated oxygen, as well as with stabilizers in solution. To simplify the measurement and data analysis, we performed these experiments on fixed cells where fluorophore is immobile.

Similar to the performance in vitro with ambient oxygen, in 50% oxygen self-healing dye pairs exhibited 250% improvement of smFRET photobleaching time compared to DY549-Alexa647 dye pairs (Table 5.1). In fully deoxygenated buffer, the photobleaching time of self-healing dye pairs further increase to 100 sec, much higher than DY549-Alexa647 in the same condition, or even with different kinds of stabilizers in solution (Table 5.1). With data demonstrate that self-healing fluorophores possessing improved photostability extend the temporal scale of cellular imaging.

We next performed live-cell smFRET. Consistent with the *in vitro* and fixed-cell data, in 50% oxygen the self-healing dye pairs also exhibit 150% improvement of photostability compared to the DY549-Alexa647 dye pairs. It worth noting that fully deoxygenation of imaging buffer, which is widely used for *in vitro* measurements, introduce significant perturbation and artifacts to the studied system. **Figure 5.5** illustrated the representative images of cells labeled with fluorophores incubated with deoxygenated buffer for 0 hour (up) or 1 hour (down). 1 hour incubation in deoxygenated buffer leads to the absence of dye-labeled membrane receptor and severe cellular autofluorescence, probably due to the internalization of membrane receptor. This phenomenon is not observed for cells incubated in buffer with 50% saturated oxygen, and is consistent with the fact that deoxygenation can perturbed many fundamental cellular processes.

4.5 Conclusion

Consistent with the enhanced photostability *in vitro*, these data demonstrated that self-healing fluorophores exhibit similarly enhanced photostability in the cellular context. Self-healing fluorophores show higher photostability than conventional

fluorophore in different buffer conditions, including with ambient oxygen, with partially or fully deoxygenation, and with stabilizer in solution. Moreover, we found that prolong incubation in fully deoxygenated buffer leads to severe imaging artifacts, suggesting that deoxygenation, a photoprotection method widely used for i*n vitro* advanced imaging, may be problematic for live-cell imaging.

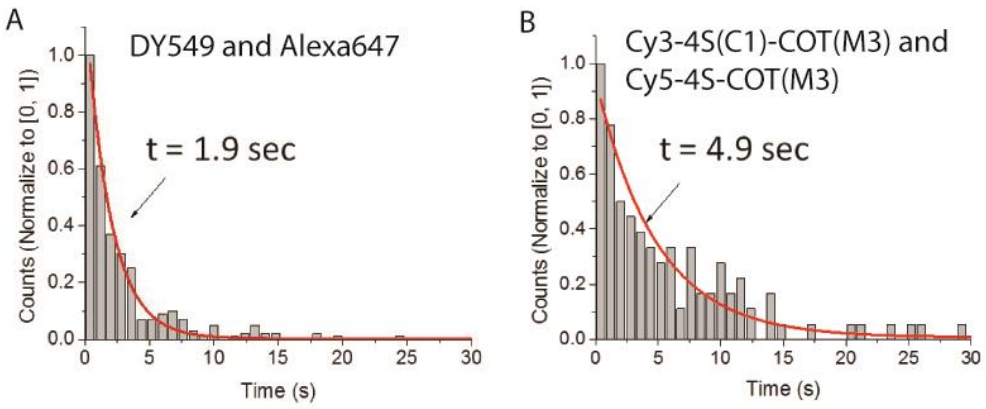

Figure 5.4. Measurement time of live-cell single-molecule FRET for self-healing fluorophores. (A) DY549 and Alexa647, and (B) Cy3-4S(C1)-COT(M3) and Cy5-4S-COT(M3). The sample was illuminated with 1.5 mW 532 nm laser.

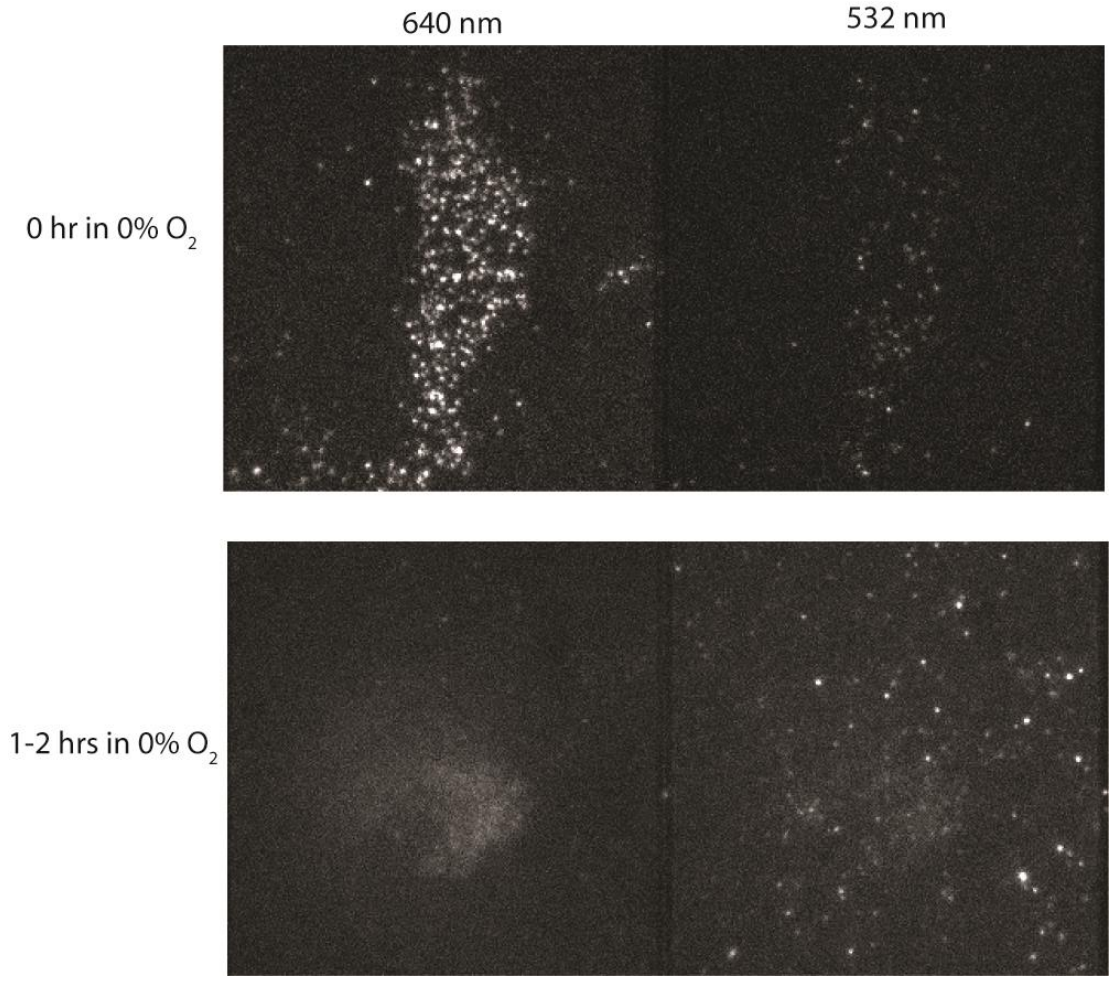

Figure 5.5. Representative images of Cy3-4S(C1)-COT(M3) and Cy5-4S-COT(M3) labeled cells that have spent (up) 0 hour or (down) 1 hours in deoxygenated buffer. Excitation wavelengths are 640nm (left) or 532 nm (right).

6. Understanding the design principles of self-healing fluorophores to improve biological imaging

6.1 Summary

Bright, long-lasting organic fluorophores are essential to address shortcomings in performance that currently limit a broad range of imaging applications. While the depletion of oxygen and the addition of stabilizers improve fluorophore photostability by quenching photo-induced reactive triplet state and radical species, such strategies suffer from potential toxicities that restrict the utility in biological settings. "Self-healing" fluorophores, which bear one or more intra-molecularly linked stabilizers, offer a powerful means of addressing both the need for enhanced fluorophore performance and biological compatibility. Although the existing self-healing fluorophores exhibits significant improvements in photostability, their performance is still far from the predicted potential of the self-healing mechanism, especially in physiologically-relevant conditions (e.g. with ambient oxygen). To guide the development of self-healing fluorophores with superior photostability, we have synthesized a series of Cy5 derivatives in which the stabilizer cyclooctatetraene (COT) is covalently attached *via* polymethylene linkers of defined lengths, and examined the relationship between the rate of intramolecular triplet energy transfer and fluorophore performance. Our data reveal key limitations of the self-healing mechanism encompassed in existing technologies, including the instability of the stabilizer itself. Exploiting this understanding, we modified COT to reduce its reactivity and demonstrated a 3-fold increase in photostability for Cy3 and nearly 10-fold for Cy5 in

ambient oxygen conditions. This is not attainable with existing photo-protection approaches and offers a new generalizable strategy to rationally engineer the self-healing mechanism to maximize the full potential of organic fluorophores commonly employed in biomedical imaging.

6.2 Introduction

Fluorescence microscopy continues to witness revolutionary advancements in both sensitivity and resolution, progress that is highlighted by the development of single-molecule and super-resolution fluorescence imaging methods[24, 150]. Fast fluorophore photobleaching (photo-induced degradation) currently limits further developments in this area as the quality and duration of the experimental signals are proportional to the total number of photons emitted and detected[8, 136, 137, 155, 156]. Photo-protection strategies that mitigate fluorophore photobleaching are therefore in high demand[8, 137, 155].

The most common photo-protection strategies employed involves the removal of molecular oxygen[88, 89] and the addition of small-molecule stabilizers, such as Trolox[53, 138], nitrobenzylalcohol (NBA)[102], and cyclooctatetraene (COT)[39], to solution[8]. While such have a proven capacity to increase fluorophore performance in a range of biological settings, the utility of current photo-protection strategies is restricted by the perturbation of oxygen depletion, the solubility limit of stabilizers (ca. 1 mM), and their potential biological toxicities[115], particularly in live-cell contexts[31, 136].

To circumnavigate the limitations of current photo-protection strategies, we have set out to engineer a modified class of probes wherein specific stabilizers are covalently

linked to organic fluorophores, e.g. Cy5. In such "self-healing" fluorophores, reactive, photo-induced fluorophore triplet and radical states are intra-molecularly quenched to reduce the probability of chemical degradation[72, 120, 133]. This approach has been shown to reduce the duration of reactive triplet states and lower the rate of photobleaching by as much as 100 fold in deoxygenated solutions, and 4 fold in the presence of ambient oxygen[116, 117, 137, 157]. The utility of intra-molecularly photostablized fluorophores has already been demonstrated both *in vitro* and in living cells[116, 158, 159].

The self-healing strategy is grounded in the principles of intra-molecular chemical reactions, which posit that the covalent attachment of stabilizers to the fluorophore will increase their effective concentration by up to ten orders of magnitude (ca. 10^7 M) beyond their aqueous solubility limit[160, 161]. Such increases should, in principle, lead to reductions in triplet state lifetime that would effectively render fluorophores inert to photo-induced reactions involving molecular oxygen[137, 162]. However, the effective concentrations of stabilizers (c.a. 1-100mM, see section 6.2.1) for current self-healing fluorophores are still far lower than 10^7 M, with only a modest increase of photostability in the presence of oxygen, a condition required for many biological and cellular functions. Here we present a plausible mechanism that limits further improvement of the current self-healing fluorophores. Exploiting this understanding, we identify design principles for self-healing fluorophores, and improve the photostability of Cy5 by nearly 10 fold in ambient oxygen conditions through reducing the reactivity of the stabilizer COT. We further show that this approach can be generalized to fluorophores across the visible spectrum.

6.2.1 Calculating the effective concentration of stabilizers for "Self-healing" fluorophores

The effective concentrations of stabilizer in self-healing fluorophores were calculated by dividing the rate of the intramolecular reaction (k_{intra}) with the bimolecular rate of intermolecular reaction (k_{inter})[163]. For intramolecular triplet energy transfer, $k_{intra} = 1/\tau_T$, which ~10^6 sec^{-1}. The k_{inter} for triplet energy transfer from an organic molecule to COT is 10^7 - 10^9 $s^{-1}M^{-1}$[70, 140, 164]. Therfore, the effective concentration for COT is k_{intra}/ k_{inter} = 1 – 100 mM.

6.3 The lifetime of the Cy5-COT(n) triplet state correlates with linker lengths

Analogous to earlier intra-molecular triplet energy transfer investigations performed on model systems[160, 165], we set out to synthesize a series of Cy5-COT fluorophores in which COT was covalently attached to the Cy5 fluorogenic center *via* defined-length polymethylene linkers (Cy5-COT(n)), where the number (n) of carbon atoms separating the COT and the Cy5 fluorophore is 1, 2, 3, 4, 5, or 10 (**Chart 6.1**). Using these model compounds, we have examined the relationship between each fluorophore's triplet state lifetime and their observed photostability both in ambient oxygen and in deoxygenated solutions.

In previous work[72], we employed laser flash photolysis to characterize the triplet state lifetime (τ_T) of Cy5 (^{3}Cy5*) using benzophenone (BP) as a sensitizer. Upon excitation with a 355 nm laser, BP undergoes efficient intersystem crossing to the

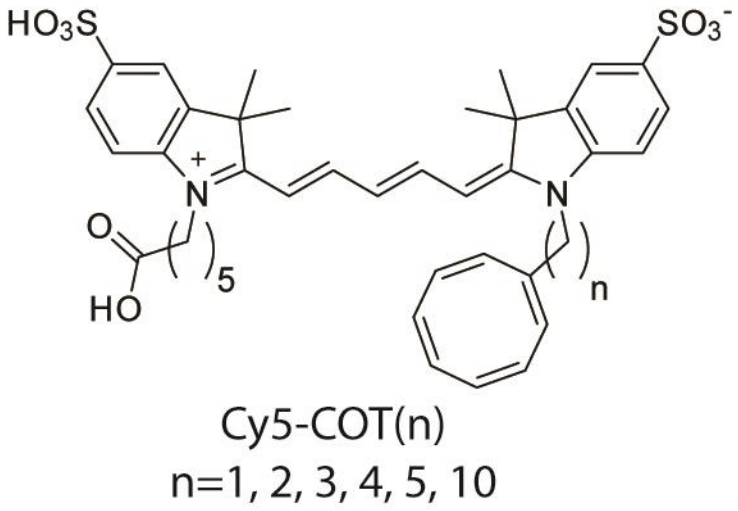

Chart 6.1. Structures of Cy5-COT(n) fluorophores used in this study.

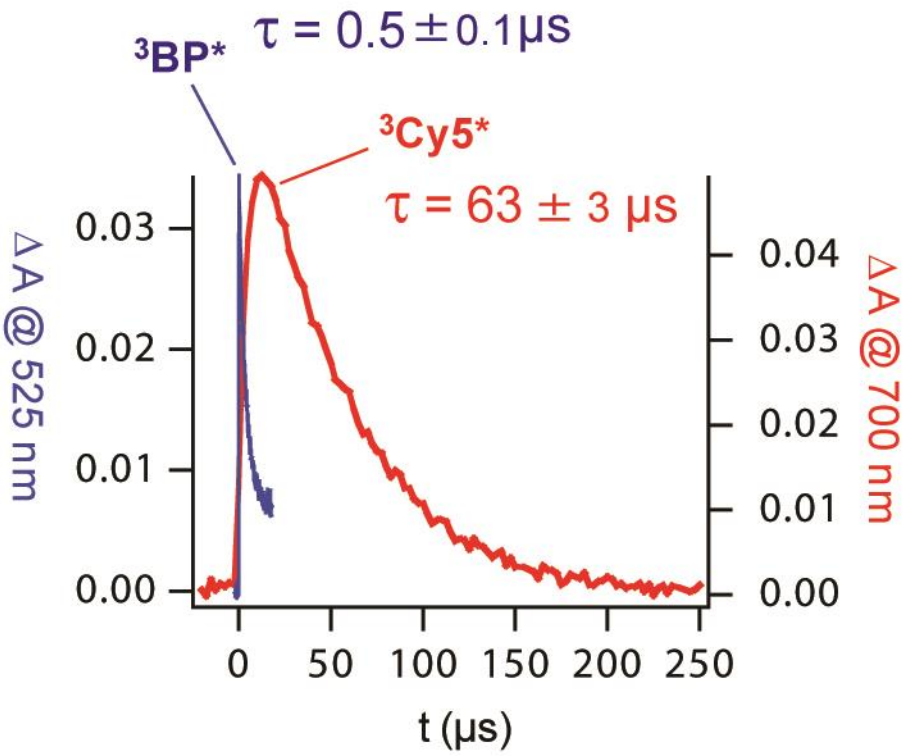

Figure 6.1. Cy5 triplet absorption traces recorded at 700 nm and BP triplet absorption traces recorded at 525 nm after pulsed laser excitation. The laser is at 355 nm with 5 ns pulse width. Experiments were performed in deoxygenated acetonitrile solutions of BP (3 mM) and Cy5 (10 μM). The triplet lifetimes (τ) are derived from a kinetic fitting model considering the growth kinetics due to energy transfer from ^{3}BP* to Cy5.

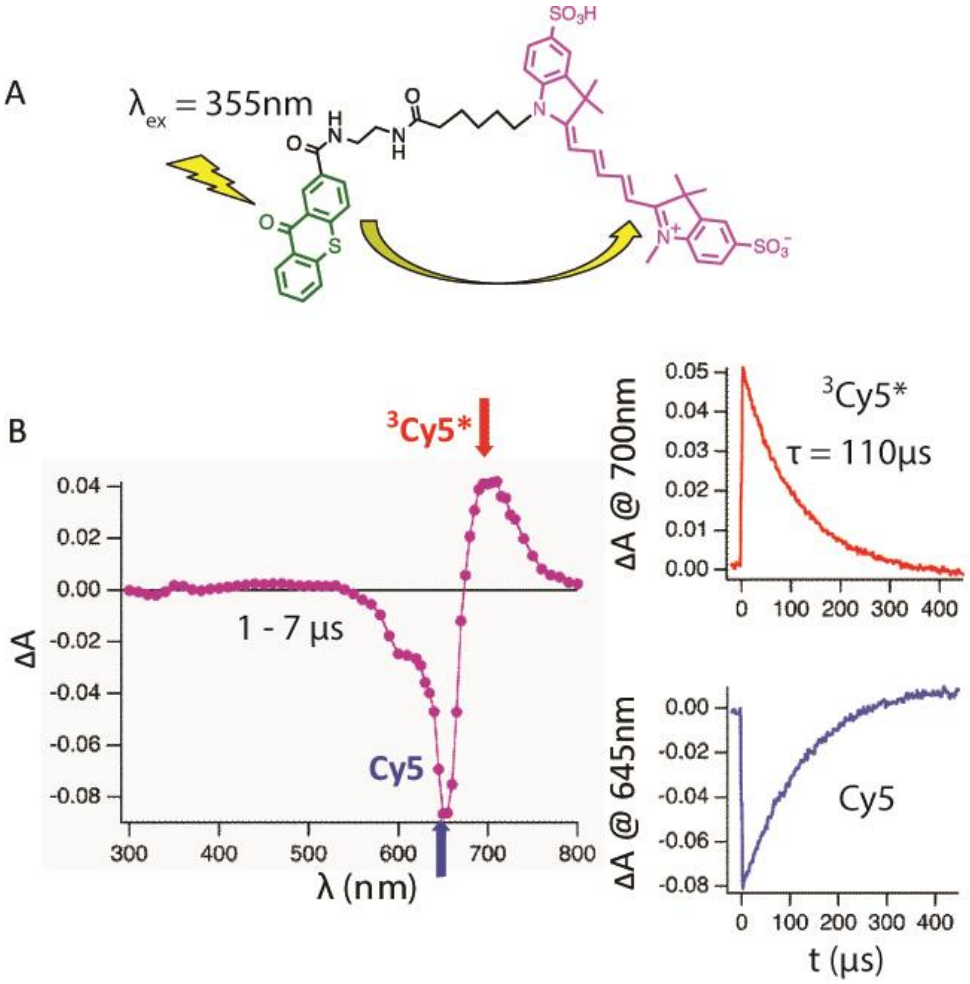

Figure 6.2. Transient absorption spectra for OTX-Cy5. (A) Reaction scheme for intramolecular sensitization of Cy5 fluorophore via OTX; (B) Transient absorption spectra recorded at 1-7 µs after the laser pulse (355 nm, 5 ns pulse width) of deoxygenated acetonitrile solutions of OTX-Cy5 (10 µM). The insets show kinetic traces at appropriate observation wavelengths.

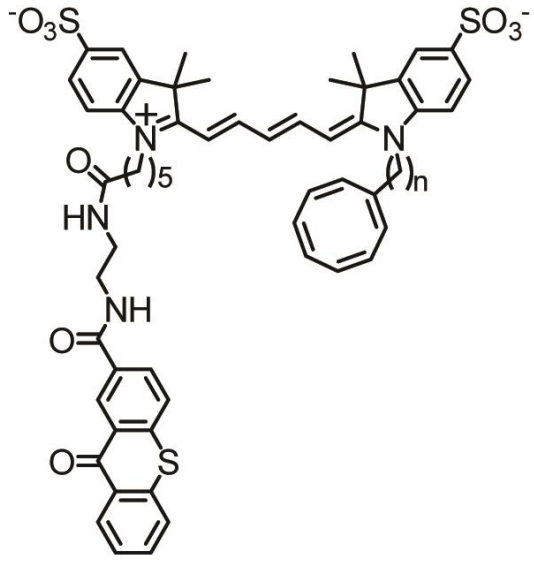

TX-Cy5-COT(n)
n=1, 2, 3, 4, 5, 10

Chart 6.2. Structures of OTX-Cy5-COT(n) used to determined triplet state lifetime of Cy5-COT(n).

triplet state and populates the Cy5 triplet state through triplet-triplet energy transfer, which was monitored by its transient absorbance at 700 nm[72]. In solution, this approach generates ^{3}Cy5* at a timescale of approximately 0.5 μs, limited by the diffusion of triplet benzophenone (^{3}BP*) and Cy5 (**Figure 6.1**). While this approach has proven useful for estimating the τ_T of ^{3}Cy5* (ca. 60 μs) and for qualitative comparisons of distinct fluorophore species[72], it suffers key drawbacks that preclude its use here. First, high concentrations of both BP (c.a. 10 mM) and fluorophore (c.a. 100 μM) are needed to rapidly populate the Cy5 triplet state, which can result in complications including dye aggregation and triplet-triplet annihilation. These effects can lead to an underestimation of τ_T as well as other potentially complicating artifacts. Second, and of paramount importance to the present investigations, the timescale for the inter-molecular triplet sensitization approach is also insufficient for determining short τ_T (<0.5 μs).

To address these shortcomings, we have used an intra-molecular approach to populate the Cy5 triplet state by covalently linking a triplet state sensitizer, 9-oxothioxanthone (OTX), to Cy5 and Cy5-COT(n) fluorophores (**Figure 6.2A, Chart 6.2**). OTX was selected as an intra-molecular sensitizer because it has high triplet quantum yield[166], higher triplet state energy than Cy5[166], and can be selectively excited at non-interfering wavelengths (eg. 355nm) due to its high molar absorptivity[167]. Using this approach, the rate of triplet-triplet energy transfer from OTX to Cy5 is increased by nearly an order of magnitude (ca. 0.05 μs) and is concentration independent. Correspondingly, triplet lifetime measurements can be performed at substantially lower dye concentrations (ca. 1-10 μM), where the τ_T of Cy5

is revealed to be approximately twice as long (~110 us) as previously estimated (**Figure 6.2B**)[72]. Hence, all τ_T measurements reported here were made using OTX-conjugated versions of the Cy5-COT(n) fluorophores (**Chart 6.2; Figure 6.3**), from which the rate constants of intra-molecular triplet energy transfer were calculated (k_{TET}=1/ τ_T). These findings were independent of the sensitizing methods as τ_T of OTX-Cy5-COT(10) (3.1±0.1 μs) was indistinguishable from τ_T of Cy5-COT(10) (3.2±0.3 μs) measured using benzophenone free in solution (**Figure 6.4**).

Cy5-COT(n) fluorophores generally exhibited longer τ_T at longer linker lengths; at linker lengths below four atoms, τ_T increased sharply (**Table 6.1, Figure 6.5A**). These data are notably consistent with previous intramolecular triplet energy transfer studies, where it was suggested that energy transfer preferentially occurs efficiently *via* a through-bond mechanism for short linkers (length < 4 atoms) whereas transfer preferentially occurs through intramolecular collision when longer linkers (length>5 atoms) are employed.[165, 168, 169] However, the most rapid triplet quenching rates achieved, where the COT was separated from Cy5 by just a single carbon atom ($1/\tau_T$(Cy5-COT(1)) = 4.5×10^6 s^{-1}), was 2-3 orders of magnitude lower than expected for the through-bond energy transfer mechanism[165, 168, 169]. This suggests that the observed rate of triplet energy transfer for Cy5-COT(n) is possibly limited by conformational changes in the COT molecule, of which the formation of planar species are thought to be required for its "non-vertical" transition to the triplet state[112, 113].

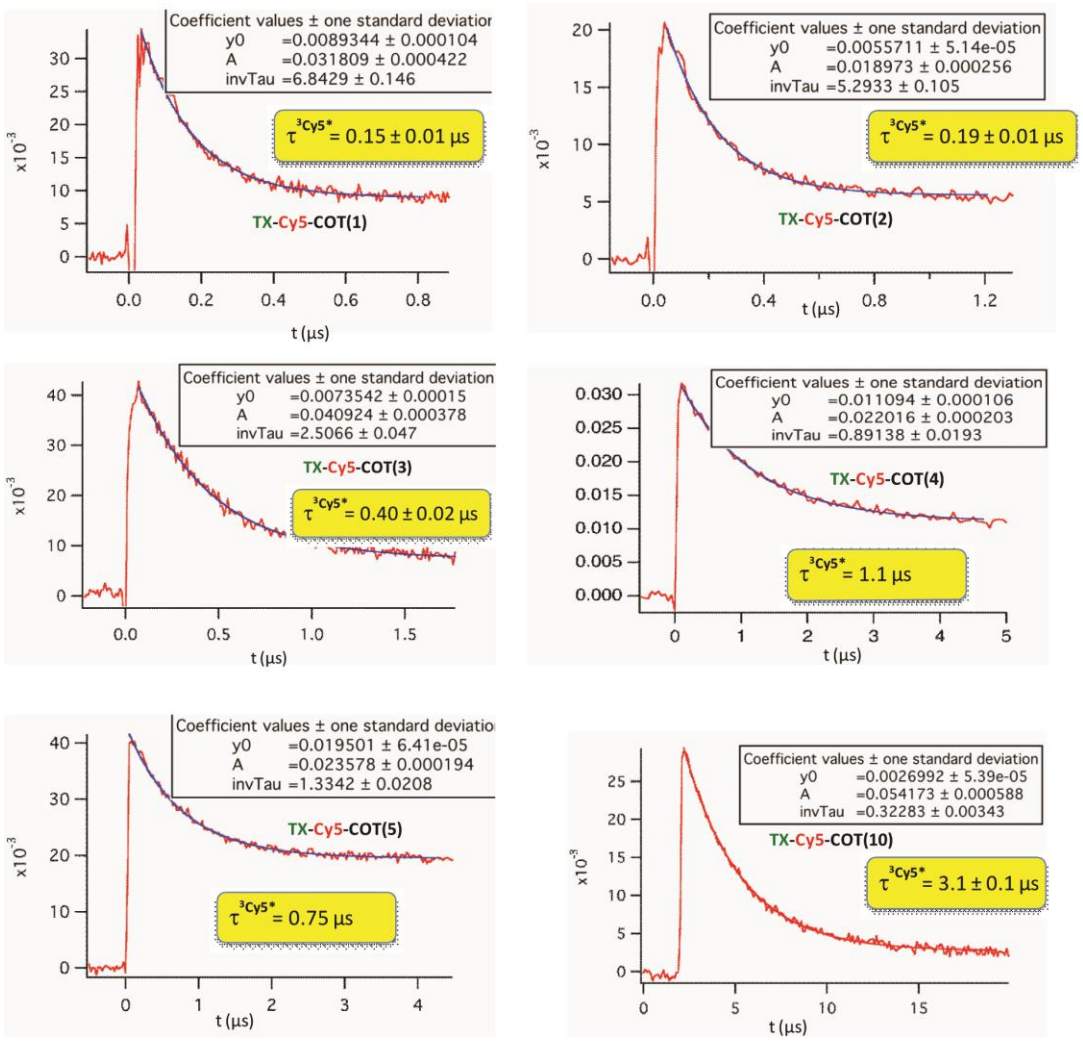

Figure 6.3. Transient absorption traces for OTX-Cy5-COT(n), n = 1, 2, 3, 4, 5, 10. Transient absorption traces at 700 nm after pulsed laser excitation (355 nm, 5 ns pulse width) of deoxygenated acetonitrile solutions of OTX-Cy5-COT(n) (~10 µM). The optical path length is 1 cm. The transient absorption at 700 nm was fit (blue line) to a single-exponential function, which accounts for the decay of Cy5 triplets.

$$\frac{d(\Delta A)}{dt} = -a_1 e^{(-k_1 t)} + a_2 e^{(-k_2 t)}$$

$$k_1 = 1.1 \times 10^6\ s$$

$$k_2 = 0.31 \times 10^6\ s$$

$$\tau^{^3Cy5^*} = 1/k_2 = 3.2 \pm 0.3\ \mu s$$

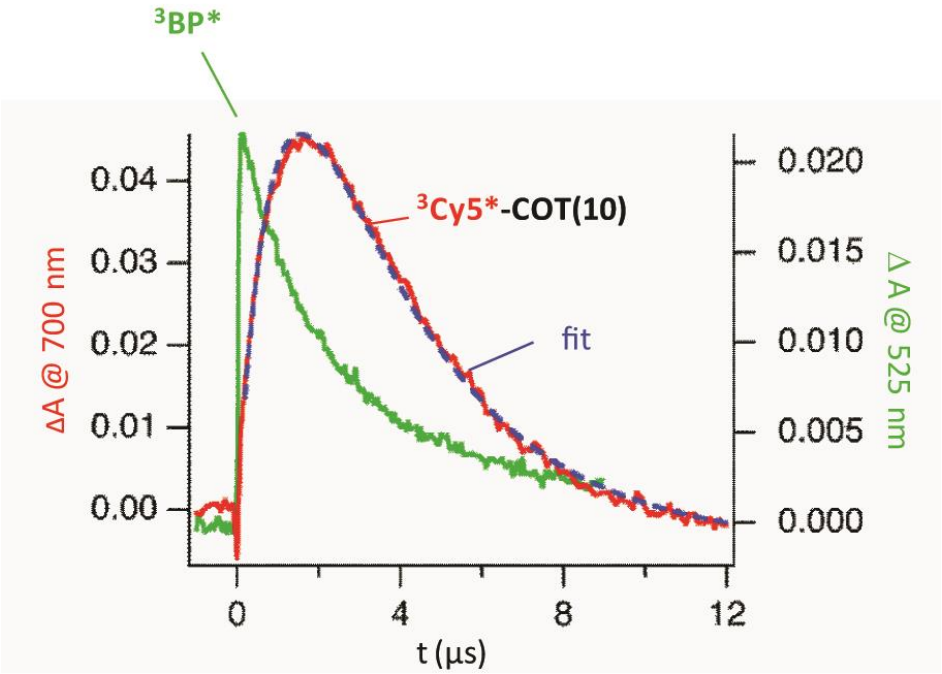

Figure 6.4. Transient absorption traces at 525 nm and 700 nm after pulsed laser excitation. Laser is at 355 nm with 5 ns pulse width. Experiments were performed in deoxygenated acetonitrile solutions of BP (~20 mM) and Cy5-COT(10) (~39 μM). The optical path length is 2 mm. The trace at 700 nm was fit (blue line) to a bi-exponential function, which accounts for the growth kinetics (k_1) and decay (k_2) of Cy5 triplets.

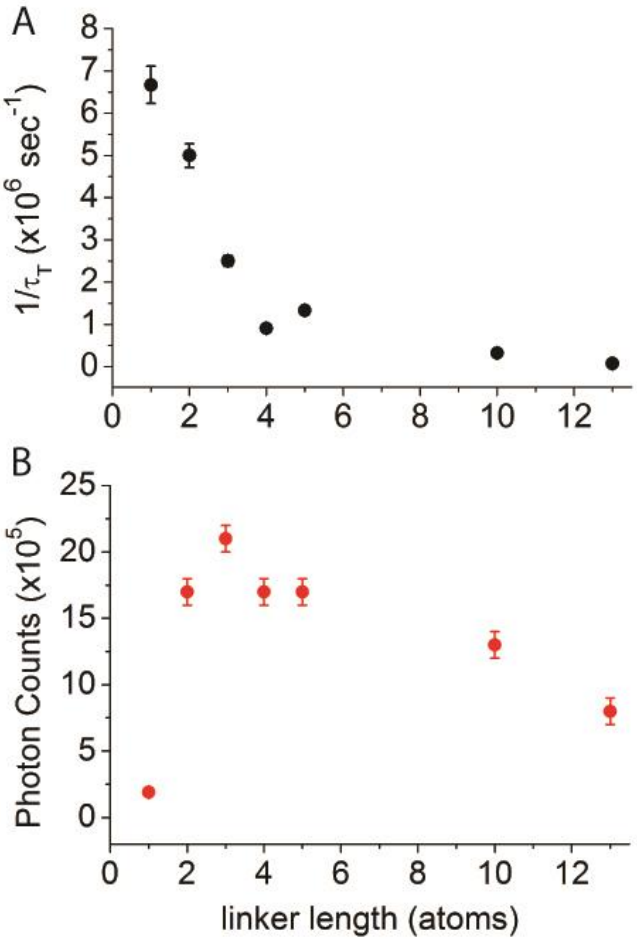

Figure 6.5. Triplet state lifetime and photostability of Cy5-COT(n). (A) The inverse of triplet state lifetime ($1/\tau_T$) and (B) the average number of photons detected before photobleaching in single-molecule measurements versus the length of linkers between Cy5 and COT. The Cy5-COT with an 13-atom linker is from our previous study.[72]

Table 6.1. Triplet state lifetime (τT), and average number of photon detected (counts) before photobleaching in single-molecule measurement of Cy5 and Cy5-COT fluorophores. The Cy5-COT with an 11-atom linker is from our previous study.[72]

	τ_T (μs)	Counts in deoxygenated buffer ($x10^6$)	Counts in ambient oxygen ($x10^4$)
Cy5	110±5	0.04±0.02	0.5±0.1
Cy5-COT(1)	0.15 ± 0.01	0.19 ± 0.02	2.4 ± 0.2
Cy5-COT(2)	0.19 ± 0.01	1.7 ± 0.1	2.1 ± 0.2
Cy5-COT(3)	0.40 ± 0.02	2.1 ± 0.1	2.1 ± 0.2
Cy5-COT(4)	1.1 ± 0.1	1.7 ± 0.1	1.9 ± 0.1
Cy5-COT(5)	0.75 ± 0.04	1.7 ± 0.1	1.9 ± 0.2
Cy5-COT(10)	3.1 ± 0.1	1.3 ± 0.1	1.9 ± 0.2
Cy5-COT(13)	13 ± 2	0.8 ± 0.1	1.6 ± 0.3
Cy5-bisCOT(3)	0.22 ± 0.01	3.1 ± 0.1	4.4 ± 0.3

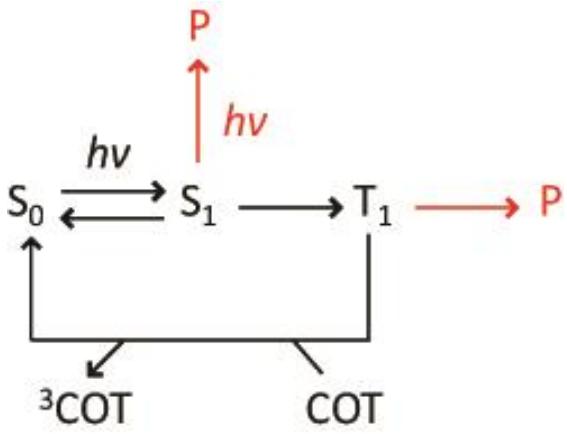

Scheme 6.1. Probable photophysical and photochemical processes of Cy5-COT fluorophores. S_0: ground state; S_1: singlet excited state; T_1: triplet excited state; P: photobleached product.

6.4 Linker-length dependence of Cy5-COT(n) photostability

To examine the relationship between triplet lifetime and photostability, each fluorophore was imaged at a single-molecule resolution through total-internal-reflection fluorescence (TIRF) microscopy using a prism-based, wide-field illumination strategy where thousands of individual fluorophores attached to DNA oligonucleotides can be imaged simultaneously[116]. The photostability of each Cy5-COT(n) fluorophore was first examined under deoxygenated conditions[89], and the total number of photons detected prior to photobleaching was quantified. As previously reported[116], marked increases in total photon count were observed relative to the parent Cy5 molecule. Consistent with the notion that fluorophores photobleach through the triplet state (**Scheme 6.1**), the photon counts of Cy5-COT(n), with n>2, increase as the $1/\tau_T$ increases (**Table 6.1, Figure 6.5**). Total photon counts were, however, notably uncorrelated with $1/\tau_T$ for Cy5-COT(2) and Cy5-COT(1) (**Table 6.1, Figure 6.5**). In particular, although Cy5-COT(1) possesses the shortest triplet state lifetime (0.15 μs), it also exhibits the least photon counts ($1.9x10^5$). Thus, at the shortest linker length, nearly all benefits of the COT-mediated intramolecular triplet quenching process were lost.

To understand these observations, we considered the most probable photophysical and photochemical pathways for Cy5 stabilization and photo-induced degradation[62, 70, 72, 82]. Fluorophores may photobleach through the first triplet state (T_1), and they may absorb multiple photons and degrade through higher excited states (S_n or T_n, n>1) (**Scheme 6.1**)[82, 83], the rate of which is expected to increase with excitation power[82, 83]. According to this model, we reasoned that at low illumination intensity

(<100W/cm^2) fluorophores photobleach mainly through their first triplet state (T_1). A kinetic scheme describing the photobleaching rate from T_1 shows that $1/\Phi_{B,T}$, the inverse of the yield of photobleaching through the triplet state, increases linearly with k_{TET} (i.e. $1/\tau_T$) (**Scheme 6.2**). Correspondingly, the photon count should be linearly dependent on $1/\tau_T$ if it is solely due to photobleaching from the triplet state. Indeed, we found that at low (80W/cm^2) illumination intensity, photon counts increase linearly with $1/\tau_T$ for Cy5-COT(n) with n>2 (**Figure 6.6A, red dots**).

The observation that Cy5-COT(n) with n<3, (Cy5-COT(1) and Cy5-COT(2)) deviates substantially from this trend (**Figure 6.6A**), suggests that these two fluorophores may exhibit a pronounced increase in photobleaching through alternative pathways. We posit that such alternative pathways for degradation may specifically arise from the proximity of COT to the Cy5 fluorophore, where at short distances excited states of COT may react with Cy5, thereby causing photobleaching. It is important to note that the lifetime of ^{3}COT* is similar to that of ^{3}Cy5* (ca. ~100 μs[164]). At short tether lengths, such ^{3}COT* lifetimes may be sufficiently long lived for secondary intramolecular reaction events to occur with Cy5 prior to COT's relaxation back the ground state through non-radiative relaxation processes.

According to the model in Scheme 6.1, the rates of photobleaching would also be expected to increase with excitation power[82, 83]. We therefore characterized the photon counts for each Cy5-COT(n) fluorophore over a range of illumination intensities. The inverse of photon counts, proportional to the photobleaching quantum yield (Φ_B), was observed to increase linearly with illumination intensity (**Figure 6.7**), indicating that higher excited states contribute to the effective rate of photobleaching.

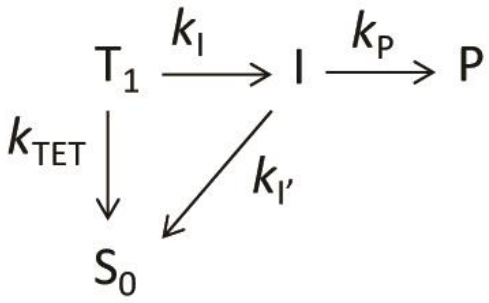

$$\Phi_{B,T} = \frac{\frac{k_P}{k_{I'}} k_I}{k_I + k_{TET}} \qquad \frac{1}{\Phi_{B,T}} = \frac{k_{I'}}{k_P k_I} k_{TET} + \frac{k_{I'}}{k_P}$$

Scheme 6.2. Photobleaching pathways from the triplet state in the absence of oxygen. T_1: triplet excited state; S_0: ground state; I: intermediate state to photobleaching; P: photobleached product. $\Phi_{B,T}$: Quantum yield of photobleaching from triplet state.

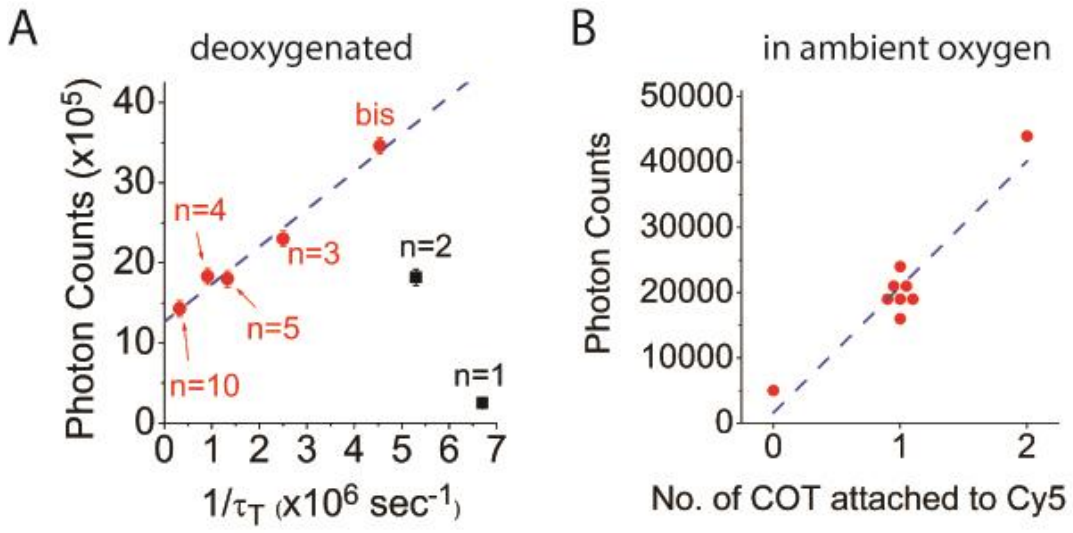

Figure 6.6. The limiting factors for the photostability of Cy5-COT(n). (A) In deoxygenated solution and at low excitation power (80W/cm^2), photon counts increase linearly with $1/\tau_T$ for Cy5-COT(n) (n>2) and Cy5-bisCOT(3) (red circles), but not for Cy5-COT(1) and Cy5-COT(2) (black rectangle). (B) In ambient oxygen, the photon counts of Cy5, Cy5-COT(n) and Cy5-bisCOT(3) fluorophores increase linearly with the number of COT molecules attached to Cy5.

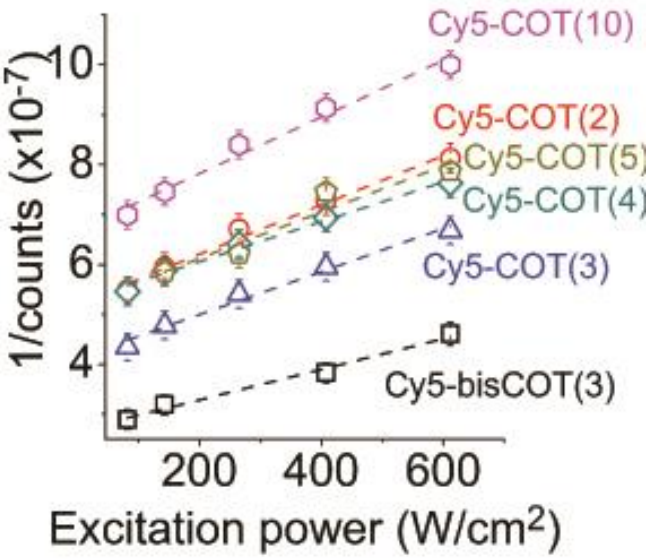

Figure 6.7. The 1/count of Cy5-COT(n) and Cy5-bisCOT(3) in deoxygenated solution as a function of excitation power.

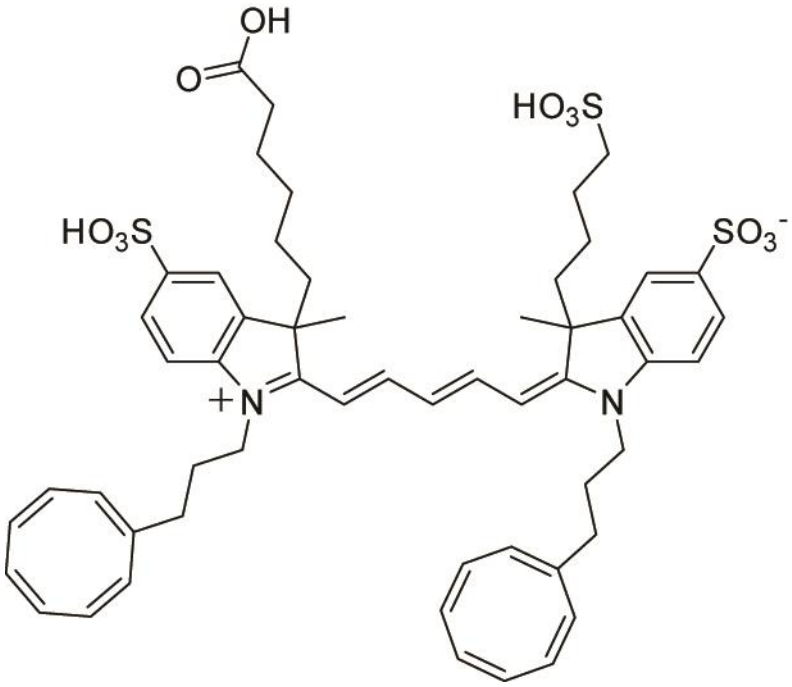

Chart 6.3. Structures of Cy5-bisCOT(3) fluorophore.

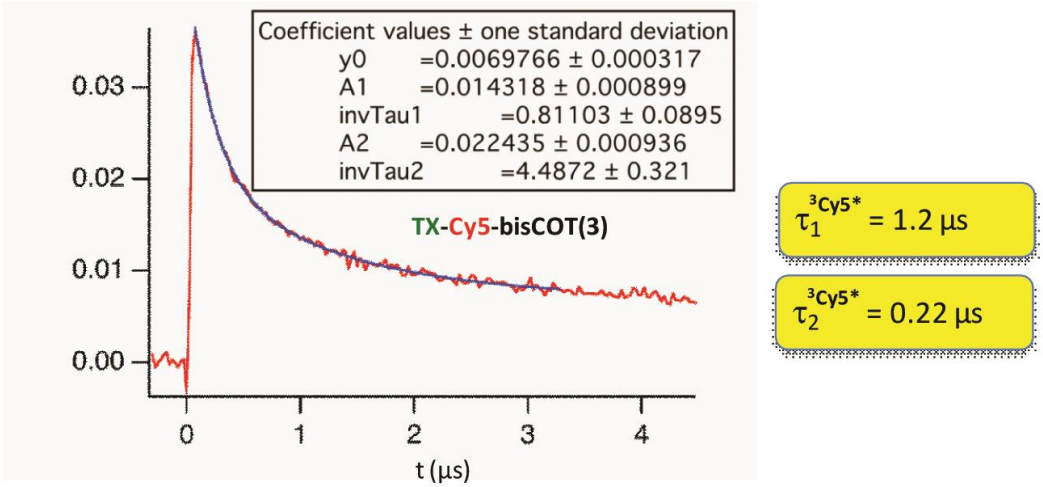

Figure 6.8. Transient absorption trace OTX-Cy5-bisCOT(3). Transient absorption traces at 700 nm after pulsed laser excitation (355 nm, 5 ns pulse width) of deoxygenated acetonitrile solutions of OTX-Cy5-bisCOT(3) (~10 µM). Optical path length is 1 cm. The transient absorption at 700 nm was fitted (blue line) to a double-exponential (down) function, which accounts for the decay of Cy5 triplets.

6.5 Additional attached COT molecule enables additive effects of photo-protection

To explore the effects of additional triplet state acceptors for intra-molecular triplet energy transfer and for improving photostability, we synthesized Cy5-bisCOT(3), where Cy5 was attached to two COT molecules *via* a three-carbon linker (**Chart 6.3**). The τ_T of Cy5-bisCOT(3) is 0.22 μs (**Table 6.1, Figure 6.8**), an approximately two-fold reduction from Cy5-COT(3) (τ_T = 0.40 μs), suggesting additive effects of triplet energy transfer for multiple COT molecules attached. The shortened triplet state translated into a nearly 50% enhancement in fluorophore photostability in a deoxygenated solution, the highest photon count of any of the Cy5-COT(n) fluorophores examined so far (3.1×10^6; **Table 6.1**).

6.6 Photostability in ambient oxygen conditions

We next sought to examine each fluorophore's photostability under ambient oxygen conditions. Compared to the parent Cy5 fluorophore, the Cy5-COT(n) fluorophore derivatives exhibited an approximately 3-5 fold increase in total photon counts; the Cy5-bisCOT(3) fluorophore showed an approximately 9 fold increase in total photon counts (**Table 6.1**). These data are consistent with the model that COT-mediated reductions in τ_T of Cy5 effectively protect the Cy5 fluorophore from damaging reactions with molecular oxygen. They are also in line with the notion that the rates of intra-molecular triplet energy transfer in self-healing fluorophores substantially exceed the rates of damaging reactions with molecular oxygen and/or reactive oxygen species[62, 137].' In this context, it is notable that Cy5 fluorophore photostability in the presence of molecular oxygen correlated linearly with the number of COT molecules attached to

Cy5 (**Figure 6.6B**) but not linker length (**Figure 6.9, Table 6.1**). This observation suggests that COT's protective function may be inactivated during imaging through reactions with molecular oxygen. Given its comparatively long lifetime[164], this may be particular to ^{3}COT*[164, 170]. In this view, each COT molecule extends the Cy5 fluorophore photon counts by an equal amount. After both COT molecules are inactivated, Cy5 photobleaches on a time scale of the parent Cy5 molecule.

6.7 COT substituted with an electron-withdrawing group increases fluorophore photostability

On the basis of this hypothesis, we reasoned that increasing the stability of COT may in turn improve fluorophore photostability, particularly in ambient oxygen. Previous works have shown that COT can react with photo-generated singlet oxygen and that the reactivity is significantly reduced if COT is substituted with an electron withdrawing group (EWG)[170]. We predicted that Cy5 linked to EWG-substituted COT would exhibit further improved photostability in oxygen. To test this hypothesis, we synthesized amide-substituted COT, linked it to Cy5 through a 11-atom linker (Cy5-amide-COT(11); **Figure 6.10A**), and characterized its photostability. Indeed, in buffer with ambient oxygen, Cy5-amide-COT(11) exhibits 35,000 photon counts, two times more than the photon counts (16,000) of Cy5-COT(13), a fluorophore with a difference of only two methylene groups (**Figure 6.10B**). Surprisingly, Cy5-amide-COT(11) also showed enhanced photostability in oxygen-depleted buffer, exhibiting three times more photon counts than Cy5-COT(13) (**Figure 6.10C**). We next tested amide-COT with other cyanine fluorophores, namely Cy2, Cy3, Cy5.5, and Cy7. In all

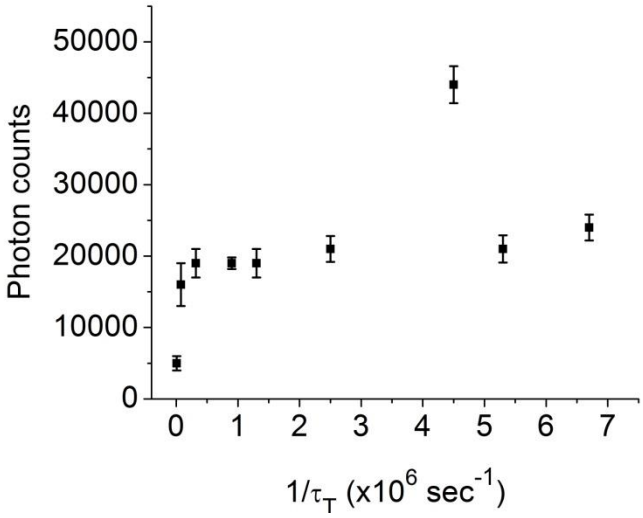

Figure 6.9. The photon counts of Cy5, Cy5-COT(n), and Cy5-bisCOT(3) in ambient oxygen conditions as a function of inverse of triplet state lifetime ($1/\tau_T$).

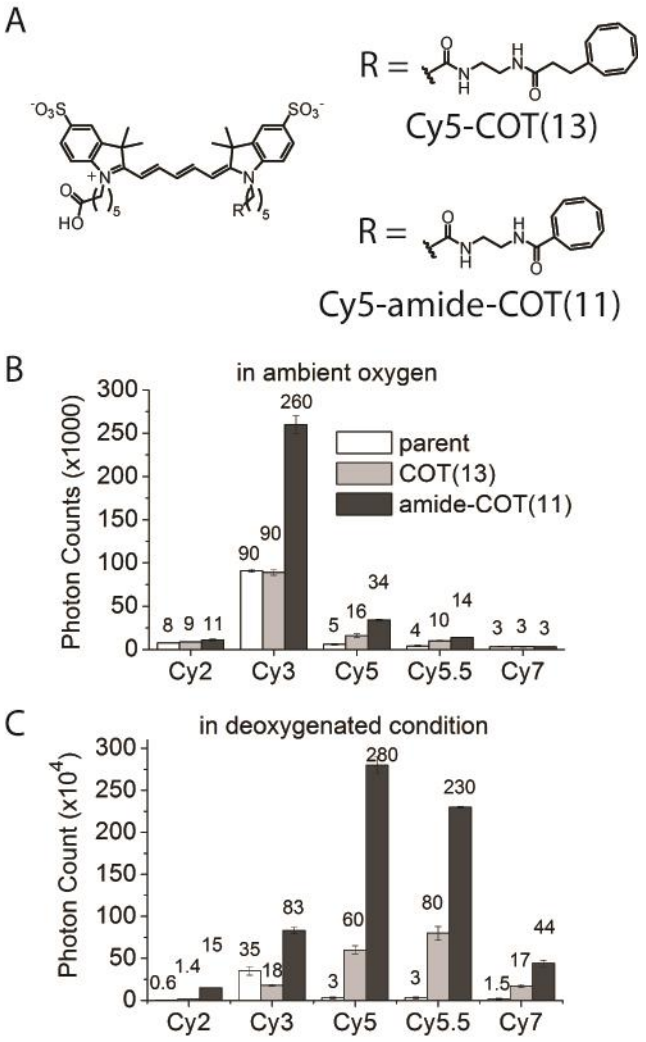

Figure 6.10. COT-amide further improves fluorophore photostability. (A) Structures of Cy5-COT(13) and Cy5-amide-COT(11). Photon counts of Cyanines fluorophores linked with COT or amide-COT (B) in buffer with ambient oxygen or (C) in oxygen-depleted buffer.

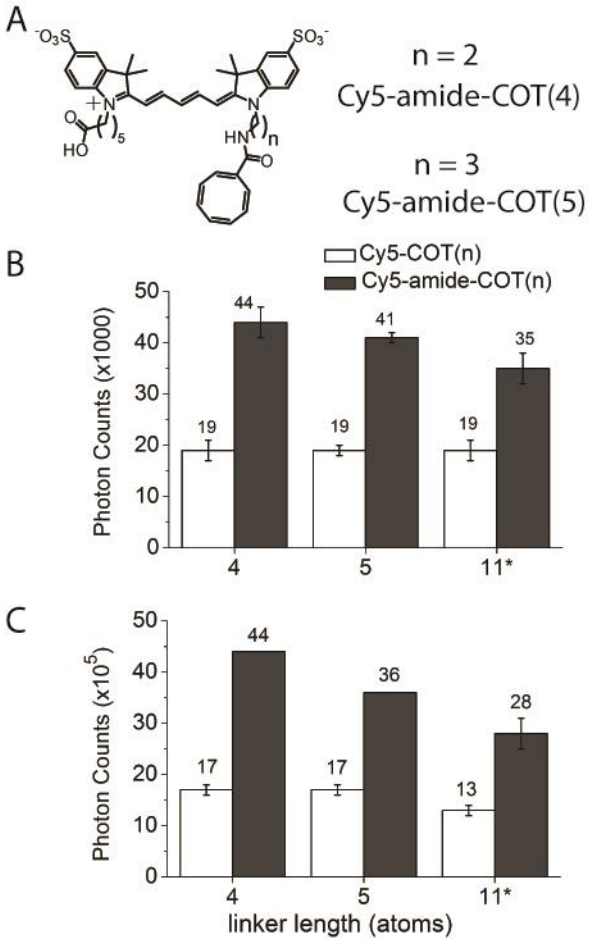

Figure 6.11. COT-amide further improves fluorophore photostability. (A) Structures of Cy5-amide-COT(4) and Cy5-amide-COT(5). (B) Photon counts of Cy5-COT(n) and Cy5-amide-COT with different lengths of linker (B) in buffer with ambient oxygen or (C) in oxygen depleted buffer. *Since Cy5-COT(11) is not available, Cy5-COT(10) is employed to compare with Cy5-amide-COT(11).

Table 6.2: Triplet state lifetime (τ_T), and average number of photon detected (counts) before photobleaching in single-molecule measurement of Cy5-amide-COT fluorophores.

	τ_T (μs)	Counts in deoxygenated solution ($x10^6$)	Counts in ambient oxygen ($x10^4$)
Cy5-amide-COT(4)	0.077 ± 0.005	4.4 ± 0.1	4.4 ± 0.3
Cy5-amide-COT(5)	0.28 ± 0.01	3.6 ± 0.2	4.1 ± 0.1
Cy5-amide-COT(11)	0.33 ± 0.01	2.8 ± 0.1	3.5 ± 0.3

cases, amide-COT improves the photostability significantly more than COT (**Figure 6.10B, C**). For Cy3, a fluorophore widely used for routine and advanced imaging applications, amide-COT improves its photon counts by about 200% both in the presence and absence of oxygen, while COT does not improve its photon count.

Based on our findings with the Cy5-COT(n) fluorophores, we sought to further improve fluorophore photostability by shortening the linkers to 4 and 5 atoms (Cy5-amide-COT(4) and Cy5-amide-COT(5)) (**Figure 6.11.A**). As expected, these fluorophores exhibit further increased photostability (**Figure 6.11.B and C**). In ambient oxygen, these fluorophores exhibit 8-9 fold more photon counts (44000 and 41000, respectively) than Cy5 (5000). Compared to Cy5-COT(n) fluorophores with the same linker length, we see an increase τ_T in photon counts by more than 100% with Cy5-amide-COT, both in ambient oxygen and in a deoxygenated environment (**Table 6.2; Figure 6.11.B and C**).

The improved photostability for Cy5-amide-COT may arise from the reduced reactivity of COT with oxygen species. Alternatively, amide-COT may more efficiently quench Cy5 triplet state than COT does, thus further improving photostability. To examine the latter possibility, we measured the triplet state lifetime of Cy5-amide-COT(n), with n=4, 5, and 11. Their τ_T is 0.077 μs, 0.28 μs, and 0.33 μs respectively (**Table 6.2**), shorter than the τ_T of Cy5-COT(n) with similar linker lengths. Although the mechanism of how amide-COT more efficiently quenches the triplet state is not clear, we speculate that the amide group may change the potential energy surface of COT, which affects the rate of "non-vertical" triplet energy transfer[113]. However, the improved photostability for Cy5-amide-COT(n) in ambient oxygen cannot be totally

attributed to the shortened triplet state, because they exhibit 100% more photons than the Cy5-COT(n) fluorophores with comparable τ_T, namely Cy5-COT(1) , Cy5-COT(2), and Cy5-COT(3) (τ_T = 0.15 μs, 0.19 μs, 0.40 μs, respectively). Therefore, the improved photostability may arise from the reduced reactivity for EWG-substituted COT.

6.8 A general module to improve fluorophore photostability

With increased rate of triplet energy transfer and reduced reactivity to molecular oxygen, amide-COT may be a general stabilizer to improve fluorophore photostability when covalently linked to a fluorophore. Here we create a general strategy for implementing intra-molecular photostabilization for organic fluorophores that are widely used to visualize intracellular processes in a broad array of biological applications. Our strategy is based on the synthesis of an adaptor molecule containing amide-COT, which can then be directly attached to NHS-activated forms of commercially available dye molecules (**Figure 6.12; Figure 6.13**). We firsted test it with Cy3B, TMR, and silicon rhodamine (SiR), fluorophores used for single-molecule and live-cell imaging[148, 149]. The –NHS activated parent and amide-COT fluorophores were labeled to DNA oligo nucleotides and characterized with TIRF microscopy. In ambient oxygen, SiR-amide-COT exhibited 2.5 fold enhancement of fluorophore photostability, demonstrating the effectiveness of the approach (Table 6.3). Modest improvement was also observed for Cy3B, but not for TMR (Table 6.3). Consistent with the result for Cyanine fluorophores, the effects of the amide-COT attached are more pronounced in the deoxygenated conditions. All of the amide-COT fluorophores exhibit 5-30 fold improvement on photostability compared to parent fluorophores (Table 6.3).

We next examined whether the improved photostability of fluorophore labeled on DNA can be extended to fluorophores labeled on protein. The parent SiR and SiR-amide-COT are tethered to the SNAP tag[153, 171] using a BG reactive group. (**Figure 6.13.B**). A ~2-fold enhancement in the total number of photons emitted was observed in the presence of oxygen (Figure 6.13.C) without any change in fluorophore brightness. This latter observation indicates that the COT-amide linker has little to no effect on lactone formation. Hence the fluorogenic nature of SiR upon protein conjugation[149] remains unperturbed. Even more substantial benefits were observed in the absence of oxygen, where the increase in photon yield was more than 15-fold (**Figure 6.13.C**). These observations demonstrate that a simple modification of fluorophore –by attaching it to an adapter molecule with a stabilizer- could lead to improved photostability that is not attainable with previous photoprotection methods.

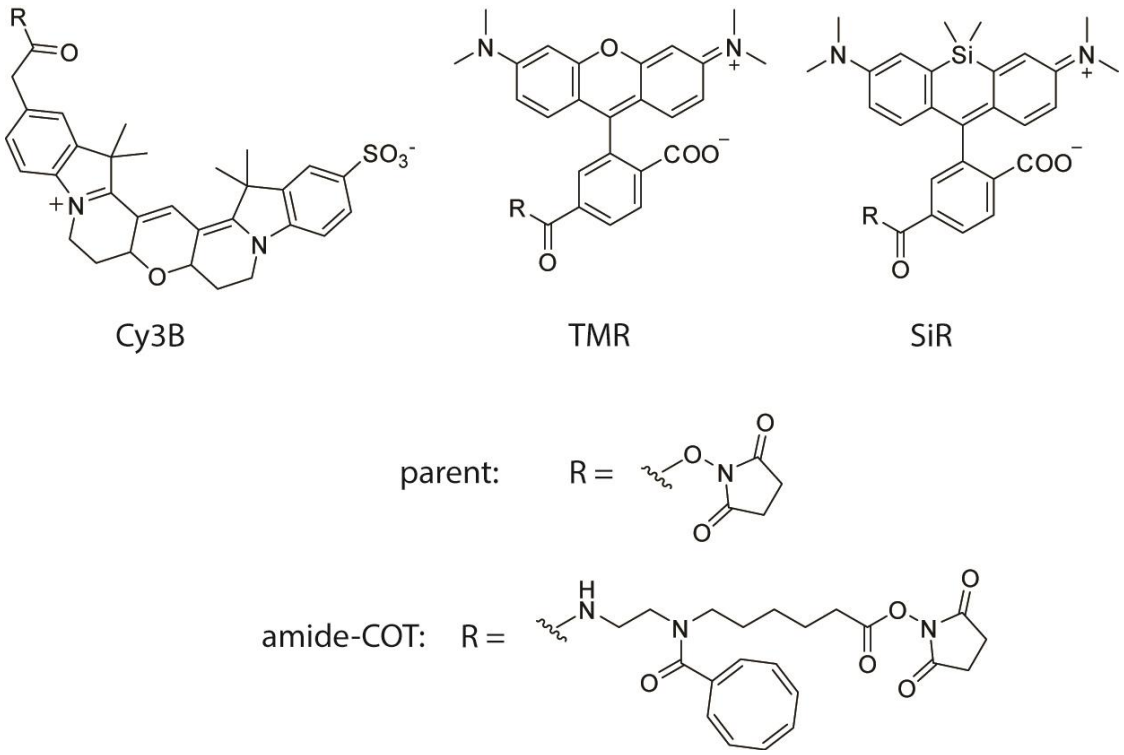

Figure 6.12. Chemical structures of Cy3B, TMR, and SiR and their COT-amide derivatives.

Table 6.3: Average number of photon detected (counts) before photobleaching in single-molecule measurement of TMR, Cy3B, SiR, and their amide-COT derivatives.

	counts in deoxygenated solution ($\times 10^5$)	counts in ambient oxygen ($\times 10^4$)
TMR (parent)	1.8 ± 0.1	12 ± 1
TMR-amide-COT	8.1 ± 0.1	13 ± 1
Cy3B (parent)	2.9 ± 0.1	4.4 ± 0.3
Cy3B-amide-COT	23 ± 1	6.0 ± 0.1
SiR (parent)	0.3 ± 0.1	8.0 ± 0.2
SiR-amide-COT	10.0 ± 0.3	20.0 ± 0.1

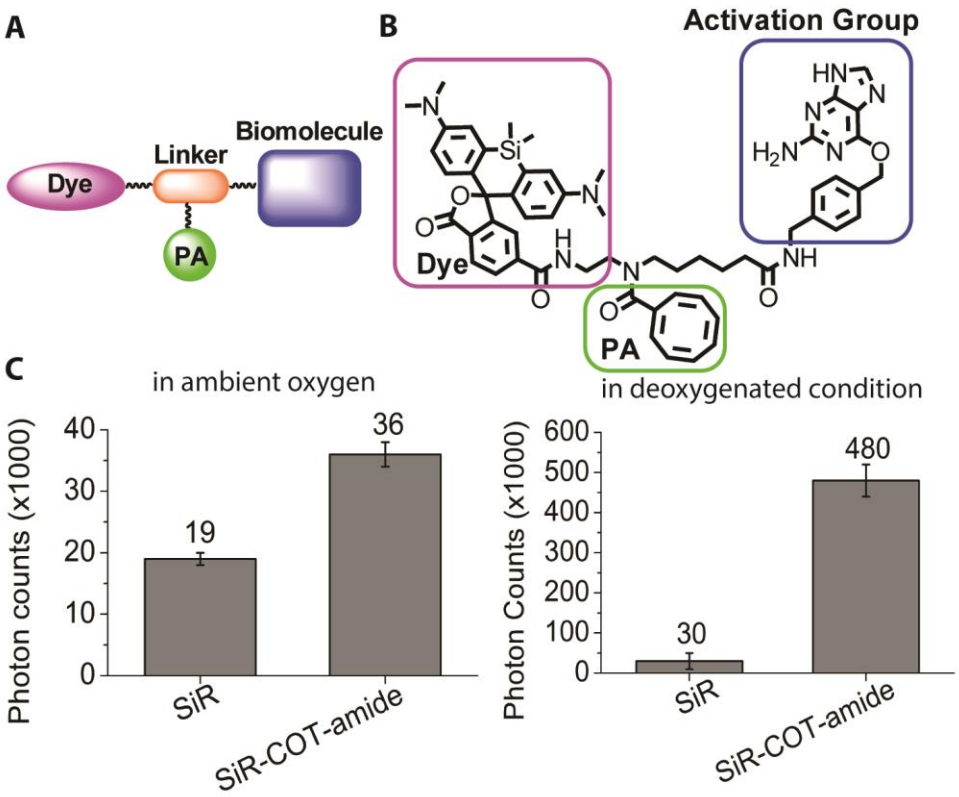

Figure 6.13. Amide-COT improves photostability for SiR. (A) a general method to covalently link a stabilizer, or stabilizer (PA, protective agent), to a dye molecule. Here the dye is labeled to the target biomolecule via an adapter, i.e., an universal linker containing a stabilizer. (B) Chemical structure of BG-reactive SiR-COT-amide fluorophores where stabilizer COT-amide is attached to a SiR fluorophore through the adapter linker. (C) Photon counts of SiR and SiR-COT-amide (left) in imaging buffer with ambient oxygen or (right) in deoxygenated imaging buffer.

6.9 Conclusions

The data obtained through these investigations serve as an important guide for the further development of self-healing fluorophores aiming to maximize their performance through intramolecular triplet energy transfer. These findings also aid our goal of establishing quantitative models for the photostability of self-healing fluorophores and identify key bottlenecks for reaching their full potential. In addition to photobleaching from the triplet state, the data presented here suggest that these bottlenecks could also include photobleaching from higher-order excited states, reactivity between the fluorophore and COT, as well as the inactivation of COT by oxygen species. Exploiting these understandings, we found that a simple structural modification – attaching amide-COT to a fluorophore - further improves photostability across the visible and near-infrared spectrum. It is worth noting that, in ambient oxygen, the amide-COT improves the photostability of Cy3 by 3 fold, Cy5 by nearly 10 fold, and SiR by 2 fold, which is not attainable with previous photo-protection approaches. These findings are critical for the development of self-healing fluorophores designed to push the frontiers of biological imaging at the single-molecule scale including live-cell imaging which requires the presence of molecular oxygen[29, 31, 136, 156, 172]. Further development of this approach could yield a new generation of self-healing fluorophores with superior photostability. For example, EWGs other than an amide group can be explored and multiple triplet state acceptors could be employed. To push the limit of biological imaging, the self-healing approach needs further generalization to fluorophores in different structural categories (e.g. Rhodamine and carbopyronine)[173], as well as combination with other protective approaches[148, 174].

7. Future directions

7.1 Benchmark fluorophore performance inside living cells

The mechanism, generalization, and application of self-healing fluorophores pave the way for the advancement of single-molecule fluorescence microscope to study biological processes in vitro, in fixed or living cells, in embryos or tissues, and *in vivo*. To achieve these goals, it is important to test the photostability of self-healing fluorophores inside living cells. The most widely used approach to label intracellular targets with organic fluorophore is to deliver net-neutral, membrane permeable fluorophores inside cells through passive diffusion and to label with a self-labeling protein tag[18, 153, 175, 176]. Because triplet energy acceptors COT and amide-COT are neutral, when attached to a fluorophore they do not change its net charge and therefore may not significantly affect its membrane permeability. We plan to label the intracellular targets with the self-healing derivatives of membrane permeable fluorophores (e.g. SiR-amide-COT). Due to the charged sulfonate group, sulfonated cyanine fluorophores and their self-healing derivatives are not permeable to cellular membrane and therefore cannot be delivered to intracellular targets through passive diffusion[18]. Delivery of fluorophore-labeled biomolecules into living cells through microinjection[31, 143] or other delivery approach[177] may represent a valuable alternates.

7.2 Development of new triplet state acceptor to further improve photostability

We have established a quantitative model of the photostability of self-healing fluorophore, and have identified rate-limiting steps and key bottle necks for further

improvement of photostability, which can guide the development of the second-generation self-healing fluorophores to push the frontier of biological imaging. The mechanistic understanding points to the searching and development of triplet state acceptor with the following properties: (1) low triplet state energy and high singlet state energy; (2) faster triplet energy transfer to the acceptor; (3) low reactivity to molecular oxygen; (4) fast relaxation to the ground state.

7.2.1 Searching for small molecules with low triplet state energy and high singlet state energy

A triplet state acceptor should possess triplet state energy lower than that of organic fluorophore, but possess singlet state energy higher than that of organic fluorophore to avoid quenching fluorescence, leading to large singlet-triplet energy difference (ΔE_{ST}). COT has an unusually low triplet state energy (c.a. 1 eV[112]) and large ΔE_{ST} (c.a. 3.1 eV [112]; ΔE_{ST}(Cy5) = 0.3eV [Chapter 4]), and we can learn from its properties in order to search other small molecules with low large ΔE_{ST}. As an annulene with 8 π-electrons, COT has aromatic triplet states and anti-aromatic singlet states (Baird's theory[178, 179]), leading to low triplet state energy and high singlet state energy. We can utilize Baird's theory to guide the search of other small molecule with low triplet state energy and large ΔE_{ST}. One example is pentafulvene and its derivatives, which forms aromatic triplet excited state with 4 π-electrons and has triplet state energy as low as 0.7 eV[180]. The triplet state energy of dimethylpentafulvene (DMPF) is 1.7 eV[180], higher than the triplet state energy of Cy2 (2.0 eV), similar than Cy3 (1.7 eV), and higher than Cy5 (1.5 eV) (measured by phosphorescence; see chapter 2 for methods). Consistent with our model and measured the triplet state energy, our preliminary data show that 1mM

DMPF in deoxygenated imaging buffer improves photostability for Cy2, but not for Cy3 and Cy5 (Figure 7.1), suggesting that fulvene derivatives with even lower triplet state energy (e.g. 1,2,3,4-Tetrachloro-6,6-dicyanopentafulvene, E_T = 0.7 eV)[180]can be a stabilizer for long-wavelength fluorophores. Computational studies predicts that other class of fulvene (e.g. benzofulvene, heptafulvene[180]) certain heterocyclic compound[181] also possess low triplet state energy and large ΔE_{ST} and therefore are promising candidates for triplet energy acceptor.

7.2.2 Increase the rate of intramolecular triplet energy transfer

Our mechanism study (Chapter 6) shows that the rate of intramolecular triplet energy transfer for Cy5-COT(n) fluorophores is 3-4 orders of magnitude lower than the rates reported for other molecules[165, 182], which can be explained by the conformational change required for the transition from COT ground state to triplet state. According to the Baird's theory[178, 179] that presented earlier (Chapter 7.2.1), COT in triplet state is aromatic and adopts a planar conformation, while COT in the singlet ground state adopts a boat-shape conformation to avoid anti-aromaticity. Therefore, a conformational change from boat shape to plane is required for triplet energy excitation, and may become a rate-limiting step for the intramolecular energy transfer from fluorophore to COT.

Our data predicts that further shortening of triplet state leads to improvement of fluorophore photostability (Chapter 2 and 6). To achieve faster intramolecular triplet energy transfer, one can employ other triplet acceptors, e.g. fulvene and its derivatives, which do not involves a significant change of conformation during triplet energy excitation. An alternate approach is to identify COT derivatives with faster energy

transfer rate. The intramolecular triplet energy transfer from Cy5 to amide-COT is 1-2 orders of magnitude faster than from Cy5 to COT (chapter 6.2). The reason for this unexpected observation is currently unknown, but according to the theoretical study[113] it may be related to the energy and gradient of the triplet potential energy surface that are affected by amide substitute. Theoretical and computational study of the mechanism of faster triplet energy transfer to amide-COT would guide the development of substituted COT with faster energy transfer.

7.2.3 Triplet state acceptor with reduced reactivity and lifetime

The mechanistic study in chapter 6 indicates that the degradation of triplet COT after intramolecular energy transfer may serve another bottleneck for improvement of photostability, especially in the presence of molecular oxygen. Previous report showed that COT substituted with electron withdrawal group (EWG) exhibited reduced reactivity to oxygen species[170]. Consistent with this model, linkage of amide-COT to a fluorophore is a general approach to improve fluorophore photostability, more effective than the linkage of COT (Chapter 6). A variety of EWG could be incorporated to COT derivatives, which may further improve fluorophore photostability. In addition, our data show that attachment of multiple triplet state acceptors further increases Cy5 fluorophore photostability, which may be generalizable to other fluorophores.

An alternate approach to slow down the degradation from the triplet state is to shorten its lifetime with heavy atom effects, which states due to spin-orbit coupling that organic molecules attached to a heavy atom (e.g. bromine or iodine) possess higher quantum yield of intersystem crossing (e.g. from the triplet state to the ground state). However,

COT substituted with bromide is not stable at room temperature and rearrange quickly. The effects of fulvene substituted with heavy atoms remain unexplored.

7.3 Combinatory approaches for photostable organic fluorophore

To maximize the potential of self-healing fluorophore for biological imaging, it is probably most effective to combine with other photo-protection approach. In deoxygenated imaging buffer, self-healing fluorophores with stabilizers in solution (e.g. COT[39, 102], NBA[39]Dave], Trolox[53, 138], ROXS[80]) exhibit higher photostability than either approach alone (chapter 5), and a number of labs have been using this combinatory approach for *in vitro* single-molecule experiments [158, 159, 183, 184]. While stabilizers in solution do not improve photostability for fluorophore in ambient oxygen (unpublished data), self-healing approach could be combined with other structural modification of fluorophore that leads to enhanced photostability, such as azetidinyl Rhodamine[148] and halogenations[174]. Moreover, to fulfill the requirement of high brightness, high chemical specificity, and low background for single-molecule imaging, self-healing fluorophore could be combined with other module that leads to high fluorescence quantum yield[93, 148] and fluorogenicity[16, 17, 149, 176, 185], altogether pushing the limit of biological imaging.

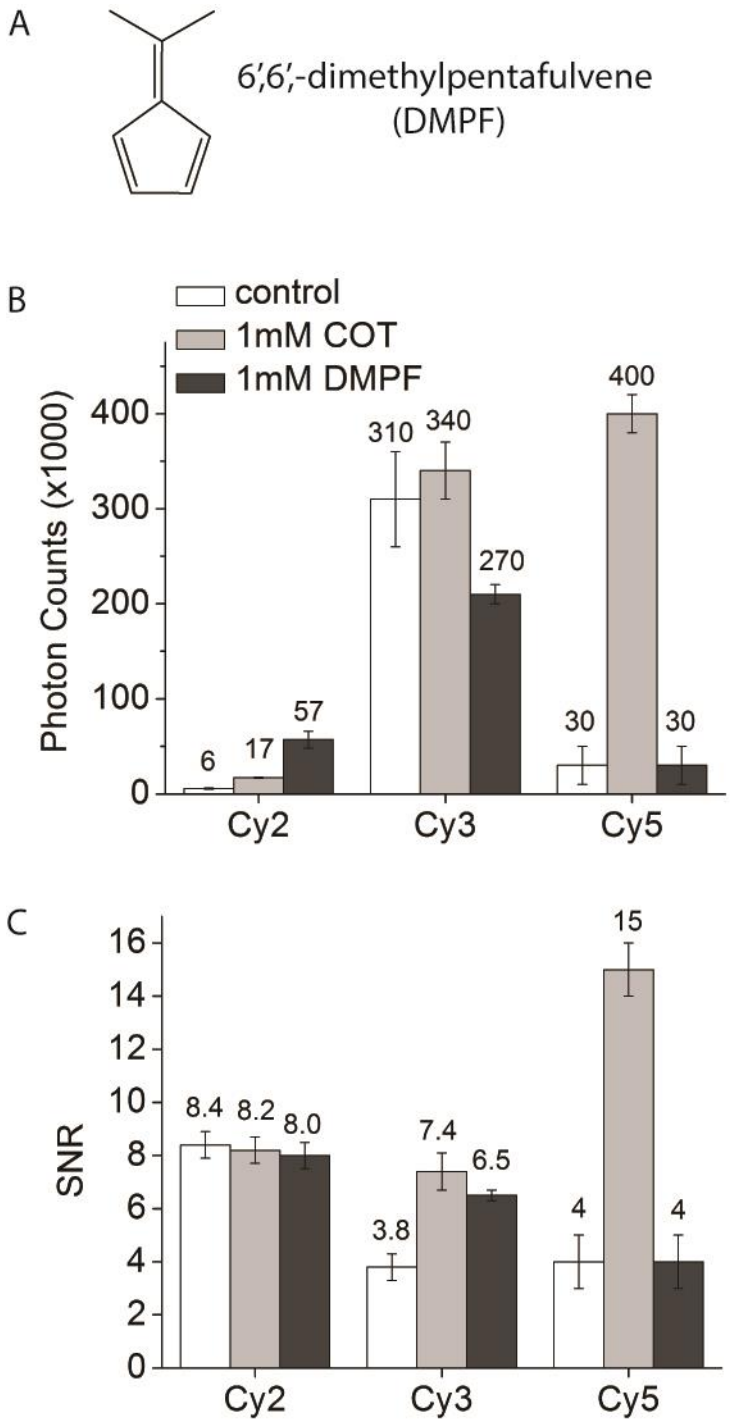

Figure 7.1. Fulvene as a candidate of potent stabilizer. (A) Structure of 6',6',-dimethylpentafulvene (DMPF). (B) Photon counts and (C) signal-to-noise ratio (SNR) of Cy2, Cy3, and Cy5 with no stabilizer, 1 mM COT, or 1 mM DMPF in solution.

REFERENCES

1. Bruchez, M.P., *Quantum dots find their stride in single molecule tracking.* Current Opinion in Chemical Biology, 2011. **15**(6): p. 775-780.

2. Loman, A., et al., *Comparison of optical saturation effects in conventional and dual-focus fluorescence correlation spectroscopy.* Chemical Physics Letters, 2008. **459**(1–6): p. 18-21.

3. Hink, M.A., et al., *Structural Dynamics of Green Fluorescent Protein Alone and Fused with a Single Chain Fv Protein.* Journal of Biological Chemistry, 2000. **275**(23): p. 17556-17560.

4. Cheng, P.C., *The Contrast Formation in Optical Microscopy*, in *Handbook of Biological Confocal Microscopy*, J.B. Pawley, Editor. 2006. p. 162-206.

5. Lakowicz, J., *Principles of Fluorescence Spectroscopy*. Third Edition ed. 2006, New York, NY: Springer Science + Business Media, LLC. 954.

6. Giepmans, B.N., et al., *The fluorescent toolbox for assessing protein location and function.* Science, 2006. **312**(5771): p. 217-24.

7. Levitus, M. and S. Ranjit, *Cyanine dyes in biophysical research: the photophysics of polymethine fluorescent dyes in biomolecular environments.* Q Rev Biophys, 2011. **44**(1): p. 123-51.

8. Ha, T. and P. Tinnefeld, *Photophysics of Fluorescent Probes for Single-Molecule Biophysics and Super-Resolution Imaging.* Annual Review of Physical Chemistry, 2012. **63**: p. 595-617.

9. Tsien, R.Y., *The green fluorescent protein.* Annu Rev Biochem, 1998. **67**: p. 509-44.

10. Shaner, N.C., P.A. Steinbach, and R.Y. Tsien, *A guide to choosing fluorescent proteins.* Nat Methods, 2005. **2**(12): p. 905-9.

11. Michalet, X., et al., *Quantum dots for live cells, in vivo imaging, and diagnostics.* Science, 2005. **307**(5709): p. 538-44.

12. Resch-Genger, U., et al., *Quantum dots versus organic dyes as fluorescent labels.* Nat Meth, 2008. **5**(9): p. 763-775.

13. Yang, F., L.G. Moss, and G.N. Phillips, *The molecular structure of green fluorescent protein.* Nat Biotech, 1996. **14**(10): p. 1246-1251.

14. Ueno, T. and T. Nagano, *Fluorescent probes for sensing and imaging.* Nat Meth, 2011. **8**(8): p. 642-645.

15. Chen, I. and A.Y. Ting, *Site-specific labeling of proteins with small molecules in live cells.* Curr Opin Biotechnol, 2005. **16**(1): p. 35-40.

16. Szent-Gyorgyi, C., et al., *Fluorogen-activating single-chain antibodies for imaging cell surface proteins.* Nat Biotech, 2008. **26**(2): p. 235-240.

17. Paige, J.S., K.Y. Wu, and S.R. Jaffrey, *RNA Mimics of Green Fluorescent Protein.* Science, 2011. **333**(6042): p. 642-646.

18. Fernandez-Suarez, M. and A.Y. Ting, *Fluorescent probes for super-resolution imaging in living cells.* Nat Rev Mol Cell Biol, 2008. **9**(12): p. 929-43.

19. Lippincott-Schwartz, J. and G.H. Patterson, *Development and Use of Fluorescent Protein Markers in Living Cells.* Science, 2003. **300**(5616): p. 87-91.

20. Fu, A., et al., *Semiconductor nanocrystals for biological imaging.* Current Opinion in Neurobiology, 2005. **15**(5): p. 568-575.

21. Dedecker, P., F.C. De Schryver, and J. Hofkens, *Fluorescent Proteins: Shine on, You Crazy Diamond.* Journal of the American Chemical Society, 2013. **135**(7): p. 2387-2402.

22. Weiss, S., *Fluorescence spectroscopy of single biomolecules.* Science, 1999. **283**(5408): p. 1676-83.

23. Moerner, W.E., *A Dozen Years of Single-Molecule Spectroscopy in Physics, Chemistry, and Biophysics.* The Journal of Physical Chemistry B, 2002. **106**(5): p. 910-927.

24. Joo, C., et al., *Advances in Single-Molecule Fluorescence Methods for Molecular Biology.* Annual Review of Biochemistry, 2008. **77**(1): p. 51-76.

25. Vale, R.D., et al., *Direct observation of single kinesin molecules moving along microtubules.* Nature, 1996. **380**(6573): p. 451-453.

26. Yildiz, A., et al., *Myosin V walks hand-over-hand: single fluorophore imaging with 1.5-nm localization.* Science, 2003. **300**(5628): p. 2061-5.

27. Zhuang, X., et al., *A single-molecule study of RNA catalysis and folding.* Science, 2000. **288**(5473): p. 2048-51.

28. Kapanidis, A.N., et al., *Initial transcription by RNA polymerase proceeds through a DNA-scrunching mechanism.* Science, 2006. **314**(5802): p. 1144-7.

29. Sako, Y., S. Minoghchi, and T. Yanagida, *Single-molecule imaging of EGFR signalling on the surface of living cells.* Nat Cell Biol, 2000. **2**(3): p. 168-72.

30. Wieser, S. and G.J. Schütz, *Tracking single molecules in the live cell plasma membrane—Do's and Don't's.* Methods, 2008. **46**(2): p. 131-140.

31. Sakon, J.J. and K.R. Weninger, *Detecting the conformation of individual proteins in live cells.* Nature Methods, 2010. **7**(3): p. 203-205.

32. Babcock, H.P., C. Chen, and X. Zhuang, *Using single-particle tracking to study nuclear trafficking of viral genes.* Biophys J, 2004. **87**(4): p. 2749-58.

33. Shav-Tal, Y., et al., *Dynamics of Single mRNPs in Nuclei of Living Cells.* Science, 2004. **304**(5678): p. 1797-1800.

34. Biteen, J.S., et al., *Super-resolution imaging in live Caulobacter crescentus cells using photoswitchable EYFP.* Nature Methods, 2008. **5**(11): p. 947-949.

35. Manley, S., et al., *High-density mapping of single-molecule trajectories with photoactivated localization microscopy.* Nature Methods, 2008. **5**(2): p. 155-157.

36. Xie, X.S., et al., *Single-Molecule Approach to Molecular Biology in Living Bacterial Cells.* Annual Review of Biophysics, 2008. **37**(1): p. 417-444.

37. Toomre, D.K. and J. Bewersdorf, *A New Wave of Cellular Imaging.* Annual Review of Cell and Developmental Biology, 2010. **26**(1): p. 285-314.

38. Persson, F., I. Barkefors, and J. Elf, *Single molecule methods with applications in living cells.* Current Opinion in Biotechnology, 2013. **24**: p. 1-8.

39. Blanchard, S.C., et al., *tRNA selection and kinetic proofreading in translation.* Nat Struct Mol Biol, 2004. **11**(10): p. 1008-14.

40. McKinney, S.A., et al., *Structural dynamics of individual Holliday junctions.* Nat Struct Mol Biol, 2003. **10**(2): p. 93-97.

41. Galletto, R., et al., *Direct observation of individual RecA filaments assembling on single DNA molecules.* Nature, 2006. **443**(7113): p. 875-878.

42. Abelson, J., et al., *Conformational dynamics of single pre-mRNA molecules during in vitro splicing.* Nat Struct Mol Biol, 2010. **17**(4): p. 504-12.

43. Stone, M.D., et al., *Stepwise protein-mediated RNA folding directs assembly of telomerase ribonucleoprotein.* Nature, 2007. **446**(7134): p. 458-61.

44. Hoskins, A.A., et al., *Ordered and Dynamic Assembly of Single Spliceosomes.* Science, 2011. **331**(6022): p. 1289-1295.

45. Abbondanzieri, E.A., et al., *Dynamic binding orientations direct activity of HIV reverse transcriptase.* Nature, 2008. **453**(7192): p. 184-189.

46. Blosser, T.R., et al., *Dynamics of nucleosome remodelling by individual ACF complexes.* Nature, 2009. **462**(7276): p. 1022-1027.

47. Zhao, Y., et al., *Single-molecule dynamics of gating in a neurotransmitter transporter homologue.* Nature, 2010. **465**(7295): p. 188-93.

48. Zhao, Y., et al., *Substrate-modulated gating dynamics in a Na+-coupled neurotransmitter transporter homologue.* Nature, 2011. **474**(7349): p. 109-13.

49. Akyuz, N., et al., *Transport dynamics in a glutamate transporter homologue.* Nature, 2013. **502**(7469): p. 114-118.

50. Rust, M.J., M. Bates, and X. Zhuang, *Sub-diffraction-limit imaging by stochastic optical reconstruction microscopy (STORM).* Nat Methods, 2006. **3**(10): p. 793-5.

51. Betzig, E., et al., *Imaging intracellular fluorescent proteins at nanometer resolution.* Science, 2006. **313**(5793): p. 1642-5.

52. Hess, S.T., T.P.K. Girirajan, and M.D. Mason, *Ultra-High Resolution Imaging by Fluorescence Photoactivation Localization Microscopy.* Biophysical Journal, 2006. **91**(11): p. 4258-4272.

53. Rasnik, I., S.A. McKinney, and T. Ha, *Nonblinking and long-lasting single-molecule fluorescence imaging.* Nature Methods, 2006. **3**(11): p. 891-893.

54. Koopmans, W.J., et al., *Single-pair FRET microscopy reveals mononucleosome dynamics.* J Fluoresc, 2007. **17**(6): p. 785-95.

55. Tomschik, M., et al., *Fast, long-range, reversible conformational fluctuations in nucleosomes revealed by single-pair fluorescence resonance energy transfer.* Proceedings of the National Academy of Sciences of the United States of America, 2005. **102**(9): p. 3278-3283.

56. Saxton, M.J. and K. Jacobson, *Single-Particle Tracking: Applications to Membrane Dynamics.* Annual Review of Biophysics and Biomolecular Structure, 1997. **26**(1): p. 373-399.

57. Kusumi, A., et al., *Paradigm Shift of the Plasma Membrane Concept from the Two-Dimensional Continuum Fluid to the Partitioned Fluid: High-Speed Single-Molecule Tracking of Membrane Molecules.* Annual Review of Biophysics and Biomolecular Structure, 2005. **34**(1): p. 351-378.

58. Cang, H., C. Shan Xu, and H. Yang, *Progress in single-molecule tracking spectroscopy.* Chemical Physics Letters, 2008. **457**(4–6): p. 285-291.

59. Dixit, R. and R. Cyr, *Cell damage and reactive oxygen species production induced by fluorescence microscopy: effect on mitosis and guidelines for non-invasive fluorescence microscopy.* The Plant Journal, 2003. **36**(2): p. 280-290.

60. Dobrucki, J.W., D. Feret, and A. Noatynska, *Scattering of Exciting Light by Live Cells in Fluorescence Confocal Imaging: Phototoxic Effects and Relevance for FRAP Studies.* Biophysical Journal, 2007. **93**(5): p. 1778-1786.

61. Kassab, K., *Photophysical and photosensitizing properties of selected cyanines.* Journal of Photochemistry and Photobiology B: Biology, 2002. **68**(1): p. 15-22.

62. Turro, N.J., V. Ramamurthy, and J.C. Scaiano, *Modern Molecular Photochemistry of Organic Molecules*. 2010: University Science Books.

63. Buschmann, V., K.D. Weston, and M. Sauer, *Spectroscopic Study and Evaluation of Red-Absorbing Fluorescent Dyes.* Bioconjugate Chemistry, 2003. **14**(1): p. 195-204.

64. *Properties of ATTO-dyes*. Available from: http://www.atto-tec.com/fileadmin/user_upload/Katalog_Flyer_Support/Dye_Properties_01.pdf .

65. Webb, J.P., et al., *Intersystem Crossing Rate and Triplet State Lifetime for a Lasing Dye.* The Journal of Chemical Physics, 1970. **53**(11): p. 4227-4229.

66. Chibisov, A.K., G.V. Zakharova, and H. Gorner, *Effects of substituents in the polymethine chain on the photoprocesses in indodicarbocyanine dyes.* Journal of the Chemical Society, Faraday Transactions, 1996. **92**(24): p. 4917-4925.

67. Menzel, R. and E. Thiel, *Intersystem crossing rate constants of rhodamine dyes: influence of the amino-group substitution.* Chemical Physics Letters, 1998. **291**(1–2): p. 237-243.

68. Kuzmin, V.A. and A.P. Darmanyan, *Study of sterically hindered short-lived isomers of polymethine dyes by laser photolysis.* Chemical Physics Letters, 1978. **54**(1): p. 159-163.

69. Tian, H. and K. Chen, *Solvent effect on the triplet lifetime of some rhodamine dyes.* Dyes and Pigments, 1994. **26**(3): p. 167-174.

70. Widengren, J., et al., *Strategies to improve photostabilities in ultrasensitive fluorescence spectroscopy.* J Phys Chem A, 2007. **111**(3): p. 429-40.

71. Jia, K., et al., *Characterization of Photoinduced Isomerization and Intersystem Crossing of the Cyanine Dye Cy3.* The Journal of Physical Chemistry A, 2007. **111**(9): p. 1593-1597.

72. Zheng, Q., et al., *On the Mechanisms of Cyanine Fluorophore Photostabilization.* The Journal of Physical Chemistry Letters, 2012. **3**(16): p. 2200-2203.

73. Montalti, M., et al., *Handbook of photochemistry*. 3rd ed. 2006, Boca Raton: CRC/Taylor & Francis. x, 650 p.

74. Byers, G.W., S. Gross, and P.M. Henrichs, *Direct and Sensitized Photooxidation of Cyanine Dyes.* Photochemistry and Photobiology, 1976. **23**(1): p. 37-43.

75. Kuramoto, N. and T. Kitao, *The contribution of singlet oxygen to the photofading of triphenylmethane and related dyes.* Dyes and Pigments, 1982. **3**(1): p. 49-58.

76. Bonnett, R. and G. Martínez, *Photobleaching of sensitisers used in photodynamic therapy.* Tetrahedron, 2001. **57**(47): p. 9513-9547.

77. Sies, H. and C.F.M. Menck, *Singlet oxygen induced DNA damage.* Mutation Research/DNAging, 1992. **275**(3–6): p. 367-375.

78. Davies, M.J., *Reactive species formed on proteins exposed to singlet oxygen.* Photochemical & Photobiological Sciences, 2004. **3**(1): p. 17-25.

79. Eggeling, C., et al., *Photostability of Fluorescent Dyes for Single-Molecule Spectroscopy: Mechanisms and Experimental Methods for Estimating Photobleaching in Aqueous Solution*, in *Applied Fluorescence in Chemistry, Biology and Medicine*. 1999, Springer Berlin Heidelberg. p. 193-240.

80. Vogelsang, J., et al., *A reducing and oxidizing system minimizes photobleaching and blinking of fluorescent dyes.* Angew Chem Int Ed Engl, 2008. **47**(29): p. 5465-9.

81. Eggeling, C., et al., *Photobleaching of Fluorescent Dyes under Conditions Used for Single-Molecule Detection: Evidence of Two-Step Photolysis.* Analytical Chemistry, 1998. **70**(13): p. 2651-2659.

82. Kong, X., et al., *Photobleaching pathways in single-molecule FRET experiments.* J Am Chem Soc, 2007. **129**(15): p. 4643-54.

83. Eggeling, C., et al., *Analysis of Photobleaching in Single-Molecule Multicolor Excitation and Förster Resonance Energy Transfer Measurements†.* The Journal of Physical Chemistry A, 2006. **110**(9): p. 2979-2995.

84. Aramendia, P.F., R.M. Negri, and E.S. Roman, *Temperature Dependence of Fluorescence and Photoisomerization in Symmetric Carbocyanines.Influence of Medium Viscosity and Molecular Structure.* The Journal of Physical Chemistry, 1994. **98**(12): p. 3165-3173.

85. Widengren, J. and P. Schwille, *Characterization of Photoinduced Isomerization and Back-Isomerization of the Cyanine Dye Cy5 by Fluorescence Correlation Spectroscopy.* Journal of Physical Chemistry A., 2000. **104**(27): p. 6416-6428.

86. Campos, L.A., et al., *A photoprotection strategy for microsecond-resolution single-molecule fluorescence spectroscopy.* Nat Meth, 2011. **8**(2): p. 143-146.

87. Lemke, E.A., et al., *Microfluidic Device for Single-Molecule Experiments with Enhanced Photostability.* Journal of the American Chemical Society, 2009. **131**(38): p. 13610-13612.

88. Benesch, R.E. and R. Benesch, *Enzymatic Removal of Oxygen for Polarography and Related Methods.* Science, 1953. **118**(3068): p. 447-448.

89. Aitken, C.E., R.A. Marshall, and J.D. Puglisi, *An oxygen scavenging system for improvement of dye stability in single-molecule fluorescence experiments.* Biophys J, 2008. **94**(5): p. 1826-35.

90. Swoboda, M., et al., *Enzymatic Oxygen Scavenging for Photostability without pH Drop in Single-Molecule Experiments.* ACS Nano, 2012. **6**(7): p. 6364-6369.

91. Schäfer, P., et al., *Methylene Blue- and Thiol-Based Oxygen Depletion for Super-Resolution Imaging.* Analytical Chemistry, 2013. **85**(6): p. 3393-3400.

92. Dempsey, G.T., et al., *Evaluation of fluorophores for optimal performance in localization-based super-resolution imaging.* Nature Methods, 2011. **8**(12): p. 1027-1036.

93. Cooper, M., et al., *Cy3B™: Improving the Performance of Cyanine Dyes.* Journal of Fluorescence, 2004. **14**(2): p. 145-150.

94. Mujumdar, R.B., et al., *Cyanine dye labeling reagents: Sulfoindocyanine succinimidyl esters.* Bioconjugate Chemistry, 1993. **4**(2): p. 105-111.

95. Rurack, K. and M. Spieles, *Fluorescence Quantum Yields of a Series of Red and Near-Infrared Dyes Emitting at 600−1000 nm.* Analytical Chemistry, 2011. **83**(4): p. 1232-1242.

96. Ponterini, G. and M. Caselli, *Photoisomerization Dynamics of 3,3'-Diethyl Oxacarbocyanine. Intramolecular and Solvent Viscosity Effects.* Berichte der Bunsengesellschaft für physikalische Chemie, 1992. **96**(4): p. 564-573.

97. Chibisov, A.K., *Triplet states of cyanine dyes and reactions of electron transfer with their participation.* Journal of Photochemistry, 1976. **6**(3): p. 199-214.

98. Roth, N.J.L. and A.C. Craig, *Predicted observable fluorescent lifetimes of several cyanines.* The Journal of Physical Chemistry, 1974. **78**(12): p. 1154-1155.

99. Sanborn, M.E., et al., *Fluorescence Properties and Photophysics of the Sulfoindocyanine Cy3 Linked Covalently to DNA.* The Journal of Physical Chemistry B, 2007. **111**(37): p. 11064-11074.

100. Mujumdar, S.R., et al., *Cyanine-Labeling Reagents: Sulfobenzindocyanine Succinimidyl Esters.* Bioconjugate Chemistry, 1996. **7**(3): p. 356-362.

101. van de Linde, S., et al., *Photoinduced formation of reversible dye radicals and their impact on super-resolution imaging.* Photochemical & Photobiological Sciences, 2011. **10**(4): p. 499-506.

102. Dave, R., et al., *Mitigating Unwanted Photophysical Processes for Improved Single-Molecule Fluorescence Imaging.* Biophys J, 2009. **96**(6): p. 2371-2381.

103. Yanagida, T., et al., *Direct observation of motion of single F-actin filaments in the presence of myosin.* Nature, 1984. **307**(5946): p. 58-60.

104. Grunwell, J.R., et al., *Monitoring the conformational fluctuations of DNA hairpins using single-pair fluorescence resonance energy transfer.* J Am Chem Soc, 2001. **123**(18): p. 4295-303.

105. Giloh, H. and J.W. Sedat, *Fluorescence microscopy: reduced photobleaching of rhodamine and fluorescein protein conjugates by n-propyl gallate.* Science, 1982. **217**(4566): p. 1252-5.

106. Von Trebra, R. and T.H. Koch, *Dabco stabilization of coumarin dye lasers.* Chemical Physics Letters, 1982. **93**(4): p. 315-317.

107. Cordes, T., et al., *Mechanisms and advancement of antifading agents for fluorescence microscopy and single-molecule spectroscopy.* Physical Chemistry Chemical Physics, 2011. **13**(14): p. 6699-6709.

108. Blanchard, S.C., et al., *tRNA dynamics on the ribosome during translation.* Proc Natl Acad Sci USA, 2004. **101**(35): p. 12893-8.

109. Cordes, T., J. Vogelsang, and P. Tinnefeld, *On the mechanism of Trolox as antiblinking and antibleaching reagent.* J Am Chem Soc, 2009. **131**(14): p. 5018-9.

110. Vogelsang, J., et al., *Make them Blink: Probes for Super-Resolution Microscopy.* ChemPhysChem, 2010. **11**(12): p. 2475-2490.

111. Marling, J.B., D.W. Gregg, and L. Wood, *Chemical Quenching of the Triplet State in Flashlamp Excited Liquid Organic Lasers.* Applied Physics Letters 1970. **17**(12): p. 527-530.

112. Wenthold, P.G., et al., *Transition-State Spectroscopy of Cyclooctatetraene.* Science, 1996. **272**(5267): p. 1456-1459.

113. Frutos, L.M., et al., *A theory of nonvertical triplet energy transfer in terms of accurate potential energy surfaces: The transfer reaction from $\pi,\pi*$ triplet donors to 1,3,5,7-cyclooctatetraene.* The Journal of Chemical Physics, 2004. **120**(3): p. 1208-1216.

114. Weninger, K., et al., *Single-molecule studies of SNARE complex assembly reveal parallel and antiparallel configurations.* Proc Natl Acad Sci U S A, 2003. **100**(25): p. 14800-5.

115. Alejo, Jose L., Scott C. Blanchard, and Olaf S. Andersen, *Small-Molecule Photostabilizing Agents are Modifiers of Lipid Bilayer Properties.* Biophysical Journal, 2013. **104**(11): p. 2410-2418.

116. Altman, R.B., et al., *Cyanine fluorophore derivatives with enhanced photostability.* Nature Methods, 2012. **9**(1): p. 68-71.

117. Altman, R.B., et al., *Enhanced photostability of cyanine fluorophores across the visible spectrum.* Nature Methods, 2012. **9**(5): p. 428-9.

118. Liphardt, B., B. Liphardt, and W. Lüttke, *Laser dyes with intramolecular triplet quenching.* Optics Communications, 1981. **38**(3): p. 207-210.

119. Ernst, L.A., et al., *Cyanine dye labeling reagents for sulfhydryl groups.* Cytometry, 1989. **10**(1): p. 3-10.

120. Tinnefeld, P. and T. Cordes, *'Self-healing' dyes: intramolecular stabilization of organic fluorophores.* Nature Methods, 2012. **9**(5): p. 426-427.

121. Munro, J.B., et al., *Identification of two distinct hybrid state intermediates on the ribosome.* Mol Cell, 2007. **25**(4): p. 505-17.

122. Qin, F., *Restoration of single-channel currents using the segmental k-means method based on hidden Markov modeling.* Biophys J, 2004. **86**(3): p. 1488-501.

123. Yagci, Y., S. Jockusch, and N.J. Turro, *Mechanism of Photoinduced Step Polymerization of Thiophene by Onium Salts: Reactions of Phenyliodinium and Diphenylsulfinium Radical Cations with Thiophene.* Macromolecules, 2007. **40**(13): p. 4481-4485.

124. Gollmer, A., et al., *Singlet Oxygen Sensor Green®: Photochemical Behavior in Solution and in a Mammalian Cell.* Photochemistry and Photobiology, 2011. **87**(3): p. 671-679.

125. Michalet, X., S. Weiss, and M. Jager, *Single-Molecule Fluorescence Studies of Protein Folding and Conformational Dynamics.* Chem. Rev., 2006. **106**(5): p. 1785-1813.

126. Huang, Z., et al., *Spectral Identification of Specific Photophysics of Cy5 by Means of Ensemble and Single Molecule Measurements.* The Journal of Physical Chemistry A, 2005. **110**(1): p. 45-50.

127. Chibisov, A.K., S.V. Shvedov, and H. Görner, *Photosensitized processes in dicarbocyanine dyes induced by energy transfer: delayed fluorescence, trans→cis isomerization and electron transfer.* Journal of Photochemistry and Photobiology A: Chemistry, 2001. **141**(1): p. 39-45.

128. Chen, P., et al., *Study on the photooxidation of a near-infrared-absorbing benzothiazolone cyanine dye.* Dyes and Pigments, 1998. **37**(3): p. 213-222.

129. Sheetz, M.P. and D.E. Koppel, *Membrane damage caused by irradiation of fluorescent concanavalin A.* Proceedings of the National Academy of Sciences, 1979. **76**(7): p. 3314-3317.

130. Vigers, G.P., M. Coue, and J.R. McIntosh, *Fluorescent microtubules break up under illumination.* The Journal of Cell Biology, 1988. **107**(3): p. 1011-1024.

131. Khan, A.U. and M. Kasha, *Direct spectroscopic observation of singlet oxygen emission at 1268 nm excited by sensitizing dyes of biological interest in liquid solution.* Proceedings of the National Academy of Sciences, 1979. **76**(12): p. 6047-6049.

132. Setsukinai, K.-i., et al., *Development of Novel Fluorescence Probes That Can Reliably Detect Reactive Oxygen Species and Distinguish Specific Species.* Journal of Biological Chemistry, 2003. **278**(5): p. 3170-3175.

133. Blanchard, S.C., *Reply to "'Self-healing' dyes: intramolecular stabilization of organic fluorophores".* Nature Methods, 2012. **9**(5): p. 427-428.

134. Chandler, D., *Electron transfer in water and other polar environments, how it happens*, in *Classical and Quantum Dynamics in Condensed Phase Simulations*, B.J. Berne, G. Ciccotti, and D.F. Coker, Editors. 1998, World Scientific: Singapore. p. 25-49.

135. Huang, B., M. Bates, and X. Zhuang, *Super-Resolution Fluorescence Microscopy.* Annual Review of Biochemistry, 2009. **78**(1): p. 993-1016.

136. Liu, Z., Luke D. Lavis, and E. Betzig, *Imaging Live-Cell Dynamics and Structure at the Single-Molecule Level.* Molecular Cell, 2015. **58**(4): p. 644-659.

137. Zheng, Q., et al., *Ultra-stable organic fluorophores for single-molecule research.* Chemical Society Reviews, 2014. **43**(4): p. 1044-1056.

138. Glazer, A.N., *Fluorescence-based assay for reactive oxygen species: a protective role for creatinine.* The FASEB Journal, 1988. **2**(9): p. 2487-91.

139. van der Velde, J.H.M., et al., *Mechanism of Intramolecular Photostabilization in Self-Healing Cyanine Fluorophores.* ChemPhysChem, 2013. **14**(18): p. 4084-4093.

140. Forward, P.J., A.A. Gorman, and I. Hamblett, *'Nonvertical' triplet energy transfer to cyclooctatetraene: support for the single-bond torsion mechanism.* Journal of the Chemical Society, Chemical Communications, 1993(3): p. 250-251.

141. Koopmans, W.J.A., et al., *spFRET Using Alternating Excitation and FCS Reveals Progressive DNA Unwrapping in Nucleosomes.* Biophysical journal, 2009. **97**(1): p. 195-204.

142. Santoso, Y., et al., *Conformational transitions in DNA polymerase I revealed by single-molecule FRET.* Proceedings of the National Academy of Sciences, 2010. **107**(2): p. 715-720.

143. Konig, I., et al., *Single-molecule spectroscopy of protein conformational dynamics in live eukaryotic cells.* Nature Methods, 2015. **12**(8): p. 773-779.

144. Willig, K.I., et al., *STED microscopy with continuous wave beams.* Nat Meth, 2007. **4**(11): p. 915-918.

145. Rieger, P.H., *Electrochemistry*. 1987: Prentice-Hall.

146. Marcus, R.A., *Electron Transfer Reactions in Chemistry: Theory and Experiment (Nobel Lecture).* Angewandte Chemie International Edition in English, 1993. **32**(8): p. 1111-1121.

147. Holzmeister, P., A. Gietl, and P. Tinnefeld, *Geminate Recombination as a Photoprotection Mechanism for Fluorescent Dyes.* Angewandte Chemie International Edition, 2014. **53**(22): p. 5685-5688.

148. Grimm, J.B., et al., *A general method to improve fluorophores for live-cell and single-molecule microscopy.* Nat Meth, 2015. **12**(3): p. 244-250.

149. Lukinavičius, G., et al., *A near-infrared fluorophore for live-cell super-resolution microscopy of cellular proteins.* Nat Chem, 2013. **5**(2): p. 132-139.

150. Huang, B., H. Babcock, and X. Zhuang, *Breaking the Diffraction Barrier: Super-Resolution Imaging of Cells.* Cell, 2010. **143**(7): p. 1047-1058.

151. Gurevich, V.V. and E.V. Gurevich, *How and why do GPCRs dimerize?* Trends in pharmacological sciences, 2008. **29**(5): p. 234-240.

152. Roy, R., S. Hohng, and T. Ha, *A practical guide to single-molecule FRET.* Nat Methods, 2008. **5**(6): p. 507-16.

153. Keppler, A., et al., *A general method for the covalent labeling of fusion proteins with small molecules in vivo.* Nat Biotech, 2003. **21**(1): p. 86-89.

154. Bosch, Peter J., et al., *Evaluation of Fluorophores to Label SNAP-Tag Fused Proteins for Multicolor Single-Molecule Tracking Microscopy in Live Cells.* Biophysical Journal, 2014. **107**(4): p. 803-814.

155. Stennett, E.M.S., M.A. Ciuba, and M. Levitus, *Photophysical processes in single molecule organic fluorescent probes.* Chemical Society Reviews, 2014. **43**(4): p. 1057-1075.

156. Sako, Y., et al., *Live cell single-molecule detection in systems biology.* Wiley Interdisciplinary Reviews: Systems Biology and Medicine, 2012. **4**(2): p. 183-192.

157. Zheng, Q., et al., *The Contribution of Reactive Oxygen Species to the Photobleaching of Organic Fluorophores.* Photochemistry and Photobiology, 2014. **90**(2): p. 448-454.

158. Akyuz, N., et al., *Transport domain unlocking sets the uptake rate of an aspartate transporter.* Nature, 2015. **518**(7537): p. 68-73.

159. Wasserman, M.R., et al., *Chemically related 4,5-linked aminoglycoside antibiotics drive subunit rotation in opposite directions.* Nat Commun, 2015. **6**.

160. Bruice, T.C. and U.K. Pandit, *The Effect of Geminal Substitution Ring Size and Rotamer Distribution on the Intramolecular Nucleophilic Catalysis of the Hydrolysis of Monophenyl Esters of Dibasic Acids and the Solvolysis of the Intermediate Anhydrides.* Journal of the American Chemical Society, 1960. **82**(22): p. 5858-5865.

161. Lightstone, F.C. and T.C. Bruice, *Ground State Conformations and Entropic and Enthalpic Factors in the Efficiency of Intramolecular and Enzymatic Reactions. 1. Cyclic Anhydride Formation by Substituted Glutarates, Succinate, and 3,6-Endoxo-Δ4-tetrahydrophthalate Monophenyl Esters.* Journal of the American Chemical Society, 1996. **118**(11): p. 2595-2605.

162. Nani, R.R., et al., *Reactive species involved in the regioselective photooxidation of heptamethine cyanines.* Chemical Science, 2015. **6**(11): p. 6556-6563.

163. Jencks, W.P., *Catalysis in Chemistry and Enzymology*. 1987: Dover.

164. Das, T.N. and K.I. Priyadarshini, *Triplet of cyclooctatetraene: reactivity and properties.* Journal of the Chemical Society, Faraday Transactions, 1994. **90**(7): p. 963-968.

165. Wagner, P.J. and P. Klán, *Intramolecular Triplet Energy Transfer in Flexible Molecules: Electronic, Dynamic, and Structural Aspects.* Journal of the American Chemical Society, 1999. **121**(41): p. 9626-9635.

166. Allonas, X., et al., *Investigation of the triplet quantum yield of thioxanthone by time-resolved thermal lens spectroscopy: solvent and population lens effects.* Chemical Physics Letters, 2000. **322**(6): p. 483-490.

167. Jockusch, S., et al., *Electron Spin Polarization Transfer from a Nitroxide Incarcerated within a Nanocapsule to a Nitroxide in the Bulk Aqueous Solution.* The Journal of Physical Chemistry Letters, 2010. **1**(18): p. 2628-2632.

168. Cowan, D.O. and A.A. Baum, *Intramolecular triplet energy transfer.* Journal of the American Chemical Society, 1971. **93**(5): p. 1153-1162.

169. Wagner, P.J. and G.M. El-Taliawi, *Through-space intramolecular triplet energy transfer: the cinnamyl esters of .omega.-benzoyl carboxylic acids.* Journal of the American Chemical Society, 1992. **114**(21): p. 8325-8326.

170. Adam, W., et al., *Synthesis of endoperoxides derived from cyclooctatetraenes via singlet oxygenation.* Tetrahedron, 1985. **41**(11): p. 2045-2056.

171. Johnsson, N. and K. Johnsson, *Chemical Tools for Biomolecular Imaging.* ACS Chemical Biology, 2007. **2**(1): p. 31-38.

172. Murakoshi, H., et al., *Single-molecule imaging analysis of Ras activation in living cells.* Proceedings of the National Academy of Sciences of the United States of America, 2004. **101**(19): p. 7317-7322.

173. Zheng, Q., et al., *Intra-molecular Triplet Energy Transfer is a General Approach to Improve Organic Fluorophore Photostability.* Photochemical and Photobiological Sciences, 10.1039/C5PP00400D.

174. Renikuntla, B.R., et al., *Improved Photostability and Fluorescence Properties through Polyfluorination of a Cyanine Dye.* Organic Letters, 2004. **6**(6): p. 909-912.

175. Huang, Y., et al., *Effects of modifying the $tRNA^{Lys}_3$ anticodon on the initiation of human immunodeficiency virus type 1 reverse transcription.* J. Virol., 1996. **70**: p. 4700-4706.

176. Chen, Z., et al., *Second-Generation Covalent TMP-Tag for Live Cell Imaging.* Journal of the American Chemical Society, 2012. **134**(33): p. 13692-13699.

177. Erazo-Oliveras, A., et al., *Protein delivery into live cells by incubation with an endosomolytic agent.* Nat Meth, 2014. **11**(8): p. 861-867.

178. Baird, N.C., *Quantum organic photochemistry. II. Resonance and aromaticity in the lowest 3.pi..pi.* state of cyclic hydrocarbons.* Journal of the American Chemical Society, 1972. **94**(14): p. 4941-4948.

179. Ottosson, H., *Organic photochemistry: Exciting excited-state aromaticity.* Nat Chem, 2012. **4**(12): p. 969-971.

180. Ottosson, H., et al., *Scope and limitations of Baird's theory on triplet state aromaticity: application to the tuning of singlet-triplet energy gaps in fulvenes.* Chemistry, 2007. **13**(24): p. 6998-7005.

181. Zeng, T., N. Ananth, and R. Hoffmann, *Seeking Small Molecules for Singlet Fission: A Heteroatom Substitution Strategy.* Journal of the American Chemical Society, 2014. **136**(36): p. 12638-12647.

182. Klán, P. and P.J. Wagner, *Intramolecular Triplet Energy Transfer in Bichromophores with Long Flexible Tethers.* Journal of the American Chemical Society, 1998. **120**(9): p. 2198-2199.

183. Munro, J.B., et al., *Conformational dynamics of single HIV-1 envelope trimers on the surface of native virions.* Science, 2014. **346**(6210): p. 759-763.

184. Lv, Z., et al., *Direct Detection of alpha-Synuclein Dimerization Dynamics: Single-Molecule Fluorescence Analysis.* Biophys J, 2015. **108**(8): p. 2038-47.

185. Sun, X., et al., *Development of SNAP-Tag Fluorogenic Probes for Wash-Free Fluorescence Imaging.* ChemBioChem, 2011. **12**(14): p. 2217-2226.